Iouri Poussep

Localização e Coerência de Excitações Elementares em Sistemas Eletrônicos Desordenados: Ligas AlGaAs e Super-redes GaAs/AlGaAs Intencionalmente Desordenadas.

Março de 2005

ÍNDICE:

I. Introdução

I.1. Metais e isolantes. Problema de localização.

Condutividade elétrica apresenta uma grandeza física fundamental quando precisa descrever a resposta de um material para o campo elétrico externo. Neste caso a condutividade é usada para caracterização quantitativa de possibilidade de transferir a carga elétrica que ocorre pela presença de portadores livres. Dependendo da magnitude de condutividade, todos ao materiais podem ser condicionalmente divididos para metais, onde a condutividade típica $\sigma > 10^6$ (ohm x cm)$^{-1}$ e isolantes onde $\sigma < 10^{-8}$ (ohm x cm)$^{-1}$. Semicondutores possuem os valores de condutividade intermediários.

Para caracterizar "degrau de liberdade" de portadores elétricos pode-se usar a razão do tempo de livre caminho médio (τ) sobre o tempo característico entre as colisões de portadores (elétrons) com defeitos (t_{coll}): τ/t_{coll}. Quando $\tau/t_{coll} \gg 1$, as colisões não influenciam significativamente o movimento dos elétrons, que por isto não desviam drasticamente da sua trajetória reta em campo elétrico externo [Fig.1(a)]. Neste caso podemos tratar o movimento de elétrons como a difusão de partículas clássicas e de acordo com a aproximação de Boltzmann:

$$\sigma_D = \frac{ne^2\tau}{m} \tag{1}$$

onde n e m são a concentração de elétrons e sua massa respectivamente.
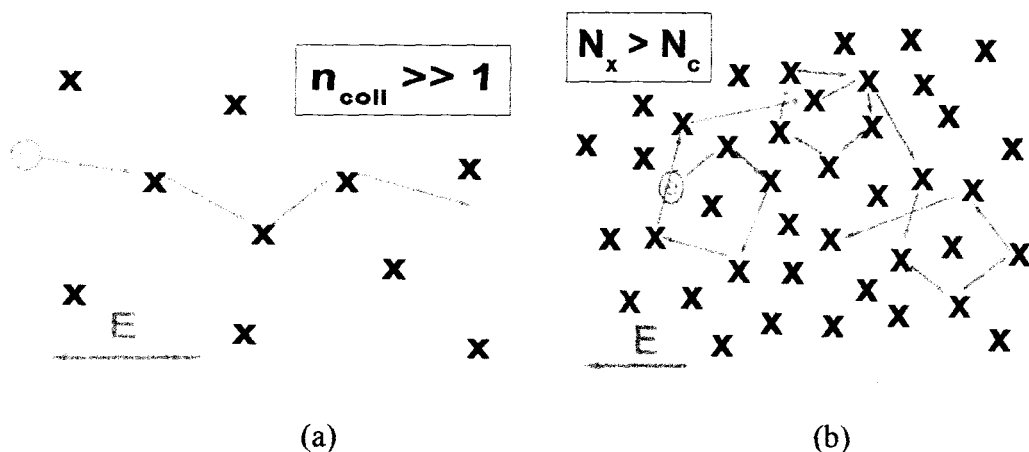

(a)   (b)

Fig.1. Trajetórias de elétrons na presença de centros de espalhamento. n_{coll} é numero de colisões que ocorrem durante o tempo de observação.

3

A formula (1) determina a condutividade metálica DC ($\omega = 0$) que é determinada por condições:

$$\sigma(T=0) \neq 0, \quad \partial\sigma / \partial T < 0 \qquad (2)$$

Num metal a condutividade diminui com a temperatura para as temperaturas maior do que a temperatura de Debye. Para as temperaturas baixas a condutividade metálica praticamente não depende da temperatura.

Aumento da concentração de centros de espalhamento N_x pode causar modificação drástica das trajetórias clássicas eletrônicas resultando em formação de trajetórias fechadas, como é apresentado na Fig.1(b). As trajetórias fechadas correspondem à localização espacial de elétrons. De acordo com P.W.Anderson [1], todos os elétrons devem ser localizados quando $N_x > N_c$, onde N_c é a concentração crítica de centros de espalhamento. Esta condição corresponde ao um isolante quando:

$$\sigma(T=0) = 0, \quad \partial\sigma / \partial T > 0 \qquad (3)$$

Assim, o comportamento da condutividade com a variação da temperatura manifesta o tipo de material (metal ou isolante).

Entretanto, quando a densidade de defeitos aumenta, a distancia média entre os centros de espalhamento diminui. Quando esta distancia for comparável ao comprimento de onda de de Broglie, propriedades ondulatórias de elétrons começam determinar o movimento deles. Neste caso a física clássica falha e o tratamento quântico deve ser usado para calcular a condutividade.

Na física quântica um elétron que propaga num sistema de centros de espalhamento é determinado por uma função de onda tipo:

$$\Psi(\vec{r}) \propto \sum_{\vec{k}} \exp(-i\vec{k}\vec{r}) \qquad (4)$$

que apresenta a soma de ondas planas com diferentes números de onda ($\vec{k}$). Enquanto o estado localizado é descrito pela função de onda que espalha-se no espaço sobre a distancia finita – o cumprimento de localização (ξ):

$$\Psi(\vec{r}) \propto \exp(|\vec{r} - \vec{r}_0| / \xi \qquad (5)$$

I.2. Interferência quântica. Localização como produto de interferência quântica

Quando os elétrons apresentam propriedades ondulatórias, a interferência entre eles pode influenciar a condutividade. Isto acontece quando se consideram as trajetórias fechadas equivalentes e opostas, como é apresentado na Fig.2.
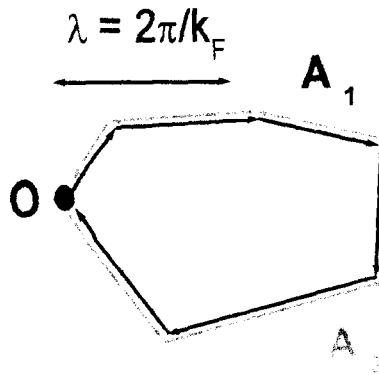

Fig.2. Trajetórias fechadas opostas que correspondem às duas amplitudes clássicos A_1 e A_2 equivalentes.

As amplitudes A_1 e A_2 acumulam fases iguais e por isso, as duas amplitudes resultam em interferência construtiva no ponto de origem (**O**). Neste caso, a probabilidade de achar um elétron no ponto de origem P_o aumenta com relação à probilidade clássica [2]:

$$P_O = |A_1 + A_2|^2 = |A_1|^2 + |A_2|^2 + 2\operatorname{Re}(A_1^* A_2) \tag{6}$$

onde o último termo apresenta o resultado de interferência.

Este efeito é chamado como a localização fraca, que ocorre em metais quando a concentração de defeitos é baixa. A interferência quântica produz uma correção para a condutividade clássica. Neste caso a condutividade total pode ser apresentada como a soma de condutividade clássica (σ_D) e da correção quântica ($\Delta\sigma$) :

$$\sigma = \sigma_D + \Delta\sigma \tag{7}$$

no limite de espalhamento fraco ($k_F l \gg 1$, onde k_F e l são o numero de onda da Fermi e o livre caminho médio) respectivamente [2]:

$$\frac{\Delta\sigma}{\sigma} \approx -\frac{1}{(k_F l)^2}(1 - \sqrt{\frac{\tau}{\tau_\varphi}}) \tag{8}$$

onde τ_φ é o tempo de defasagem da função de onda.

No campo magnético externo (H), as duas amplitudes (A_1 e A_2) adquirem as fases diferentes; a diferença entre as fases é: $\Delta\varphi = 2\pi\dfrac{\Phi}{\Phi_0}$, onde Φ e Φ_0 são o fluxo de campo magnético através da trajetória fechada e o quantum de fluxo magnético. Isto significa que o campo magnético destruiu a coerência entre as amplitudes e assim, a correção quântica $\Delta\sigma$ desaparece. A teoria diz que a correção quântica depende do campo magnético como [2]:

$$\Delta\sigma(H) = \frac{e^2}{2\pi^2\hbar l_H}F(\delta) \sim \sqrt{H} \tag{9}$$

onde l_H é o cumprimento magnético, $\delta = \dfrac{l_H^2}{4D\tau_\varphi}$, com D é o coeficiente de difusão.

No limite de localização forte ($k_F l < 1$) a condutividade é causada por pulos de elétrons entre os estados localizados, como é apresentado na Fig.3.
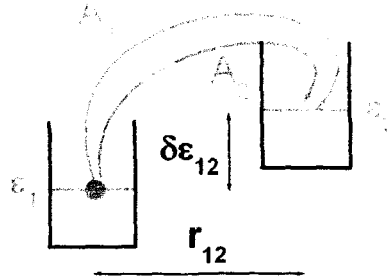
Fig.3. Processos de ativação de elétrons localizados.

Neste caso as diferentes amplitudes de pulos (A_1 e A_2) podem interferir causando a correção para condutividade; os cálculos teóricos resultam em seguinte dependência da condutividade do campo magnético [3]:

$$\Delta\sigma(H) = \frac{e^2\delta^{-3/2}}{192\pi^2\hbar l_H} \sim H^2 \tag{10}$$

As duas formulas (9) e (10) apresentam diferentes dependências de condutividade do campo magnético nos estados metálico e isolante. Assim, de acordo com as teorias, medidas de magneto-condutividade podem também manifestar o tipo de material na forma equivalente às medidas de dependências de condutividade sobre a temperatura.

I.3. Problemas de coerência de elétrons em sistemas anisotrópicos e

desordenados

De acordo com a lei de Ohm, densidade de corrente j_i é proporcional ao aplicado campo elétrico E_k :

$$j_i = \sigma_{ik}E_k \qquad (11)$$

onde o coeficiente de proporcionalidade σ_{ik} é a condutividade que num cristal tem a forma de tensor. No campo magnético externo $H = 0$ o tensor de condutividade tem somente as componentes diagonais (apresentados na Fig.4):

$$\sigma_{ik} = \begin{vmatrix} \sigma_{xx} & 0 & 0 \\ 0 & \sigma_{yy} & 0 \\ 0 & 0 & \sigma_{zz} \end{vmatrix} \qquad (12)$$

Num cristal perfeito os movimentos de elétrons em todas as três direções principais $(x, y$ e $z)$ são independentes e por isto, as propriedades dinâmicas de um elétron em cristal podem ser descritas por três equações de movimento independentes. No entanto, a situação pode mudar drasticamente em sistemas eletrônicos fortemente anisotrópicos. Um exemplo respeitável é dado por sistemas metálicos de multicamadas. Estes sistemas tem importância significativa porque incluem um classe de materiais que revelam a super-condutividade com temperaturas altas ("high-temperature superconductors").

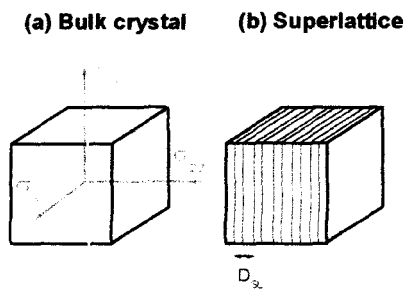**(a) Bulk crystal   (b) Superlattice**

Fig.4. Componentes de condutividade num cristal (a) e a estrutura de super-rede (b).

Em tais metais os blocos metálicos bidimensionais fracamente conectados formam um cristal inteiro. Os experimentos mostram que nestes materiais a variação de condutividade com a temperatura depende significativamente da direção da corrente [4-6].

7

A dependência da condutividade da temperatura foi mostrada sendo diferente nas duas direções: paralelo e perpendicular às camadas. Acima de uma típica temperatura (50-200 K) a condutividade paralela das camadas é metálica enquanto a condutividade através de camadas corresponde ao comportamento isolante. Com as temperaturas baixas, ambas condutividades mostram o comportamento metálico.

Este resultado não tem uma explicação dentro da teoria convencional de condutividade de metais de Bloch-Peierls que prediz isotropia de dependência térmica da condutividade [7]. Nesta teoria a condutividade é expressada através de um produto de velocidade de elétron e o tempo de relaxação dele (determinado por processos de espalhamento). A velocidade é genericamente anisotrópica, mas independente da temperatura, enquanto o tempo de relaxação é genericamente dependente da temperatura mas não apresenta a dependência significativa da direção de corrente. Os exemplos deste comportamento surpreendente incluem cuprates [8], cristais moleculares orgânicos [9], strontium ruthenate [10] e oxidos de cobalto [11]. A estrutura cristalina destes materiais forma planos sobre quais um elétron pode mover-se fácil, mas a ligação entre os planos está fraca.

Em [11] foi demonstrado que quando a temperatura aumenta, as quase-partículas responsáveis para o transporte dentro das camadas desaparecem aproximadamente com as mesmas temperaturas quando a condutividade inter-planos cruza seu comportamento de metálico para isolante. A teoria [12] mostra que as quase-partículas existem dentro das camadas quando o momentum na direção perpendicular as camadas é conservado durante o processo de tunelamento entre as camadas. Isto significa que em sistemas metálicos multicamadas o movimento de elétrons paralelo das camadas depende do transporte entre as camadas. Ainda não está claro, como apresentar o transporte metálico dentro das camadas quando as quase-partículas desaparecem. Isto levanta um problema ligado ao uso da teoria de liquido de Fermi e o conceito de quase-partículas para descrição de comportamento metálico [13].

A solução deste problema é importante para entender a física de processos de supercondutividade de alta temperatura que acontece em materiais eletronicamente anisotrópicas, com a clara estrutura de multicamadas. O estado supercondutivo tem o caráter tridimensional; por isso, a ligação entre as camadas deve fortemente influenciar a formação dele [11]. Porém, em metais multicamadas naturais a anisotropia é dada pela

estrutura destes materiais e não pode ser modificada para variar condições de transporte (ligação entre as camadas) e assim, distinguir uma razão de desacordo com a teoria.

A coerência de elétrons é profundamente ligada ao problema de localização. O tempo de defasagem da função de onda eletrônica determina a força de localização. Este tempo é considerado como um tempo mais curto no sistema eletrônico e assim, o comprimento de coerência $L_\varphi = \sqrt{D\tau_\varphi}$ determina o comprimento mínimo de pacote de onda eletrônica [14]. Conseqüentemente, o comprimento de coerência pode servir como uma estimativa mínima ("lower cutoff") para o cumprimento de localização. De acordo com W.Kohn [15], a localização de elétrons ocorre no espaço de configuração, e por isso se relaciona mais à natureza da função de onda do que à distribuição de carga eletrônica no espaço real. Portanto, o estado isolante é determinado pela localização da função de onda básica ('ground wave function"). Por isso, uma prova direta das propriedades de funções de ondas eletrônicas é um assunto central do problema de localização.

Quaisquer excitações elementares que têm a natureza ondulatória revelam mesmos aspectos qualitativos da localização. Porém, especifica de traços delas pode causar diferentes representações características. Em nossos experimentos comparamos as propriedades de localização de excitações uni-partículas e excitações coletivas (plasmons) sujeitas do potencial aleatório em super-redes GaAs/AlGaAs desordenadas. A diferença essencial entre elas consiste em polarização dinâmica que determina o movimento coletivo de elétrons. A interação entre os elétrons que produz esta polarização intrinsecamente determina traços de excitações coletivas. Por isso, a comparação entre propriedades de localização de elétrons e plasmons pode esclarecer como a interação influencia a localização.

II. Super-redes intencionalmente desordenadas

II.1. Desordem monitorada

A idéia deste projeto foi usar super-redes semicondutoras para estudar o transporte quântico (processos de interferência quântica e problemas de coerência de elétrons) em estruturas de multicamadas. Neste caso as super-redes semicondutoras tem uma vantagem evidente – possibilidade de monitorar acoplamento entre as camadas e assim, avistar como isto influencia o transporte.

9

As super-redes semicondutoras apresentam um grande benefício para fabricar as estruturas com desejado potencial eletrônico e assim, modelar propriedades dinâmicas de elétrons. Já na primeira proposta de materiais super-estruturados [16] foi mencionado que o controlado desvio de super-rede da estrutura ideal fornece uma base para testar as teorias de sistemas desordenados. Uma delas, mais interessante até hoje, é a teoria de localização. A localização de elétrons pode ocorrer em super-rede com a desordem bastante forte, onde a energia de localização domina a energia cinética. Também, a variação de composição e largura das barreiras permite controlar a interação entre os elétrons em poços vizinhos e assim, modificar a dimensionalidade do sistema eletrônico. Assim, em super-redes pode-se controlar ambos, a desordem e a interação que fundamentalmente determinam o efeito de transporte e localização de elétrons [17]. Neste caso, dependentemente da forca de desordem, o sistema eletrônico revela dois estados – um metálico e outro isolante.

O método de crescimento por epitaxia de feixes moleculares permite colocar camadas atômicas "one by one" e assim, controlar a estrutura das amostras em escala atômica. Isso apresenta uma possibilidade única de fabricação de materiais super-estruturados com controle de estrutura na direção de crescimento.

Estudamos as super-redes semicondutoras (GaAs/AlGaAs) que apresentam uma seqüência das camadas de materiais diferentes (GaAs e AlGaAs); esta seqüência de camadas (poços quânticos e barreiras) modula as propriedades eletrônicas do sistema, formando um espetro energético que depende dos parâmetros geométricos da estrutura (larguras das camadas). O heterosistema GaAs/AlGaAs foi escolhido, pois possui alta qualidade de interfaces que diminui os efeitos da desordem incontrolada associada com imperfeições interfaciais. Assim, as propriedades de transporte eletrônico em super-redes podem ser bem definidas. É bem conhecido que em super-redes periódicas, como a conseqüência de reflexões de Bragg causadas pela interferência construtiva entre as ondas propagadas nas opostas direções sobre o eixo da super-rede (direção de crescimento), o espectro energético dos elétrons apresenta uma seqüência de minibandas (intervalos energéticos permitidos) separadas por minigaps (intervalos energéticos proibidos) [18]. As propriedades dinâmicas dos elétrons dependem fortemente de estrutura das minibandas. A violação da periodicidade da super-rede quebra a coerência de elétrons e assim, produz estados eletrônicos localizados. Conseqüentemente, a transição metal-isolante em

transporte vertical (perpendicular às camadas) pode ser conseguida quando se introduz a desordem na direção de crescimento pela variação aleatória de espessuras de camadas.

As propriedades dos elétrons em super-redes desordenadas podem ser caracterizadas pelo parâmetro $\delta_{SL} = \Delta/W$. A energia Δ mede o grau de desordem e é determinada pela espessura da distribuição dos elétrons não-interagentes calculada nos poços quânticos isolantes. A energia W é a força de interação entre os elétrons que no caso de super-redes coincide com a largura da minibanda considerada. Evidentemente, a maioria dos elétrons deve ser localizada quando $\delta_{SL} > 1$.
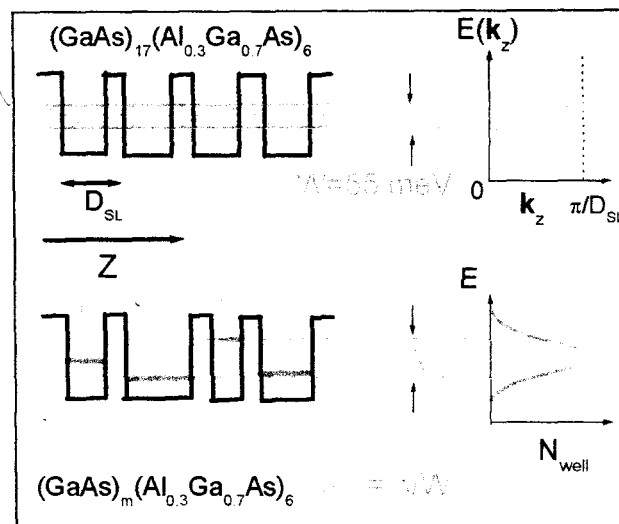

Fig.5. Formação dos estados eletrônicos propagativos em super-rede periódica (painel em cima) e os estados localizados em super-rede desordenada (painel embaixo).

Para produzir a desordem desejada, as super-redes $(GaAs)_m(AlGaAs)_n$ com a variação aleatória das espessuras dos poços quânticos GaAs e com as espessuras de barreiras de AlGaAs fixas ($n = 6$ ML) devem ser preparadas. Nestas super-redes a desordem vertical foi formada pela a variação aleatória controlada das espessuras de camadas de GaAs sobre o valor nominal m = 17 ML. As amostras foram crescidas nos substratos de GaAs orientados em [001] direção cristalográfica. Para evitar flutuações das espessuras de camadas laterais que provocam a desordem incontrolada, o crescimento foi interrompido por 20 s nas interfaces normais (AlGaAs crescido sobre de GaAs). O

11

acoplamento entre as camadas foi acertado pela variação das larguras das barreiras. As camadas metálicas foram formadas pela dopagem homogênea pelo Si.

Outro tipo de desordem pode ser produzida em super-redes por rugosidade de interfaces. Como é apresentado na Fig.6., as propriedades de "bulk"cristal dominam quando a espessura dos poços quânticos de super-rede d é maior do que o comprimento de livre caminho médio l. Neste caso as impurezas causam o espalhamento de elétrons. Porém, o espalhamento por rugosidades interfaciais aumenta-se quando a espessura de poços quânticos diminui. Quando $d < l$, o espalhamento pela rugosidade interfacial domina o transporte paralelo formando estados localizados.
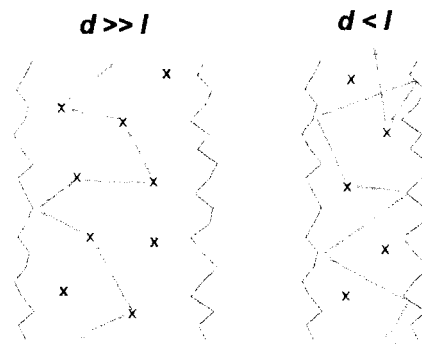
$$d \gg l \qquad\qquad d < l$$

Fig.6. Movimento eletrônico em camadas de super-rede.

Assim, a transição metal-isolante em transporte paralelo pode ser obtida em super-redes com a variação da espessura dos poços quânticos.

As amostras com vários níveis de desordem e do acoplamento vertical foram estudadas e assim, o papel da desordem na propagação e na localização dos elétrons em super-redes foi revelado e investigado.

II.2. Controle e caracterização da desordem

Um problema freqüentemente encontrado em sistemas eletrônicos desordenados é caracterização quantitativa da forca de desordem. Na maioria das realizações de tais sistemas a desordem pode ser definida somente qualitativamente. Ainda mais, a variação de desordem normalmente é acompanhada pela alteração da densidade de elétrons, que influencia interação entre eles. Isto acontece em tais sistemas comuns como

12

semicondutores dopados, onde a dopagem produz ambos a desordem e excesso de elétrons e em dispositivos de efeito de campo ("field effect devices") onde a alteração de espessura da camada da depleção influencia ambos, o efeito da desordem superficial e a densidade de elétrons.

Em super-redes semicondutoras a desordem pode ser controlada pela estrutura da super-rede, entretanto a dopagem pode prover elétrons. O controle separado da forca de desordem e da concentração de elétrons pode ser obtido quando o efeito da desordem artificial estrutural domina a desordem por impurezas.

Usamos vários métodos para caracterizar o efeito de desordem sobre elétrons em super-redes investigadas, tais como medidas de capacitância, fotoluminescência, e efeito Hall. As medidas de capacitância fornecem os dados sobre a densidade de elétrons na direção de crescimento que é diretamente influenciada pela desordem vertical. A modificação da densidade de elétrons nas bandas de valência e de condução pela desordem pode ser medida usando a fotoluminescência. As medidas de mobilidade de Hall aprovisionam os valores do parâmetro $k_F l$, que caracterizam tipo de material ($k_F l \gg 1$ corresponde de estado metálico, enquanto $k_F l < 1$ significa a presença de estados localizados). Os perfis CV medidos em super-redes com diferentes forcas de desordem são apresentados na Fig.7. Estes resultados mostram que a modulação vertical da densidade de
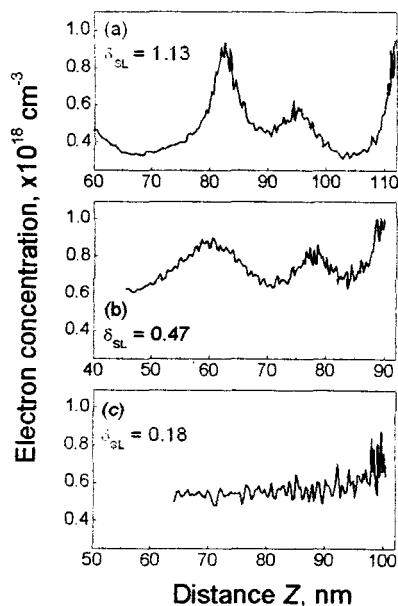

Fig.7. Densidades de elétrons medidas com temperatura T = 10 K em super-redes $(GaAs)_m(Al_{0.3}Ga_{0.7}As)_6$ com diferentes forças de desordem δ_{SL} [19].

13

elétrons aumenta com o acréscimo da força de desordem que manifesta diretamente a localização espacial.

Em semicondutores dopados degenerados a posição do pico de fotoluminescência é associado à energia de Fermi. Na presença de desordem, a energia de Fermi diminui por causa da redistribuição de elétrons sobre o potencial aleatório [20]. Isso resulta em deslocamento "red shift" da linha de fotoluminescência. De acordo cm a teoria [20], o decréscimo da energia de Fermi é aproximadamente igual à amplitude de flutuações de potencial aleatório, que no caso de super-redes desordenadas é dado pela largura da distribuição de níveis eletrônicos $\Delta = W \cdot \delta_{SL}$.
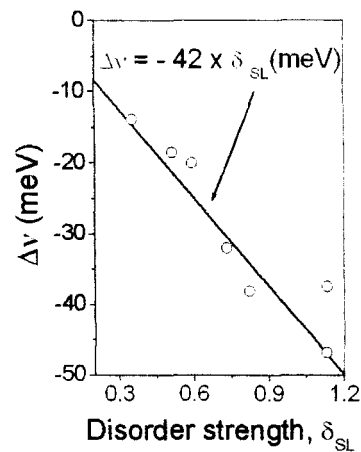

Fig.8. Deslocamentos "red shift" das linhas de fotoluminescência medidos com temperatura T = 4.2 K em super-redes desordenadas $(GaAs)_m(Al_{0.3}Ga_{0.7}As)_6$ com diferentes forças de desordem δ_{SL}. [21].

Os resultados apresentados na Fig.8 mostram a correspondência boa entre os deslocamentos de fotoluminescência medidos em super-redes com varias forcas de desordem e o deslocamento calculado com a largura da minibanda W = 42 meV (enquanto, a largura da minibanda esperada é 55 meV).

Estes dados demonstram que a força de desordem produzida em super-redes pela variação de espessuras de poços quânticos pode ser bem-controlada e pode ser caracterizada pelo único parâmetro δ_{SL}.

Os resultados de medidas de mobilidades Hall paralelas em super-redes desordenadas e em super-redes periódicas com diferentes espessuras de camadas GaAs (poços quânticos) são apresentados na Fig.9.
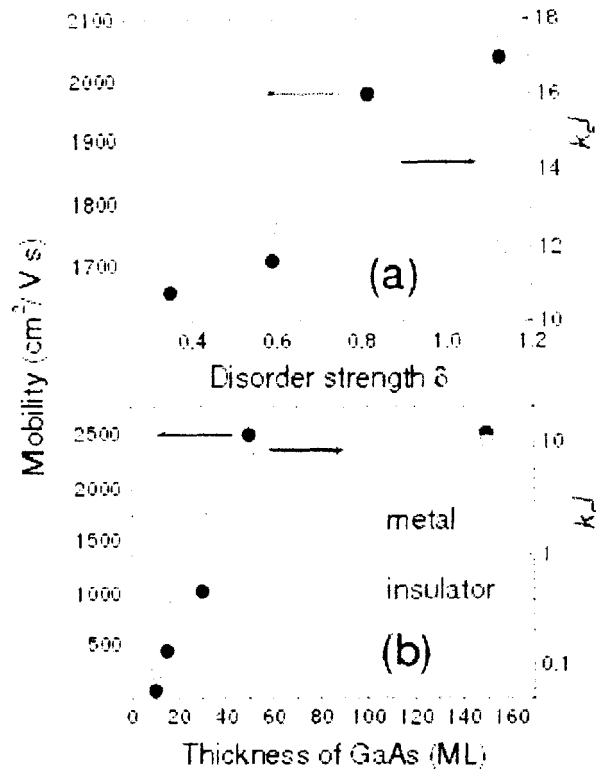
14

Fig.9. Mobilidades Hall paralelas (círculos fechados) e valores de $k_F l$ (círculos abertos) obtidos com T = 1.6 K em super-redes $(GaAs)_m(Al_{0.3}Ga_{0.7}As)_6$ desordenadas com variação aleatória de espessuras de camadas de GaAs (a) e em super-redes periódicas $(GaAs)_m(Al_{0.3}Ga_{0.7}As)_6$ com diferentes espessuras de GaAs (b) [22].

A concentração de dopagem nominal foi $1.2x10^{18}$ cm^{-3} em super-redes desordenadas e $7.0x10^{17}$ cm^{-3} em super-redes periódicas. Em ambos os casos a mobilidade diminuiu com aumento da força de desordem. De acordo com os valores do parâmetro $k_F l$ a variação de espessuras de camadas de GaAs nas super-redes periódicas causou a transição metal-isolante: as super-redes com espessuras de GaAs maior do que 30 monocamadas apresentaram comportamento metálico, enquanto os parâmetros $k_F l$ <1 obtidos nas super-redes com espessuras de poços menores do que 30 monocamadas demonstraram formação de estados localizados.

Assim, demonstramos que o arranjo de estrutura de super-redes semicondutoras fornece controle da força de desordem.

III. Transporte quântico em super-redes GaAs/AlGaAs desordenadas

III.1. Regimes de transporte quântico em super-redes desordenadas

As correções quânticas para a condutividade causam a magneto-resistência negativa em semicondutores desordenados [23,24]. Em tais materiais o transporte é acompanhado pela interferência quântica entre as funções de onda eletrônicas – o processo conhecido como a localização fraca de elétrons. As correções associadas à localização fraca determinam a magneto-resistência em campos magnéticos fracos $\omega_c \tau \ll 1$, (onde ω_c é a freqüência ciclotrônica e τ é o tempo elástico) quando a interação entre os elétrons pode ser desprezada [25]. A desordem tem um papel considerável na localização fraca providenciando dois processos de espalhamento coerentes que contribuem para a interferência quântica. A localização fraca também é considerada como um "precursor" da localização forte [26]. Na presença de localização forte (como em super-redes artificialmente desordenadas) as correções quânticas fazem a contribuição ainda mais relevante [27].

As correções de localização fraca para a condutividade de super-redes com acoplamento vertical fraca foram recentemente consideradas em Ref.[28]. Enquanto a teoria da interferência quântica em super-redes no caso da localização forte foi desenvolvida em Ref.[29].

Assim, em super-redes desordenadas distinguimos três regimes de transporte quântico:

i) regime de superfície de Fermi propagativa (regime de localização fraca com $k_F l \gg 1$) quando $t_z \tau > \hbar$, onde t_z e τ são a energia de acoplamento vertical e o tempo de espalhamento elástico, respectivamente;

ii) regime de superfície de Fermi difusiva (regime de localização fraca com $k_F l \gg 1$) quando $t_z \tau < \hbar$; neste caso um elétron sofre muitos espalhamentos até sair camada;

iii) regime de localização forte quando $k_F l < 1$.

As fórmulas que determinam as correções da localização fraca em diferentes regimes de transporte são as seguintes [28]:

$$\Delta\sigma_{PFS}^{x} = \frac{e^2}{2\pi^2 \hbar L_B}\alpha F(\delta), \Delta\sigma_{PFS}^{z} = \frac{\Delta\sigma_{PFS}^{x}}{\alpha^2} \tag{13}$$

$$\Delta\sigma^x_{DFS} = -\frac{e^2}{2\pi^2\hbar D_{SL}}\alpha F(\delta,\delta'), \Delta\sigma^z_{DFS} = \frac{\Delta\sigma^x_{DFS}}{\alpha^2} \tag{14}$$

Onde indexes x e z denotam os componentes perpendiculares e paralelas à direção de crescimento respectivamente, $L_B = \sqrt{\hbar/eB}$ é o comprimento magnético, $\alpha = \sqrt{D_x/D_z}$ é o coeficiente da anisotropia (D_x e D_z são os coeficientes de difusão paralelo e normal respectivamente), D_{SL} é o período da super-rede e as funções $F(\delta)$ e $F(\delta,\delta')$ com $\delta = \dfrac{L_B^2}{4D_z\tau_\varphi}$, $\delta' = \dfrac{L_B^2}{4D_x}(\dfrac{1}{\tau_\varphi}+2\dfrac{l_z^2\tau}{\hbar^2})$ (aqui τ_φ é o tempo de defasagem da função de onda eletrônica) foram determinadas em [28].

A diferença essencial entre as equações (1) e (2) é em prefatores em frente das funções $F(\delta)$ e $F(\delta,\delta')$. Em regime PFS o prefator é determinado pelo comprimento magnético enquanto em regime DFS – pelo período da super-rede. Esta diferença produz comportamentos de magnetoresistência muito diferente nos dois regimes, como é demonstrado na Fig.10.

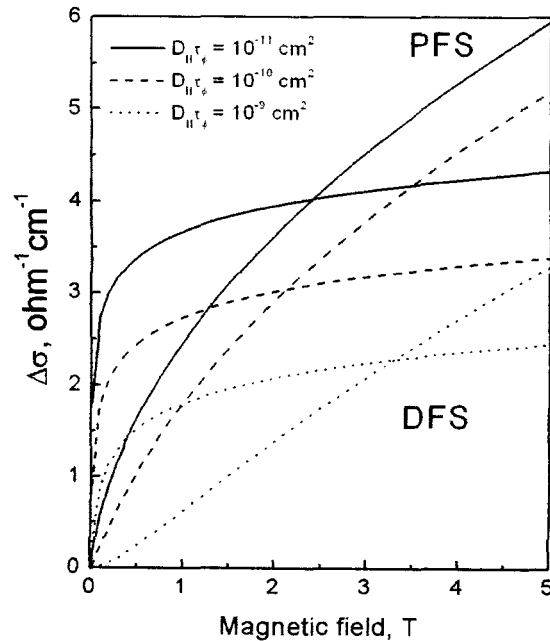

Fig.10. Correções quânticos para a condutividade clássica calculadas em dois regimes de transporte (PFS e DFS) em acordo com as equações (13) e (14) .

No caso de localização forte a correção quântica é dada por [29]:

$$\Delta\sigma^x_{loc} = \frac{e^2\delta^{-3/2}(\cos^2\varphi + \alpha^2\sin^2\varphi)}{192\pi^2\hbar\alpha l_H} \tag{15}$$

onde φ é o ângulo entre a direção da corrente e o campo magnético.

Estudamos magneto-resistências em todos os regimes e obtemos resultados em boa concordância com as predições teóricas [30,31]. Foi mostrado que a forte desordem vertical (regime DFS) modifica tanto o transporte vertical quanto o transporte paralelo resultando em diferentes dependências das condutividades (vertical e paralela) do campo magnético em relação às dependências que correspondem ao regime PFS (sem desordem).

III.2. Interferência quântica na presença de transição metal-isolante

Em super-redes com poços quânticos extremamente curtos (menores do que 10-15 monocamadas) a esperada mobilidade é tão baixa que $k_F l < 1$. Neste caso os elétrons estão localizados e ao contrario das formulas no limite da localização fraca (13,14) a teoria prediz a magneto-resistência parabólica (15). Resultados de cálculos de magneto-resistência em regimes metálico e isolante são apresentados na Fig.11.
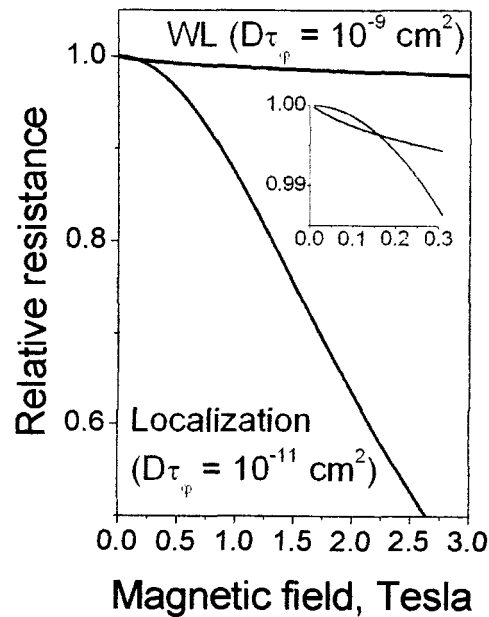

Fig.11. Dependências de resistências do campo magnético calculadas em regime metálico ("WL") e em regime isolante ("Localization").

Uma fraca dependência da resistência do campo magnético foi obtida no regime metálico (13,14), enquanto a magneto-resistência forte corresponde ao regime isolante (15). Esta diferença pode ser usada para distinguir os estados metálico e isolante. Assim, de acordo com a teoria, a correspondente modificação da interferência quântica deve manifestar a transição metal-isolante, tal como a dependência de resistência da temperatura.

Realizamos a transição metal-isolante em super-redes com variação de período. A influência de rugosidade interfacial (flutuações de monocamadas etc.) nas propriedades eletrônicos de super-redes aumenta com o decréscimo do período. Como foi mostrado em cima, em super-redes com os períodos curtos a mobilidade dos elétrons baixa pode resultar em localização (e assim, em estado eletrônico isolante) quando $k_F l < 1$. No entanto, quando as larguras dos poços quânticos são muito maiores do que o alargamento de interfaces (em super-redes com períodos longos), o regime metálico ($k_F l \gg 1$) deve determinar o transporte. Assim, a variação das larguras dos poços quânticos resulta em transição metal-isolante. Fig. 12. apresenta as resistências como funções da temperatura, medidas em super-redes com diferentes larguras de poços GaAs (*m*). As super-redes com *m* =10,15 monocamadas revelam decrescemos exponenciais característicos do estado isolante, enquanto as super-redes metálicas (m ≥ 15 monocamadas) revelam as resistências praticamente independentes da temperatura. Os decrescemos fracos ($\approx 1\%$) ocorrem em todas as super-redes metálicas por causa de destruição da interferência quântica pela temperatura.
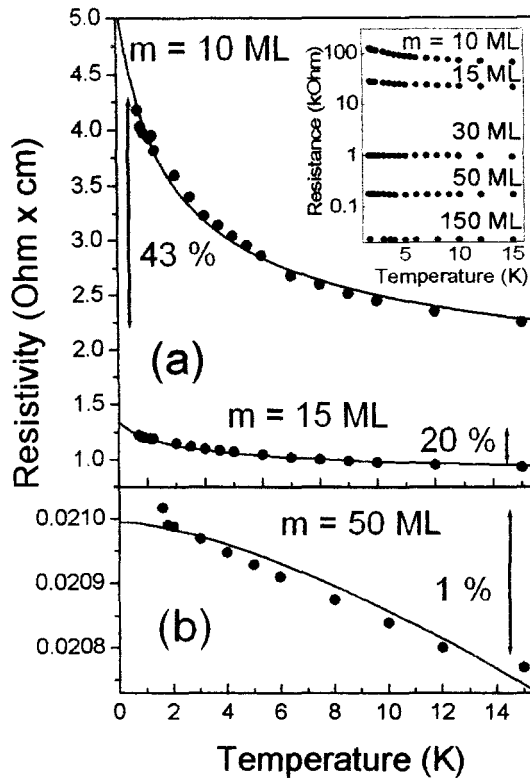
Fig.12. Dependências térmicas das resistências medidas nas super-redes $(GaAs)_m(Al_{0.3}Ga_{0.7}As)_6$ com diferentes espessuras de camadas de GaAs [32].

Investigamos a modificação da interferência quântica na presença da transição metal-isolante [32]. As magneto-resistências medidas nestas super-redes são apresentadas na Fig.13 onde as linhas vermelhas mostram resultados de cálculos usando as formulas (13) e (15). Achamos os resultados experimentais em boa concordância com predições teóricas. Isto comprova que a interferência quântica é drasticamente modificada quando se passa a transição metal-isolante.
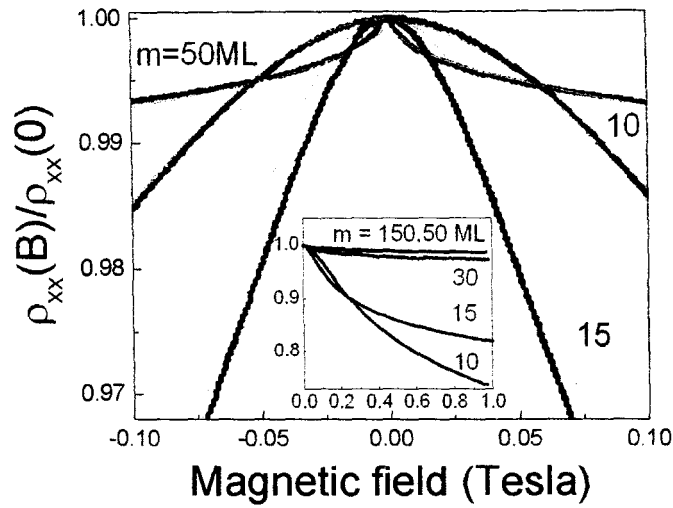
Fig.13. Magneto-resistências relativas medidas em super-redes metálicas e isolantes com temperatuta T = 1.6 K [32].

Os tempos de defasagem apresentados na Fig.14, obtidos por ajuste de magneto-resistências teóricas aos dados experimentais mostram dependências diferentes em super-redes metálicas e isolantes. Isto implica em diferentes mecanismos de defasagem: pela interação entre elétrons e fônons nas super-redes metálicas e por um mecanismo desconhecido nas super-redes isolantes.
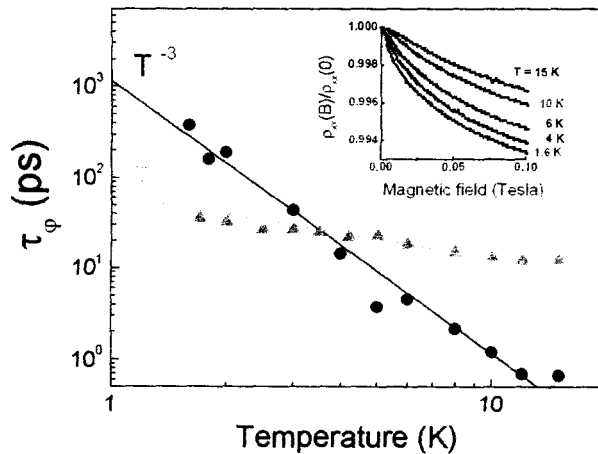
Fig.14. Dependências térmicas de tempos de defasagem obtidas nas super-redes metálicas (preta) e isolantes (vermelha). A inserção apresenta magneto-resistências medidas nas super-redes metálicas com diferentes temperaturas.

21

Fig. 15 apresenta o tempo de defasagem como função do parâmetro de desordem $k_F l$.
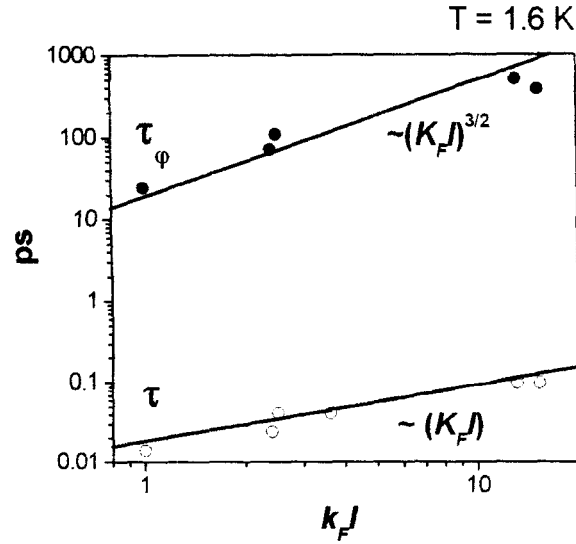
Fig. 15. Tempos de defasagem e tempos elásticos obtidos em super-redes com diferentes parâmetros da desordem $k_F l$.

O acrescentamento observado de tempo de defasagem com aumento do $k_F l$ ocorre por causa de interação entre os elétrons num sistema desordenado [33]:

$$\tau_{ee} = 4\hbar \sqrt{\frac{E_F}{3}} \left(\frac{k_F l}{k_B T}\right)^{3/2} \tag{16}$$

Portanto, mostramos que a transição metal-isolante manifesta-se em correspondente modificação da interferência quântica. No estado isolante observamos um novo mecanismo de defasagem da função da onda dos elétrons.

Finalmente, Fig. 16 apresenta magneto-resistências medidas em super-redes GaAs/AlGaAs em todos os regimes de transporte quântico.

22
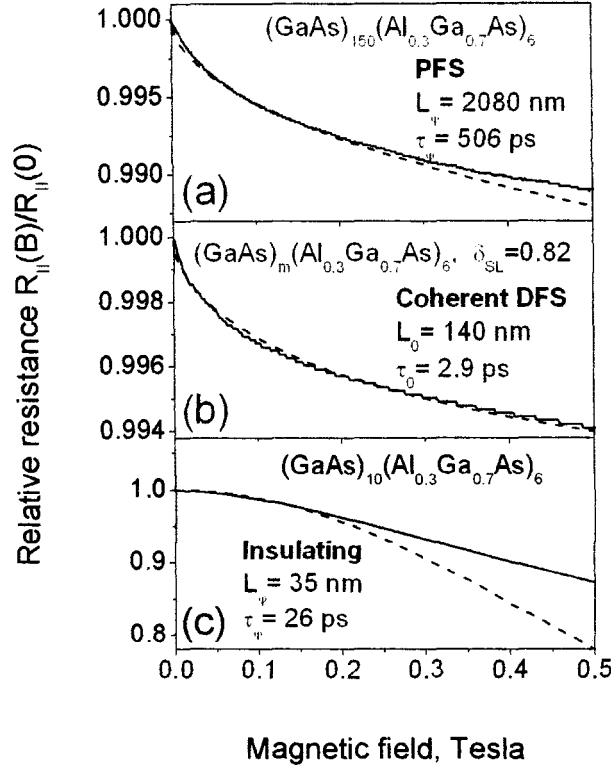
Fig. 16. Magneto-resistências medidas em super-redes GaAs/AlGaAs com T = 1.6 K em diferentes regimes de transporte quântico.

III.3. Efeitos de anisotropia

O estudo de processos de transporte em direções paralela e perpendicular à direção de crescimento de super-rede é importante, por causa da natureza anisotrópica de espectro energético dos elétrons em super-redes. A comparação entre os resultados obtidos nas ambas direções pode mostrar como esta anisotropia corresponde à estrutura nominal da super-rede investigada e assim, mostrar a validade das conclusões teóricas.

Em Ref. [28] foi mostrado que quando $h/\tau > t_z$ a desordem forte anisotrópica (sobre a direção de crescimento z) muda os características do sistema eletrônico de comportamento simples tridimensional para uma mistura de comportamento bi- e tridimensional. Isto produz efeitos anisotrópicos em processos de defasagem da função de onda eletrônica.

Medimos magneto-resistências em super-redes desordenadas na direção de crescimento (z) e na direção paralela às camadas (x) com diferentes orientações de campo magnético. As magneto-resistências verticais foram medidas em estruturas tipo mesas com

23

o diâmetro 1 mm. Os resultados apresentados nas Figs.17-19 demonstram forte efeito da desordem vertical que causa a variação de comprimento de coerência em uma ordem de grandeza. Neste caso (corrente vertical), mesmo na presença de desordem forte, somente as trajetórias tridimensionais contribuem para a condutividade e não tem a contribuição de trajetórias bidimensionais, como no caso da condutividade paralela (corrente paralela às camadas). Por isso, para fazer ajuste podemos usar a formula (13).

Fig.17. Magneto-resistências verticais, medidas em estruturas tipo mesa formadas de super-redes $(GaAs)_m(Al_{0.3}Ga_{0.7}As)_6$ desordenadas com diferentes forças de desordem com T = 1.6 K [31].
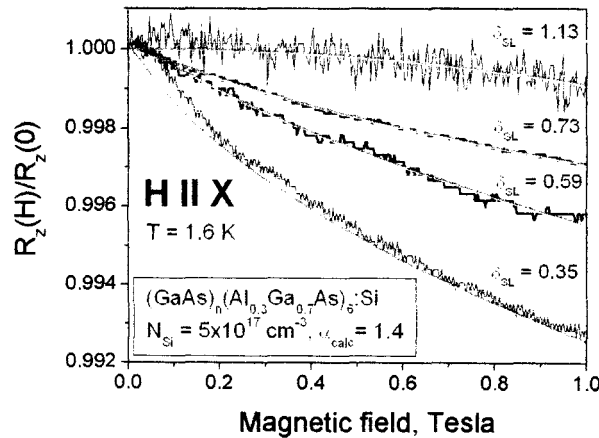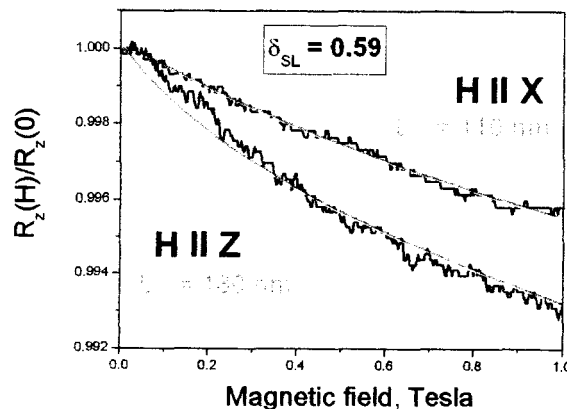

Fig.18. Magneto-resistências verticais, medidas em estruturas tipo mesa formadas de super-rede $(GaAs)_m(Al_{0.3}Ga_{0.7}As)_6$ desordenadas com a forças de desordem δ_{SL} = 0.59 com diferentes orientações de campo magnético, com T = 1.6 K [31].
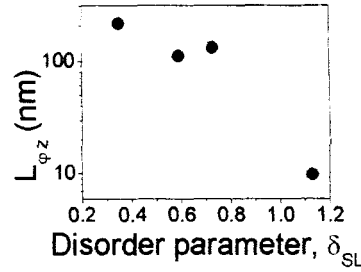
Fig.19. Comprimentos de coerência na direção de crescimento obtidos em super-redes $(GaAs)_m(Al_{0.3}Ga_{0.7}As)_6$ desordenadas diferentes forças de desordem, com T = 1.6 K.

As magneto-resistências paralelas (medidas com a corrente paralela às camadas), obtidas com varias orientações de campo magnético em super-redes metálicas e isolantes são apresentadas na Fig.20. Os resultados mostram efeito da anisotropia muito mais forte na super-rede isolante do que na super-rede metálica. Com diferentes orientações de campo magnético obtemos seguintes tempos de defasagem: na super-rede isolante $\tau_\varphi^\perp = 1.5ps$, $\tau_\varphi^{//} = 38ps$ e na super-rede metálica $\tau_\varphi^\perp = 60ps$, $\tau_\varphi^{//} = 80ps$.
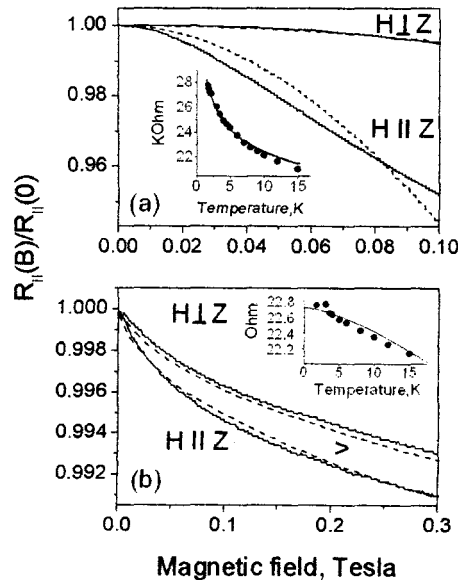
Fig.20. Magneto-resistências paralelas medidas em super-rede $(GaAs)_m(Al_{0.3}Ga_{0.7}As)_6$ isolante com m = 15 monocamadas (a) e em super-rede metálica com m = 150 monocamadas (b) com diferentes orientações de campo magnético, com T = 1.6 K. As inserções mostram dependências das resistências correspondentes da temperatura [31].

Assim, mostramos que a desordem anisotrópica resulta em anisotropia de tempo de defasagem. Achamos este efeito mais forte nas super-redes isolantes do que nas super-redes metálicas.

III.4. Transição coerência-incoerência induzida por desordem

Sistemas eletrônicos multicamadas revelam vários efeitos interessantes ligados à anisotropia deles, quando as condutividades perpendicular e paralela às camadas são significativamente diferentes. A relação entre as condutividades intracamadas e intercamadas é essencialmente ligada à dimensionalidade do sistema: a condutividade intercamadas desaparecida resulta em bidimensionalização de propriedades eletrônicas. A anisotropia de sistemas multicamadas naturalmente coloca duas escalas temporais: o tempo de defasagem τ_φ e o tempo que um elétron precisa para trocar o plano τ_0. Quando $\tau_\varphi \ll \tau_0$ um elétron sofre muitos espalhamentos antes de sair do plano; neste caso o sistema eletrônico multicamadas comporta-se como uma meda de planos bidimensionais incoerentes. No limite oposto, quando $\tau_\varphi \gg \tau_0$ um elétron troca a camada sem a perda significativa de fase e portanto, as camadas são coerentemente acopladas. Assim, a relação entre estes dois tempos característicos estabelece a transição entre regime coerente e incoerente em sistemas eletrônicos multicamadas.

Em super-redes intencionalmente desordenadas a desordem artificial produzida na direção de crescimento (z) controla o acoplamento entre as camadas. Deste modo a transição coerência-incoerência pode ser conseguida com a variação da forca de desordem. Anteriormente, na Fig.19 já mostramos que a desordem vertical afeta fortemente coerência de elétrons propagados perpendicularmente às camadas. Em seguida mostraremos que a desordem vertical influencia igualmente a coerência de elétrons propagados paralelamente às camadas.

Ainda mais, o acoplamento entre as camadas depende fortemente do caráter da superfície de Fermi. Quando a energia de Fermi é localizada dentro da minibanda ($E_F < W$) a superfície de Fermi é fechada. Neste caso elétrons apresentam propriedades de um sistema tridimensional anisotrópico. Enquanto a superfície de Fermi é aberta (tem a forma do cilindro ondulatório) quando a energia de Fermi é situada no minigap ($E_F > W$).
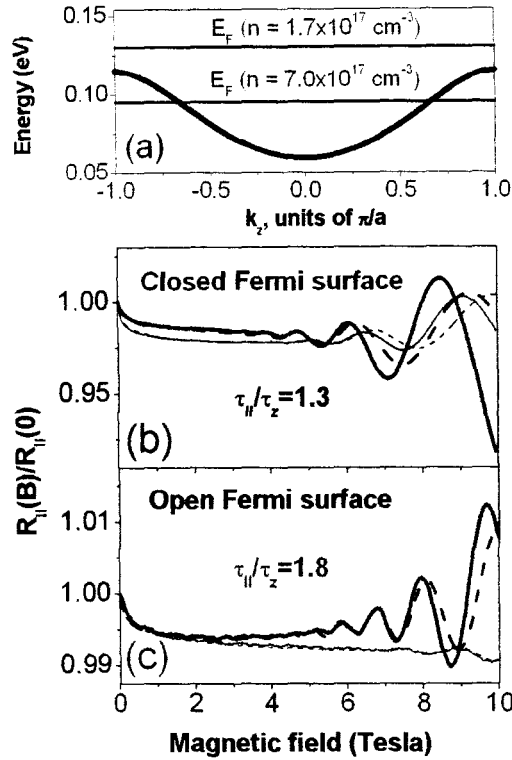
Fig.21. Magneto-resistências medidas com diferentes orientações de campo magnético com T = 1.6 T nas super-redes $(GaAs)_{17}(Al_{0.3}Ga_{0.7}As)_6$ com a dopagem baixa (a) e alta (b). As linhas estreitas e largas correspondem aos campos magnéticos paralelo e perpendicular às camadas respectivamente. O painel em cima mostra posições de níveis de Fermi em super-redes correspondentes.

Em forte campo magnético perpendicular das camadas a aberta superfície de Fermi resulta em sistema eletrônico bidimensional. Esta bidimensionalização de elétrons em super-redes induzida pelo campo magnético foi observada em Ref.[34].

Os resultados de medidas de oscilações de Shubnikova – de Haas em super-redes com superfícies de Fermi fechadas e abertas, apresentados na Fig.21, mostram esta bidimensionalização.

A influência de desordem sobre propriedades dinâmicas de elétrons depende da relação entre a energia de desordem e a energia de Fermi. Para aumentar o efeito de desordem nos diminuímos a dopagem. Com isto o efeito da desordem vertical sobre o tempo da defasagem aumentou (reduzindo τ_φ), enquanto a taxa de tunelamento diminuiu causando correspondente aumento do tempo τ_0. De tal modo os regimes coerente e incoerente foram realizados em super-redes com a dopagem alta e baixa respectivamente.

Em super-redes esta transição é esperada no regime de transporte difusivo (DFS) quando $\hbar/\tau > t_z$. Neste regime um dos dois parâmetros que determinam a dependência de correção quântica em campo magnético é [28]:

$$\delta' = \frac{L_B^2}{4D_x}(\frac{1}{\tau_\varphi} + \frac{2}{\tau_0})$$

(17)

27

$$\text{com} \quad \tau_0 = \frac{\hbar^2}{l_z^2 \tau} \tag{18}$$

Assim, no regime de transporte difusivo a correção quântica da super-rede é determinada pelos dois tempos τ_φ e τ_0. No regime incoerente, quando $\tau_\varphi \ll \tau_0$ a contribuição do tempo de difusão intercamadas e insignificante; entretanto, a correção quântica é principalmente determinada por este tempo no regime coerente, quando $\tau_\varphi \gg \tau_0$.

Fig.22 apresenta as magneto-resistências medidas nas super-redes periódicas com várias espessuras de barreiras em regime coerente e nas super-redes intencionalmente desordenadas nos regimes coerente e incoerente.
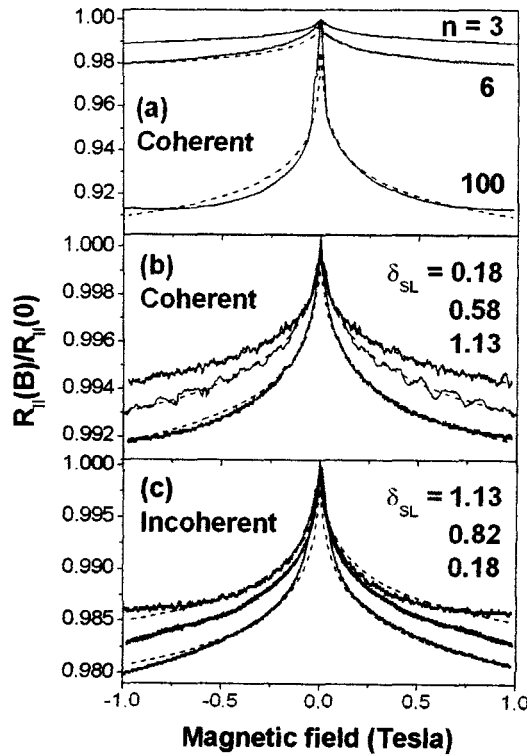

Fig.22. Magneto-resistências medidas com T = 1.6 K: (a) nas super-redes periódicas $(GaAs)_{50}(Al_{0.3}Ga_{0.7}As)_n$ com diferentes espessuras de barreiras no regime de transporte coerente, (b) nas super-redes desordenadas $(GaAs)_m(Al_{0.3}Ga_{0.7}As)_6$ altamente dopadas no regime coerente e (c) nas super-redes desordenadas com dopagem baixa no regime incoerente.

No regime de transporte coerente os medidos de magneto-resistência permitem obter o tempo τ_0, e através da formula (18) o tempo de tunelamento t_z, enquanto o tempo de defasagem pode ser determinado no regime incoerente. Os resultados são apresentados na Fig.23. Eles mostram que ambos, o tempo de tunelamento e o tempo de defasagem diminuem com aumento da força de desordem. O decréscimo de tempo de tunelamento vertical observado em super-redes desordenadas com aumento da desordem vertical ocorre por causa de decréscimo de acoplamento entre as camadas. O mesmo efeito foi observado nas super-redes periódicas com aumento de espessuras de barreiras. Enquanto o decréscimo de tempo de defasagem relaciona ao problema de coerência de quase-partículas em fortemente correlacionados sistemas metálicos multicamadas. Nossos resultados mostram que o tunelamento entre as camadas controla a coerência de quase-partículas que se movem paralelo às camadas. De acordo com a teoria [12], em sistemas eletrônicos multicamadas com acoplamento fraco as quase-partículas existem dentro das camadas quando o momento vertical deles conserva-se durante o tunelamento entre as camadas. A desordem vertical viola a conservação de momentum vertical. Como conseqüência, o tempo de defasagem diminui e as quase-partículas desaparecem.
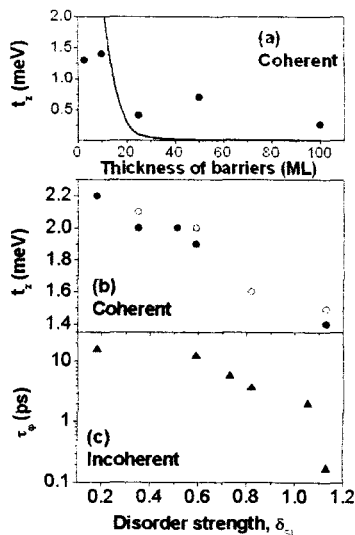
Fig.23. Energias de acoplamento vertical t_z obtidas: (a) nas super-redes periódicas $(GaAs)_{50}(Al_{0.3}Ga_{0.7}As)_n$ com diferentes espessuras de barreiras no regime de transporte coerente e (b) nas super-redes desordenadas $(GaAs)_m(Al_{0.3}Ga_{0.7}As)_6$ altamente dopadas no regime coerente e tempos de defasagem obtidos nas super-redes desordenadas $(GaAs)_m(Al_{0.3}Ga_{0.7}As)_6$ com dopagem baixa no regime incoerente (c).

IV. Excitações coletivas em sistemas eletrônicos desordenados

IV.1. Prova de Raman de função da onda de excitações coletivas na presença da desordem. Efeito da dispersão de plasmons sobre a forma da linha de Raman

Em super-redes a intensidade de espalhamento Raman por excitações coletivas eletrônicas (plasmons) é proporcional à densidade local de estados em espaço recíproco [35]:

$$I(\omega, q_{/\!/}, q_z) \cong \sum_{v} |\Psi_v(q_z)|^2 \delta(\omega - \omega_{pv})^2 \qquad (19)$$

with $\Psi_v(q_z) = \sum_{n} e^{iq_z z_n} \Psi_v(n)$,

onde ω é a freqüência de luz, $q_{/\!/}$ e q_z são os vetores de onda paralelo e perpendicular as camadas da super-rede respectivamente, ω_{pv} e $\psi_v(n)$ são auto-valores e auto-vetores de plasmons, z_n é a posição da n-a camada. Portanto, espalhamento Raman diretamente prova a função de onda de plasmons $\psi_v(q_z)$.

Assim, na presença da desordem plasmons podem ser apresentadas como uma superposição de ondas planas com os vetores de onda distribuidos num intervalo finito Δq, o que produz uma extensão espacial finita das ondas (comprimento de localização $L_c \sim 1/\Delta q$). Isto implica que ao contrario de um cristal perfeito, onde excitações coletivas com numero de onda q_0 contribuem ao espalhamento Raman, como é apresentado na Fig.24, em sistema desordenado todos os modos no intervalo de incerteza de numero de onda $\Delta q \approx 2\pi/L_p$ determinam a intensidade de Raman.

Como conseqüência, as linhas Raman adquirem uma assimetria específica, que pode ser vista claramente em espectros de semicondutores desordenados [36].
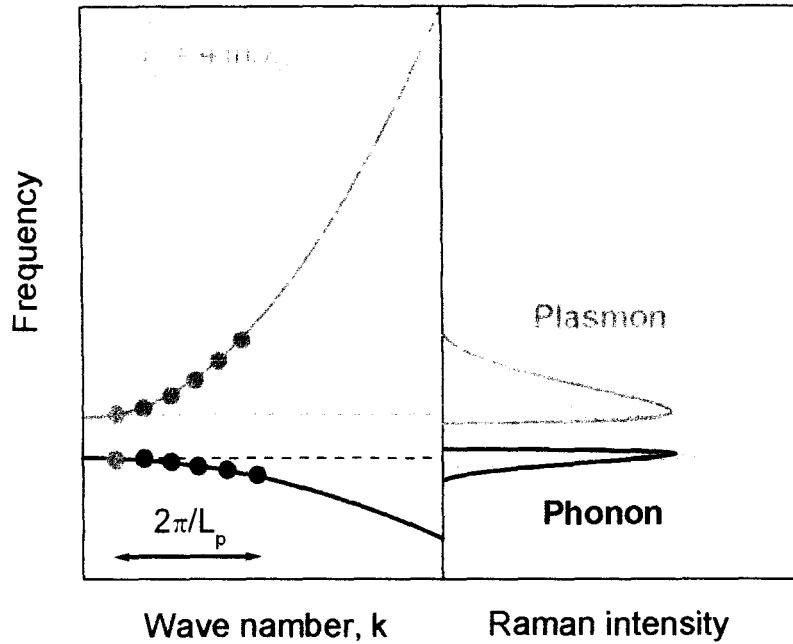
Fig.24. Painel esquerdo – as dispersões de excitações coletivas (tipo fônons e plasmon-fônons acoplados); painel direto – as intensidades de espalhamento Raman na presença da desordem.

Para obter os parâmetros característicos das excitações coletivas, a intensidade Raman pode ser calculada de acordo com a fórmula [36]:

$$I(\omega) \propto \int \exp\left[-\frac{(q-q_0)^2 L_p^2}{4}\right] \frac{d^3 q}{[\omega - \omega_p(q)]^2 + (\Gamma/2)^2} \tag{20}$$

onde q_0 é o numero de onda de luz usado pela excitação, $\omega_p(q)$ é a dispersão de excitações que contribuem para o espalhamento Raman, L_p e Γ são o comprimento de localização e a constante de amortecimento.

31

IV.2. Localização de excitações coletivas em ligas AlGaAs

Nesta parte estudamos e comparamos comprimentos de localização de excitações uni-eletrônicos e de excitações coletivas. Assim, podemos distinguir a contribuição de interação entre os elétrons que fundamentalmente determina a natureza de excitações coletivas e não influência a localização de elétrons em campos magnéticos fracos.

A influencia da desordem sobre propriedades dinâmicos de elétrons depende da relação entre a energia de desordem (Δ) e a energia de Fermi (E_F). Utilizamos dois tipos de sistemas desordenados: ligas semicondutoras AlGaAs, onde a desordem é produzida pelo potencial aleatório de liga e super-redes GaAs/AlGaAs artificialmente desordenadas.

O efeito de localização de elétrons que aparece quando $\Delta > E_F$ é apresentado em ligas AlGaAs nas Figs.25,26. Em ambas, a dependência de resistência da temperatura e a magnetoresistencia manifestam a formação de estados localizados em ligas com a dopagem baixa. Como é demonstrado na Fig.27, a transição metal-isolante também manifesta-se em variação de comprimento de localização de excitações coletivas (L_p). Em ligas isolantes (com a dopagem baixa) o comprimento de localização medido por espalhamento Raman corresponde aos fônons ópticos. Enquanto o abrupto aumento de comprimento de localização L_p foi observado quando se passa a transição de estado isolante para estado metálico. O decréscimo de comprimento de localização com aumento de dopagem, observado em ligas metálicas é causado por espalhamento por impurezas ionizadas [37].
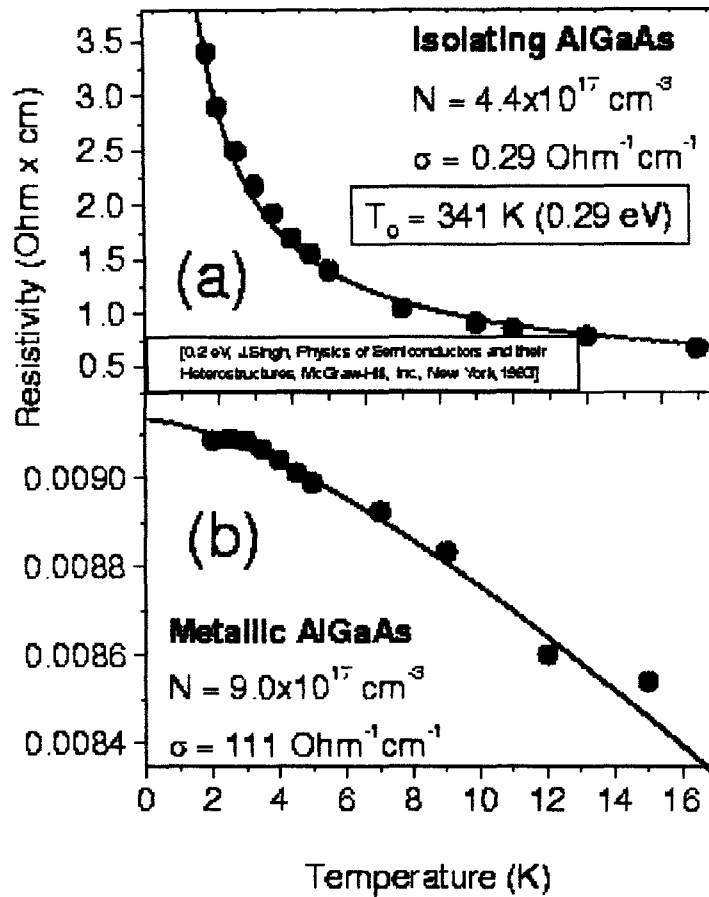
Fig.25. Dependências de resistividade da temperatura medidas em ligas $Al_{0.11}Ga_{0.89}As$ isolante (a) e metálica (b). As linhas apresentam resistividade tipo "hopping" e resistividade causada pelos efeitos de interferência quântica em ligas isolantes e metálicas respectivamente.
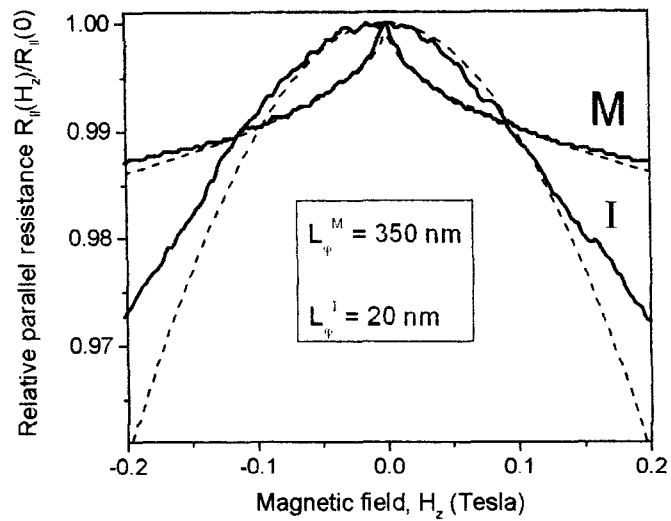
Fig.26. Magnetoresistênsias relativas medidas com T = 1.6 K em ligas $Al_{0.11}Ga_{0.89}As$ metálica (M) e isolante (I).
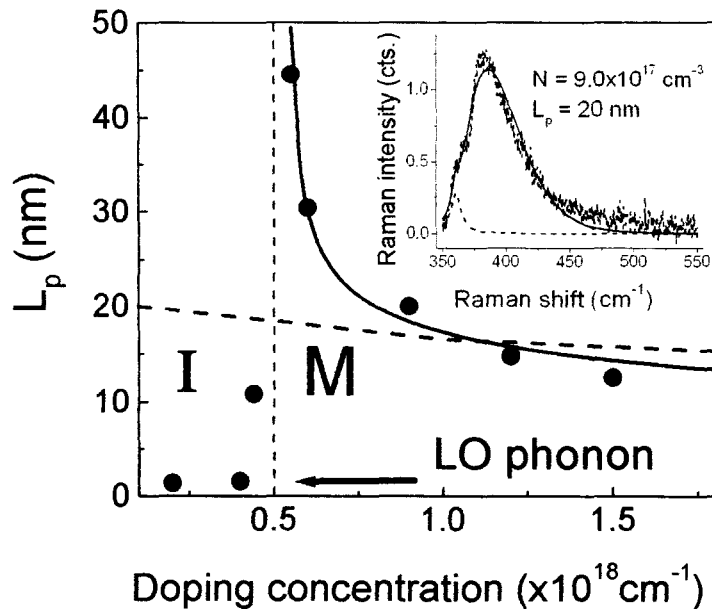
Fig.27. Comprimentos de localização de excitações coletivas medidos em ligas $Al_{0.11}Ga_{0.89}As$ isolantes (I) e metálicas (M) por espalhamento Raman com $T = 10$ K. As linhas cheia e pontilhada mostram as calculadas dependências causadas por espalhamento por impurezas ionizadas [36] e por amortecimento de Landau, respectivamente.

34

Entretanto, de acordo com a Ref.[38], em sistemas fortemente desordenados tridimensionais a localização de excitações coletivas é limitada por efeito de amortecimento de Landau. Os calculados comprimentos de localização de excitações coletivas limitadas por amortecimento de Landau estão apresentados em Fig.27 pela linha pontilhada. No caso de dopagens baixas ($N<1x10^{18}$ cm^{-3}) a localização de excitações coletivas em ligas está determinada pela desordem. Neste caso observamos que em ligas metálicas os comprimentos de localização de elétrons (350 nm) são muito maiores do que os comprimentos de localização de excitações coletivas (20 nm). Entretanto, com aumento da dopagem o amortecimento de Landau começa dominar a localização de excitações coletivas. Isto significa que em tais ligas altamente dopadas não podemos distinguir o efeito de interação sobre a localização de excitações elementares porque enquanto a localização de elétrons é determinada por desordem, a localização de plasmons é determinada por outra razão - amortecimento de Landau.

O efeito de amortecimento de Landau pode ser evitado em super-redes onde a energia de excitações coletivas cai na região de "minigap". Neste caso a interação estabelece a diferença entre localizações de elétrons e excitações coletivas.

V. Comparação entre localização de excitações uni-partículas e coletivas em super-redes GaAs/AlGaAs

V.1. Problema de interação em sistema eletrônico desordenado

Um problema fundamental ainda não resolvido é ligado à descrição de transição metal-isolante incorporando tanto a desordem quanto a interação entre os elétrons. De acordo com P.W.Anderson [1] a presença da desordem causa a localização espacial da função de onda de um elétron. É bem estabelecido que os elétrons não-interagentes em um sistema tridimensional conseguem a localização com uma desordem finita. Ao contrario, de

acordo com a teoria de "scaling"[2] todos os estados eletrônicos não-interagentes são localizados em sistemas bi- e unidimensionais, mesmo quando a desordem é infinitesimalmente fraca. Porém, acredita-se que a transição metal-isolante, que acontece num sistema eletrônico real, não pode ser explicada baseando-se em elétrons não-interagentes [39]. Os resultados recentes mostram a importância das correções causadas por interação em sistemas eletrônicos bidimensionais [40]. Até hoje existem opiniões controversas sobre como a interação influencia a localização [41].

V.2. Coerência de excitações elementares em super-redes GaAs/AlGaAs desordenadas

Comparamos comprimentos de localização de elétrons e de excitações coletivas em uma super-rede metálica intencionalmente desordenada. Desenhamos a super-rede assim que evitamos efeitos de amortecimento de Landau. A desordem artificial permitiu controlar extinções espaciais de funções de onda das excitações elementares propagadas perpendicularmente às camadas e permitiu também optar a estrutura de amostras onde os ambos, elétrons e plasmons, revelam propriedades de localização no mesmo tempo. O comprimento de localização de elétrons foi medido por magnetoresistencia numa estrutura do tipo mesa, formada de super-rede GaAs/AlGaAs desordenada (δ_{SL} =0.4). Enquanto o comprimento de localização de excitações coletivas foi determinado na mesma amostra pela assimetria de linha de Raman associada aos modos acoplados tipo LO fônon-plasmon. Fig.28(a) apresenta o espectro de Raman obtido na região de vibrações tipo AlAs. A linha marcada como L_3 corresponde às excitações coletivas acopladas tipo LO fônon-plasmon. De acordo com os cálculos de dispersões de excitações uni-eletrons e coletivas apresentadas na Fig.29, na ausência de amortecimento de Landau o comprimento de localização de excitações coletivas L_p = 5 nm é limitado pela desordem. O ajuste de magneto-resistência vertical resultou em comprimento de coerência de elétrons L_φ = 252 nm.
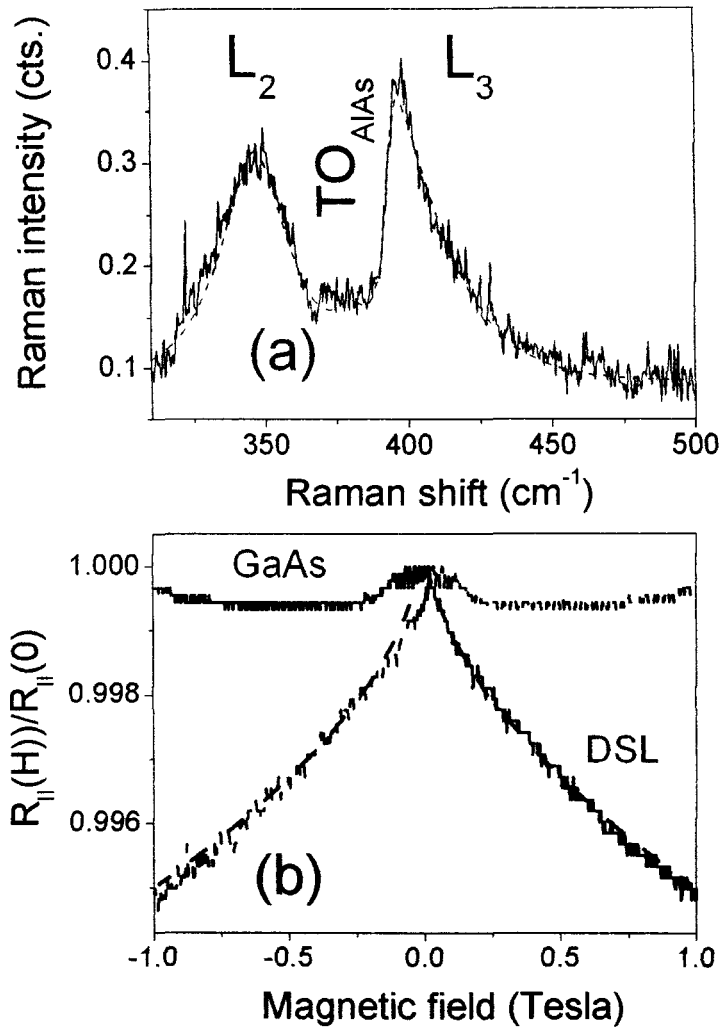
Fig.28. (a) Intensidade de espalhamento Raman medido com T = 10 K em super-rede $(GaAs)_m(Al_{0.3}Ga_{0.7}As)_6$ com a força de desordem δ_{SL} = 0.4. A linha interrompida apresenta a intensidade calculada de acordo com Eq.(19) com o comprimento de localização de excitações coletivas L_p = 5 nm. (b) Magneto-resistência vertical relativa medida na mesma super-rede com T = 10 K (DSL). A linha interrompida foi calculada de acordo com a teoria [28] com comprimento de coerência L_φ =252 nm. Os dados marcados como GaAs relacionam à estrutura tipo mesa fabricada no mesmo substrato dopado sem a super-rede.
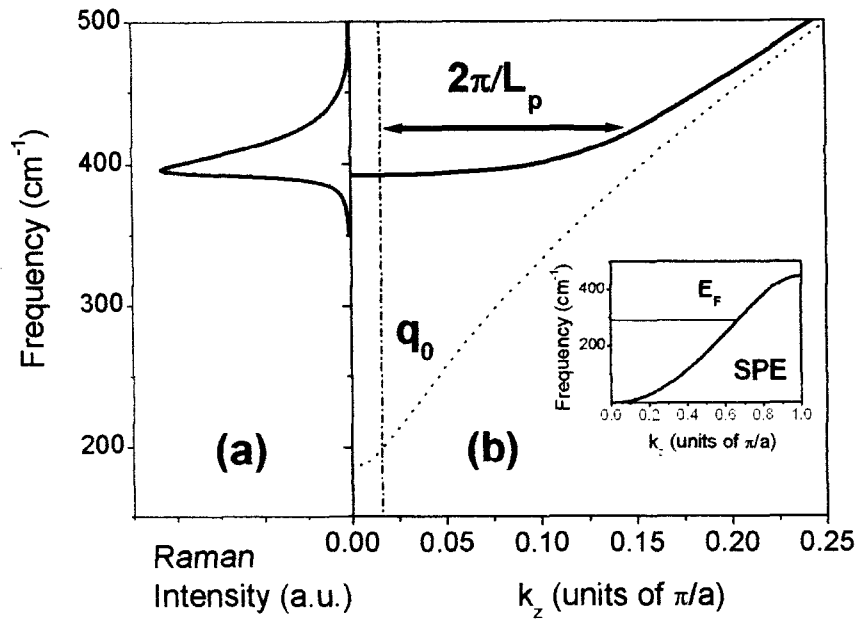
Fig.29. Espectros energéticos das excitações uni-elétrons (inserção) e coletivas (b) calculados em super-rede $(GaAs)_{17}(Al_{0.3}Ga_{0.7}As)_6$ com a concentração de elétrons n = $5.0x10^{17}$ cm^{-3}. As linhas pontilhadas e interrompidas mostram as dispersões dos plasmons não acoplados e dos plasmons acoplados aos fônons LO de AlAs. O painel (a) apresenta a intensidade calculada de espalhamento Raman obtida pelo ajuste de espectro experimental [Fig.28(a)].

Assim, achamos o comprimento de localização de excitações coletivas (5 nm) muito menor do que o comprimento de localização de elétrons individuais (252 nm). Isto confirma os dados obtidos em ligas AlGaAs com a dopagem modesta ($5x10^{17}$ cm^{-3} < N < $1x10^{18}$ cm^{-3}), onde o amortecimento de Landau ainda não foi observado. Estes resultados significam que a desordem afeta mais forte as excitações coletivas do que as excitações uni-partículas. Isto também indica que a interação que causa o movimento de elétrons correlacionado aumenta localização deles.

VI. Conclusões

Estudamos processos de transporte quântico em sistemas eletrônicos desordenados: ligas AlGaAs e super-redes GaAs/AlGaAs intencionalmente desordenadas crescidas por epitaxia de feixes moleculares. Demonstramos que em super-redes a desordem Gaussiana causada por variação aleatória de espessuras de camadas pode ser quantitativamente controlada e caracterizada pelo único parâmetro δ_{SL}. Nestes sistemas eletrônicos observamos os efeitos de anisotropia de transporte quântico causados por estrutura de super-redes e pela desordem anisotrópica. Descobrimos que a extinção espacial de excitações elementares pode ser controlada pela desordem artificial. Assim, conseguimos realizar regimes metálico e isolante com variação da desordem artificial e estudar os processos de interferência quântica durante a passagem da transição metal-isolante. Mostramos que esta transição manifesta-se em correspondente variação de magneto-resistência e em significante modificação de comprimento de localização de excitações coletivas. Ainda mais, descobrimos a transição coerente-incoerente e mostramos que de acordo com predições teóricas a desordem fabricada na direção de crescimento de super-redes desordenadas resulta em localização de elétrons propagados em ambas direções: perpendicular e paralelo às camadas. Comparamos os comprimentos de localização de excitações unipartículas e coletivas e concluímos que a interação entre os elétrons causa aumento de localização.

REFERÊNCIAS:

1. P.W.Anderson, *Phys.Rev.* **109**, 1492 (1958).

2. P.A.Lee, T.V.Ramakrishnan, *Rev.Mod.Phys.* **57**, 287 (1985).

3. V.V.Bryksin, P.Kleinert, Z.Phys. B **101**, 91 (1996).

4. Y.Maeno et al., *Nature* **372**, 532 (1994).

5. I. Terasaki et al., *Phys. Rev. B* **56**, R12685 (1997).

6. S.M.Loureiro et al.,*Phys. Rev. B* **63**, 094109 (2001).

7. N.W.Ashcroft e N.D.Mermin, *Solid State Physics,* Holt, Rinehart and Winstin, New York, 1976.

8. Y.Ando et al., *Phys.Rev.Lett.* **77**, 2065 (1996).

9. G.Mihali et al., *Phys.Rev.Lett.* **84**, 2670 (2000).

10. N.E.Hussey et al., *Phys. Rev.* B **57**, 5505 (1998).

11. T.Valla et al., *Nature* **417**, 627 (2002).

12. U.Lundin e R.H.McKenzie, *Phys.Rev.B* **68**, 801101(R), (2003).

13. A. Millis, *Nature* **417**, 599 (2002).

14. B.L.Altshuler, A.G.Aronov, D.E.Khmelnitsky, *J.Phys.C* **15**, 7367 (1982).

15. W.Kohn, *Phys.Rev.* **133**, A171 (1964).

16. L.Esaki e R.Tsu, *IBM J.Res.Dev.* **14**, 61 (1970).

17. N.F.Mott e E.A.Davis, *Electron Processes in Non-Crystalline Materials,* Clarendon Press, Oxford, 1979.

18. *Physics of Low-Dimensional Semiconductor Structures,* ed. By P.Butcher, N.H.March, M.P.Tosi, Plenum Press, New York, 1993.

19. Yu. A. Pusep, A. J. Chiquito, S. Mergulhão, A.I.Toropov, *J. Appl. Phys.* **92**, 3830 (2002).

20. B.I.Schklovskii, A.L.Efros, Electron *Properties of Doped Semiconductors,* Springer-Verlag (1984).

21. Yu.A.Pusep, F.E.G.Guimarães, M.B.Ribeiro, H.Arakaki, C.A. de Souza, P.A.Zanello, S.Malzer, G.H.Döhler, submetido ao *Phys.Rev.B*.

22. Yu.A.Pusep, M.B.Ribeiro, H.Arakaki, C.A. de Souza, P.A.Zanello, S.Malzer, G.H.Döhler, *J.Phys.Cond.Matter* **16**, 2447 (2004).

23. E.Abrahams, P.W.Anderson, D.C.Licciardello, and T.V.Ramakrishnan, *Phys.Rev.Lett.* **42**, 673 (1979)

24. B.L.Al'tshuler and A.G.Aronov, *Zh.Eksp.Teor.Fiz.* **77**, 2028 (1979) [*Sov.Phys.JETP* **50**, 968 (1979)]

25. B.L.Al'tshuler and A.G.Aronov, in *Electron-electron Interaction in Disordered Conductors*, ed. by A.L.Efros and M.Pollak (North Holland, Amsterdam, 1985)

26. P.A.Lee, T.V.Ramakrishnan, *Rev.Mod.Phys.* **57**, 287 (1985).

27. O.Farah and Z.Ovadyahu, *Phys.Rev.B* **38**, 5457 (1988).

28. A.Cassam-Chenai, D.Mailly, *Phys.Rev.B* **52**, 1984 (1995).

29. P.Kleinert, V.V.Bryksin, *Phys.Rev.B* **55**, 1469 (1997).

30. A.J.Chiquito, Yu.A.Pusep, G.M.Gusev, A.I.Toropov, *Phys.Rev.B* **66**, 035323 (2002).

31. Yu.A.Pusep, M.B.Ribeiro, H.Arakaki, C.A. de Souza, P.A.Zanello, S.Malzer, G.H.Döhler, *J.Phys.Cond.Matter* **16**, 2447 (2004).

32. Yu.A.Pusep, H.Arakaki, C.A. de Souza, Phys.Rev.B **68**, 205321 (2003).

33. B.L.Altshuler, A.G.Aronov, JETP Lett. **30**, 482 (1979)

34. Yu.A.Pusep, G.M.Gusev, A.J.Chiquito, A.K.Bakarov, A.I.Toropov, and J.C.Leite, *Phys.Rev. B* **63**, 165307 (2001).

35. P.Hawrylak, J.J.Quinn, *Phys.Rev.Lett.* **57**, 380 (1986).

36. Yu. A. Pusep, M. T. O. Silva, J. C. Galzerani, N. N. Moshegov, P. Basmaji - *Phys. Rev. B* **58** (16), 10683 (1998).

37. Yu. A. Pusep, S. S. Sokolov, J. C. Galzerani, *J. Phys.: Cond. Matter.* **13**, 10165-10174 (2001).

38. A.Pinzuck, G.Abstreiter, R.Trommer, M.Cardona, *Sol.St.Comm.*, **21**, 959 (1977).

39. E.Abrahams, *Ann.Phys.* (Leipzig) **8**, 539 (1999).

40. G.Zala, B.N.Narozhny, I.L.Aleiner, Phys.Rev. B **64**, 214204 (2001).

41. T.Vojta, F.Epperlein, M.Schreiber, Phys.Rev.Lett. **81**, 4212 (1998).

Iouri Poussep

ANEXOS

Localização e Coerência de Excitações Elementares em Sistemas Eletrônicos Desordenados: Ligas AlGaAs e Super-redes GaAs/AlGaAs Intencionalmente Desordenadas.

Agosto de 2004

LISTA DE ANEXOS:

1. Yu. A. Pusep, M. T. O. Silva, J. C. Galzerani, N. N. Moshegov, P. Basmaji - Influence of crystal potential fluctuations on Raman spectra of coupled plasmon-LO phonon modes in disordered systems, *Phys. Rev.* B **58** (16), 10683 (1998).

2. Yu.A.Pusep, G.M.Gusev, A.J.Chiquito, A.K.Bakarov, A.I.Toropov, and J.C.Leite, Vertical longitudinal magnetoresistance of superlattices, *Phys.Rev.* B**63**, 165307 (2001).

3. Yu. A. Pusep, S. S. Sokolov, J. C. Galzerani - Raman probing of the spatial extended collective excitations, *J. Phys.: Cond. Matter.* **13**, 10165-10174 (2001).

4. A.J.Chiquito, Yu.A.Pusep, G.M.Gusev, A.I.Toropov, Quantum interference in intentionally disordered doped GaAs/AlGaAs superlattices, *Phys.Rev.* B**66**, 035323 (2002).

5. Yu. A. Pusep, A. J. Chiquito, S. Mergulhão, A.I.Toropov, Parallel conductivity of random GaAs/AlGaAs superlattices in regime of controlled disorder, *J. Appl.Phys.* **92**, 3830 (2002).

6. Yu.A.Pusep, M.B.Ribeiro, H.Arakaki, C.A. de Souza, P.A.Zanello, A.J.Chiquito, S.Malzer, G.H.Döhler, Anisotropy of quantum interference in disordered GaAs/AlGaAs superlattices, *Phys.Rev.* B **68**, 195207 (2003).

7. Yu.A.Pusep, H.Arakaki, C.A. de Souza, Quantum interference in the presence of a metal-to-insulator transition, *Phys.Rev.* B **68**, 205321 (2003).

8. Yu.A.Pusep, M.B.Ribeiro, H.Arakaki, C.A. de Souza, P.A.Zanello, S.Malzer, G.H.Döhler, Regimes of quantum transport in superlattices in a weak magnetic field, *J.Phys.Cond.Matter* **16**, 2447 (2004).

9. Yu.A.Pusep, F.E.G.Guimarães, M.B.Ribeiro, H.Arakaki, C.A. de Souza, P.A.Zanello, S.Malzer, G.H.Döhler, Effect of compensation of electron and hole scattering potentials on the optical band edge of heavily doped GaAs/AlGaAs superlattices, *Phys.Rev.* B **70**, *092301 (2004).*

10. Yu.A.Pusep, M.B.Ribeiro, Disorder driven coherence-incoherence crossover in random GaAs/AlGaAs superlattices, *Phys.Rev.* B **71**, (2005).

11. Yu.A.Pusep, Managing disorder in random GaAs/AlGaAs superlattices, aceito em *Physica E.*

12. Yu.A.Pusep, M.B.Ribeiro, V.E.Carrasco, G.Zanelato, J.C.Galzerani, Coherence of elementary excitations in a disordered electron system, aceito em *Phys.Rev.Lett.*.

Influence of crystal-potential fluctuations on Raman spectra of coupled plasmon–LO-phonon modes in disordered systems

Yu. A. Pusep, M. T. O. Silva, and J. C. Galzerani

Universidade Federal de São Carlos, 13565-905 São Carlos, São Paulo, Brazil

N. T. Moshegov

Instituto de Fisica de São Carlos, Universidade de São Paulo, 13560-970 São Carlos, São Paulo, Brazil
and Institute of Semiconductor Physics, 630090 Novosibirsk, Russia

P. Basmaji

Instituto de Fisica de São Carlos, Universidade de São Paulo, 13560-970 São Carlos, São Paulo, Brazil

(Received 20 April 1998)

The effect of the structural disorder in the Raman scattering of the coupled plasmon–LO phonon modes was studied in doped $Al_xGa_{1-x}As$ alloys and in doped GaAs/AlAs superlattices. It was observed that the asymmetry in the Raman lines, caused by this effect, is opposite to that observed for the optical phonons. This fact is explained by the differences in the dispersion curves of the optical phonons and plasmons—a negative dispersion for the phonons and a positive one for the plasmons. The analysis of the Raman line shapes by means of a Gaussian spatial correlation function allowed us to obtain the localization lengths for the LO phonons and for the plasmons in the alloys and in the superlattices; the dispersions of the coupled plasmon–LO-phonon modes were studied and an evidence for a metal-dielectric transition occurring in superlattices when the lowest miniband is completely occupied was found. [S0163-1829(98)08239-3]

I. INTRODUCTION

Fluctuations of the crystal potential destroy its translational invariance and, as a consequence, a breakdown of the Raman selection rules occurs, leading to the broadening and asymmetry of the Raman lines. This effect was found to determine the shapes of the optical-phonon Raman lines in microcrystalline semiconductor materials[1] and in semiconductor alloys;[2] moreover, the violation of the coherency of the elementary collective excitations (phonons or plasmons) leads to localization effects. However, to our knowledge, an analysis of the influence of the crystal potential fluctuations on the plasmon Raman lines has not yet been done.

The volume where the collective excitations are localized is determined by a spatial localization length (L); this length can serve as a parameter characterizing the microscopic nature of the crystal potential fluctuations. Then a study of phonons in disordered materials will give us a possibility to characterize the structural quality, while plasmons, in addition, will provide us with information about the influence of the crystal potential fluctuations on the electron transport.

In this paper we study the effect of the crystal-potential fluctuations on the plasmon–LO-phonon Raman scattering in doped $Al_xGa_{1-x}As$ alloys and in doped $(GaAs)_n(AlAs)_m$ superlattices (n and m are the thicknesses of the corresponding layers expressed in monolayers). Both the systems under consideration reveal fluctuations of the crystal potential caused either by the random alloy potential or by the disordered character of the interface between the GaAs and AlAs layers in superlattices. Moreover, the fluctuations of the impurity potential contribute to both systems as well.

The samples were grown by molecular-beam epitaxy, and

were doped with Si in order to obtain free electron concentrations in the range $(1-5)\times10^{18}$ cm^{-3}. $Al_{0.2}Ga_{0.8}As$ alloys 1 μm thick were deposited on (100)-oriented GaAs substrates. $(GaAs)_{17}(AlAs)_2$ superlattices (with 20 periods) were also grown on (100) GaAs substrates. The superlattices were prepared with ultrathin AlAs barriers (2 ML thick) in order to allow the occurrence of vertical motion of electrons through the superlattices and, therefore, to study the superlattice plasmons (the plasmons polarized normal to the layers). Backscattering unpolarized Raman spectra were performed at $T=8$ K with a Jobin-Yvon double-grating spectrometer supplied with an usual photocounting system; the 5145-Å line of an Ar$^+$ laser was utilized for excitation.

II. THEORY

As is well known, in doped semiconductors free electrons electrically couple with the LO phonons, producing coupled plasmon–LO-phonon modes. In the $Al_xGa_{1-x}As$ alloy and in $(GaAs)_n(AlAs)_m$ superlattices, two types of LO phonons are distinguished: GaAs-like and AlAs-like. The interaction of these phonons with free electrons produces two coupled optical modes ω_1^+ and ω_2^+; the first one is due to the coupling of the GaAs-like LO phonons with electrons, while the second one originates from the AlAs-like LO phonons. In addition, the low-frequency acousticlike ω^- coupled mode appears in the frequency range below the frequency of the GaAs-like TO phonon.

Both the deformation potential (DP) and the Fröhlich interaction (FI) mechanisms are responsible for the Raman scattering by the coupled plasmon–LO-phonon modes. In

this case the scattering efficiency close to the E_1 resonance is given by[3]

$$\frac{\partial^2 R}{\partial\Omega\partial\omega} \sim -\int d^3q \; g_r(\mathbf{q})\cdot f_{sc}(\mathbf{q})\mathrm{Im}\,\frac{1}{\epsilon(q,\omega)}, \qquad (1)$$

where $g_r(\mathbf{q})$ is the function which takes into consideration the enhancement of the Raman efficiency when the excitation laser has an energy close to the E_1 critical point (this function is different for DP and FI), $f_{sc}(\mathbf{q})=[4\pi/(q^2+q_0^2)]^2$ is the screening correlation function (here q_0 is the screening wave vector), and $\epsilon(q,\omega)$ is the dielectric function which includes contributions due to both optical phonons and plasmons.

According to Ref. 1, the relaxation of the conservation of the crystal momentum caused by the crystal potential fluctuations can be taken into account by introducing a Gaussian spatial correlation function $\exp(-4R^2/L^2)$, which yields

$$\frac{\partial^2 R}{\partial\Omega\partial\omega} \sim -\int d^3q \; g_r(\mathbf{q})\cdot f_{sc}(\mathbf{q})\exp\!\left(-\frac{q^2L^2}{4}\right)\cdot\mathrm{Im}\,\frac{1}{\epsilon(q,\omega)}. \qquad (2)$$

Without lost of generality, far from resonance, the Raman intensity can be written in a phenomenological form

$$I(\omega)\sim\int f_{sc}(\mathbf{q})\exp\!\left(-\frac{q^2L^2}{4}\right)\frac{d^3q}{[\omega-\omega(q)]^2+(\Gamma/2)^2}, \qquad (3)$$

where $\omega(q)$ is the dispersion of the relevant collective excitations, and Γ is their damping constant.

We used the dispersions of the optical LO phonons for bulk $Al_xGa_{1-x}As$ in the form

$$\omega(q)=\omega_{LO}(1-Aq^2), \qquad (4)$$

where ω_{LO} is the frequency of the longitudinal-optical phonons. This formula gives a good approximation of the experimental data[4] with $A(\mathrm{GaAs})=0.18(a/2\pi)^2$ and $A(\mathrm{AlAs})=0.05(a/2\pi)^2$, where a is the lattice constant.

The dispersion of the plasmons was taken in the random-phase approximation[5]

$$\omega(q)=\omega_p\left[1+\frac{3}{10}\left(\frac{v_F}{\omega_p}\right)^2 q^2\right], \qquad (5)$$

where $\omega_p=(4\pi e^2 n/m)^{1/2}$ is the plasma frequency, and v_F is the Fermi velocity.

At the electron densities relevant to the samples under investigation, $\omega_p\sim\omega_{LO}$; then, the dispersion of the coupled plasmon–LO-phonon modes is almost completely determined by the dispersion of plasmons, which is much stronger than that of the LO phonons.

As it is seen from Eq. (3), the dispersion of collective excitations $\omega(q)$ and the value of the localization length L are responsible for an asymmetry of the Raman line. It follows from Eqs. (3)–(5) that the asymmetry of the plasmon–LO-phonon Raman line should be opposite to that of the LO phonon; this is explained by the different dispersions of the optical phonons and plasmons–a negative dispersion for the LO phonons and a positive one for the plasmons.
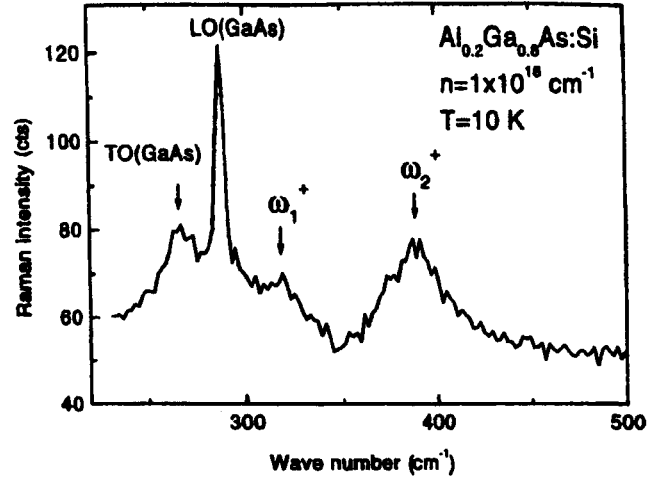

FIG. 1. The Raman spectrum of the doped $Al_{0.2}Ga_{0.8}As$ alloy with an electron density $n=1\times10^{18}$ cm^{-3} measured at $T=8$ K.

We assumed an isotropic spatial correlation and a spherical Brillouin zone in alloys. Superlattices present anisotropic systems with the electron energy defined as

$$E(q_1,q_z)=\frac{\hbar^2 q_1^2}{2m_1}+E(q_z), \qquad (6)$$

where q_1 and q_z are the electron momenta parallel and perpendicular to the layers, respectively.

In such anisotropic systems there is no way to take into account the screening effects correctly. Therefore, in superlattices we used the isotropic approximation (3) where all the parameters have a meaning of values averaged over directions. Thus the average dispersion of plasmons was calculated according to Eq. (5) with the average effective mass $\bar{m}^{-1}=\frac{1}{3}(2m_1^{-1}+m_z^{-1})$, where the electron effective mass in-plane of the layers m_1 was taken to be equal to the effective mass of electrons in bulk GaAs ($m=0.068m_0$), while the effective mass normal to the layers m_z was calculated by the envelope function approximation as has been done in Ref. 6.

In the case of thick enough barriers when quantum wells are well isolated, the only contribution to the Raman intensity is due to the plasmons polarized in plane of the layers (which become active in the backscattering configuration due to the electron scattering); therefore, the problem becomes a two-dimensional one and can be easily solved with an appropriate modification of Eq. (3) and with the two-dimensional screening correlation function[7] $f_{sc}(\mathbf{q})=[1/(q+q_0)]$, with $q_0=2g_v/a^*$ where g_v is a valley degeneracy factor which gives the number of equivalent energy bands, and a^* is the effective Bohr radius.

III. EXPERIMENTAL RESULTS AND DISCUSSION

The Raman spectra of one of the doped $Al_{0.2}Ga_{0.8}As$ alloys is shown in Fig. 1. The two lines assigned as ω_1^+ and ω_2^+ are the GaAs and AlAs-like coupled modes, respectively. In addition, the TO and LO GaAs-like phonons of the alloy were observed at 266 and 286 cm^{-1}, respectively. The uncoupled LO phonon is seen because of the surface depletion layer.
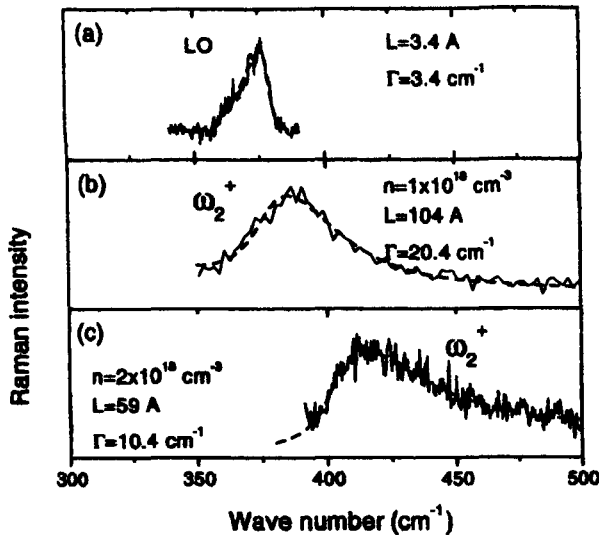
The Raman spectra measured in the spectral range of the

FIG. 2. The Raman spectra of doped $Al_{0.2}Ga_{0.8}As$ alloys with different electron densities measured at $T=8$ K in the spectral range of AlAs-like optical phonons: intrinsic alloy (a), $n=1\times10^{18}$ cm^{-3} (b), and $n=2\times10^{18}$ cm^{-3} (c).

AlAs-like LO phonon in the samples with different electron densities are presented in Fig. 2. The asymmetry of the LO Raman line observed in the intrinsic alloy [Fig. 2(a)] was found similar to that observed in $Al_xGa_{1-x}As$ alloys.[2] The coupling of the LO phonons with the plasmons in the doped alloy causes a blueshift of the Raman line, and, in addition, drastically changes its shape—the asymmetry of the Raman line becomes opposite to that due to the LO phonons.

As mentioned above, different asymmetries of the LO-phonon line and of the coupled mode line are caused by the different dispersions of the LO phonons and plasmons. The Raman spectra calculated by Eq. (3) with Eqs. (4) and (5) reveal a good fitting to the experimental results with the values of the localization lengths L depicted in Fig. 2. In order to calculate the screening correlation function in the doped alloy, we used the Thomas-Fermi screening radius as the value of q_0.

If the localization length L is small enough, then collective excitations in a broad interval of their dispersions will be involved in the Raman scattering. In this case the width of the asymmetrical Raman line is determined by the dispersion of the relevant collective excitations. Our results show that the phonon states from almost the whole Brillouin zone contribute to the Raman scattering in the intrinsic $Al_{0.2}Ga_{0.8}As$ alloy because the half-width of the asymmetrical LO-phonon line (≈14 cm^{-1}) is almost equal to the dispersion of the AlAs-like LO phonon (≈20 cm^{-1}).

The situation is somewhat different in the doped alloy where, as is well known, the dispersion of the plasmons is well defined until a critical value of the wave number q_c, while the plasmons with $q>q_c$ decay into single-particle electron excitations.[5] In the samples studied, the estimatives give $q_c\approx3\times10^6$ and 3.6×10^6 cm^{-1} in the alloys with the electron concentrations $n=1\times10^{18}$ and 2×10^{18} cm^{-3}, respectively; this yields totals dispersions of the plasmons of ≈46 and ≈75 cm^{-1} in the corresponding samples, while the half-widths of the asymmetrical plasmon-LO-phonon lines are about 40 and 50 cm^{-1}, respectively. This means that the
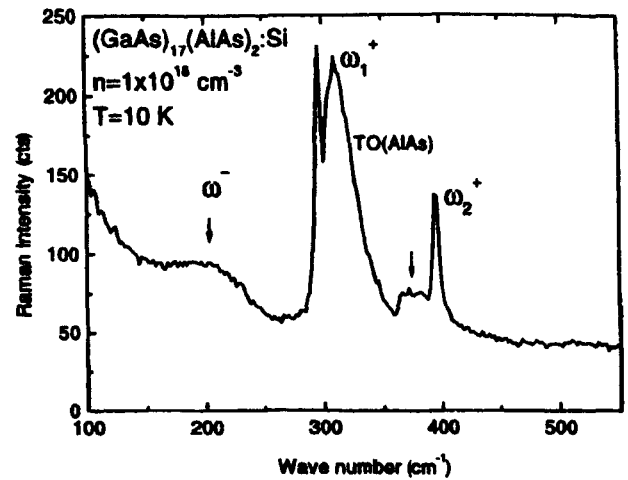

FIG. 3. The Raman spectrum of the doped $(GaAs)_{17}(AlAs)_2$ superlattice with an electron density $n=1\times10^{18}$ cm^{-3} measured at $T=8$ K.

largest part of the available plasmon states contribute to the Raman scattering.

Results similar to those obtained in the doped $Al_{0.2}Ga_{0.8}As$ alloys were observed in the doped $(GaAs)_{17}(AlAs)_2$ superlattices, where Raman lines corresponding to the coupled plasmon-LO-phonon modes revealed the same kind of asymmetry caused by the dispersion of the plasmons. Figure 3 displays the Raman spectrum of a doped $(GaAs)_{17}(AlAs)_2$ superlattice with the electron concentration $n=1\times10^{18}$ cm^{-3}. Again, as in the alloys, the two coupled modes (GaAs and AlAs-like) were observed, both revealing an inverted asymmetry as compared to the one found for the optical phonon line. Additionally, due to a better structural quality of the superlattices in comparison with the alloys, the low-frequency ω^- coupled mode was observed as well. The LO-phonon line of the GaAs layers was found as a sharp line at 296 cm^{-1}; as in the case of the doped alloys, it appears to be due to the surface depletion layer. The TO phonon of the AlAs barriers (and probably the LO phonon as well, appearing by the same reason as the LO phonon of the GaAs layers) was found around 370 cm^{-1}. The Raman spectra measured in superlattices with different electron densities are shown in Fig. 4. The spectrum in Fig. 4(a) corresponds to the sample with a partially occupied lowest Γ miniband, while those in Figs. 4(b) and 4(c) were measured in the samples with completely filled lowest Γ minibands, when the Fermi level is located close to the top of the miniband or even in a minigap (see calculations presented for similar samples in Ref. 6). The strong decrease of the localization length L, found when the Fermi level enters a minigap, reflects the localization of electrons and serves as evidence of the metal-dielectric transition which takes place with an increase of the electron density in superlattices. Two effects can be responsible for this localization: the formation of one-dimensional conducting channels in superlattices due to the fluctuations of the electron potential,[6] and the "reentrant localization" found to occur for the electron states at the top of a miniband.[8]

The percentage of states of the total plasmon dispersion involved in the Raman scattering of the doped superlattices can be estimated from the following data: in the superlattices with the electron concentrations 1×10^{18}, 3×10^{18}, and 5.6
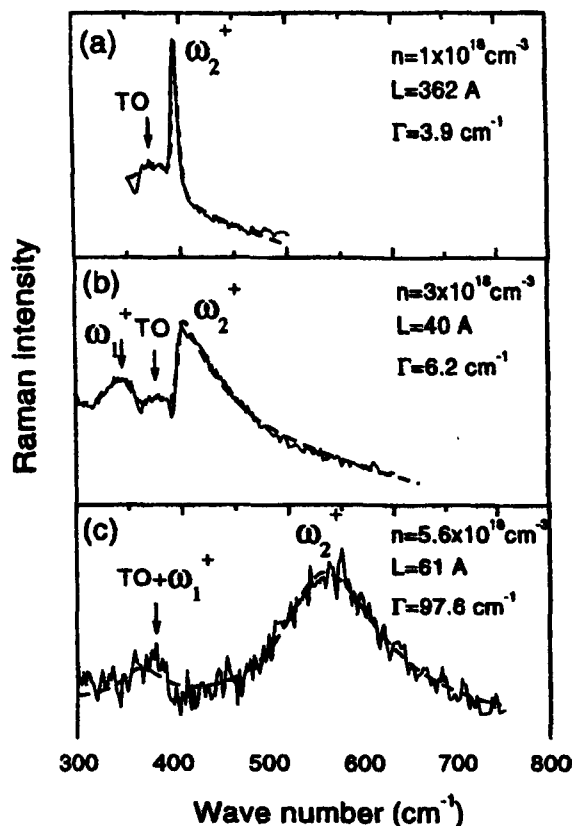
FIG. 4. The Raman spectra of doped $(GaAs)_{17}(AlAs)_2$ superlattices with different electron densities measured at $T=8$ K in the spectral range of AlAs-like optical phonons: $n=1\times10^{18}$ cm^{-3} (a), $n=3\times10^{18}$ cm^{-3} (b), and $n=5.6\times10^{18}$ cm^{-3} (c).

$\times10^{18}$ cm^{-3} the calculated widths of the plasmon dispersions are 50, 112, and 175 cm^{-1}, respectively, while the corresponding half-widths of the plasmon–LO-phonon lines are 7.5, 52, and 130 cm^{-1}. Therefore, while in the lower

doped superlattice only a small part of the plasmon dispersion is involved, in the highly doped samples the situation is similar to that of the alloys—almost all the available plasmon states contribute to the Raman process. This shows the importance of the impurity potential fluctuations in doped superlattices.

It is worth mentioning that different localization lengths were observed in the superlattice where the Raman spectrum reveals well-defined GaAs and AlAs-like coupled modes (Fig. 3). We obtained $L\sim89$ and 362 Å for the GaAs-like (ω_1^+) and AlAs-like (ω_2^+) coupled modes, respectively. It is evident that the atomic vibrations contributing to the coupled modes are responsible for this difference. Therefore, in spite of the fact that the dispersions of the coupled modes are determined mostly by the plasmons, the phonon origin influences their localization lengths.

IV. CONCLUSIONS

The influence of a structural disorder on coupled plasmon–LO-phonon modes was studied in doped $Al_xGa_{1-x}As$ alloys and in doped $(GaAs)_n(AlAs)_m$ superlattices. A relaxation of the momentum selection rules due to the breakdown in the crystal ordering was observed. This effect allows a large interval of the plasmon density of states to be involved in the Raman scattering. The analysis of the experimental results made it possible to determine the localization lengths of the carriers in the samples under investigation, and, thus, to estimate the range of the plasmon dispersion active in the Raman process; it further reveals the evidence of a metal-dielectric transition occurring in superlattices when the lowest miniband is completely filled.

[1] H. Richter, Z. P. Wang, and L. Ley, Solid State Commun. 39, 625 (1981).

[2] P. Parayanthal and F. H. Pollak, Phys. Rev. Lett. 52, 1822 (1984).

[3] D. Olego and M. Cardona, Phys. Rev. B 24, 7217 (1981).

[4] Yu. A. Pusep, S. W. da Silva, J. C. Galzerani, A. G. Milekhin, V. V. Preobrazhenskii, B. R. Semyagin, and I. I. Marahovka, Phys. Rev. B 52, 2610 (1995).

[5] D. Pines, Elementary Excitations in Solids (Addison-Wesley, Reading, MA, 1963).

[6] Yu. A. Pusep, A. J. Chiquito, S. Mergulhão, and J. C. Galzerani, Phys. Rev. B 56, 3892 (1997).

[7] T. Ando, A. B. Fowler, and F. Stern, Rev. Mod. Phys. 54, 437 (1982).

[8] H. A. Fertig and S. Das Sarma, Phys. Rev. B 42, 1448 (1990).

Vertical longitudinal magnetoresistance of semiconductor superlattices

Yu. A. Pusep,[1,2] G. M. Gusev,[1] A. J. Chiquito,[2] S. S. Sokolov,[2,3] A. K. Bakarov,[4] A. I. Toropov,[2,4] and J. R. Leite[1]

[1]*Instituto de Física da Universidade, São Paulo, 05315-970 São Paulo, São Paulo, Brazil*

[2]*Departamento de Física, Universidade Federal de São Carlos, Caixa Postale 676, 13565-905 São Carlos, Brazil*

[3]*Institute for Low Temperature Physics and Engineering, National Academy of Sciences of Ukraine, 61164 Kharkov, Ukraine*

[4]*Institute of Semiconductor Physics, 630090 Novosibirsk, Russia*

(Received 17 October 2000; revised manuscript received 19 January 2001; published 2 April 2001)

Vertical longitudinal magnetoresistance (VLMR) caused by the peculiar shape of the Fermi surface of a superlattice has been observed in GaAs/Al$_x$Ga$_{1-x}$As superlattices. This VLMR occurs when the electrons occupy the open Fermi surface and their motion in the plane of the layers is quantized by a magnetic field. It was shown that there exists a critical magnetic field that cancels the contribution of the electrons occupying the open Fermi surface to the vertical conductivity in the case when the chemical potential exceeds the width of the miniband, thus resulting in the observed VLMR. This effect produces the conditions necessary to observe the quantized Hall effect in the three-dimensional electron system of a superlattice.

I. INTRODUCTION

During the last decade, there has been considerable interest in studying the integer quantum Hall effect (QHE) in anisotropic three-dimensional electronic systems—semiconductor superlattices (SL's) where the minima of the resistivity ρ_{xx} were found to be accompanied by similar minima of the vertical conductivity σ_{zz}. Thus, a significant role of the vertical conductivity in formation of quantized states in a quasi-three-dimensional electronic system was determined.[1,2] In later studies two different contributions to the vertical conductivity of a superlattice in a strong magnetic field were distinguished: one due to the bulk and the other caused by the hybridization of the edge states of the superlattice layers.[3–5] The latter was shown to form the so-called two-dimensional chiral metal, which was observed at low enough temperatures ($T<1$ K) when all bulk quantum Hall states are localized and therefore the surface conductivity contributes significantly.

Moreover, the vertical longitudinal magnetoresistance (VLMR) of superlattices (the magnetoresistance that occurs when both electric and magnetic fields are directed along the growth direction of the superlattice) was studied in Refs. 6–11. As a result, specific Shubnikov–de Haas oscillations in the form of resistance resonances were predicted and anisotropy of the vertical magnetotransport in SL's was found: it was shown that the vertical magnetoresistance is much weaker, although still significant, for a magnetic field applied normal to the layers than for one directed parallel to the layers. Thus the observed nonzero VLMR was considered to be the result of nonuniform fluctuations of the widths of the layers, which caused localization of the electrons.[12,13]

In this paper we present results showing that even in an ideal SL, in appropriate conditions, there exists a strong VLMR originating from the peculiar shape of the Fermi surface of the SL. It is shown that when the Fermi energy lies in a minigap, in the case when the inter-Landau-level spacing is larger than the electron broadening energy ($\hbar/\tau$), the vertical conductivity tends to zero in a magnetic field applied parallel to the growth direction of the SL. In this case, the three-

dimensional electron system of a SL behaves like a stack of two-dimensional quantum Hall conductors thus producing conditions necessary for observation of the QHE.

The paper is organized as follows. The theory is considered in Sec. II. The electronic properties of the samples are characterized in Sec. III. The experimental results together with their discussion are given in Sec. IV, and conclusions are outlined in Sec. V.

II. THEORY

As shown in Refs. 14 and 15, at $T=0$ the vertical conductivity of a SL (along the z direction) can be written in the Drude form

$$\sigma_z = \frac{n^* e^2 \tau}{m_z} \tag{1}$$

with the effective electron concentration

$$n^* = \frac{m_\parallel W_{SL}}{2\pi^2 \hbar^2 D_{SL}} \int_0^{k_F} dk_z \left| \frac{v_z(\mathbf{k})}{v_{max}} \right|^2, \tag{2}$$

where m_z and $m_\parallel$ are the effective masses normal and parallel to the layers, respectively, W_{SL} is the miniband width, D_{SL} is the period of the SL, and v_{max} is the maximum electron velocity. The electron velocity v_z along the superlattice axis, which is responsible for the vertical conductivity of an ideal SL, is determined by the electron spectrum $E(\mathbf{k})$ along all possible directions of the wave vector $\mathbf{k}$:

$$v_z(\mathbf{k}) = \frac{1}{\hbar} \frac{\partial E(\mathbf{k})}{\partial k_z}. \tag{3}$$

Thus, a nonvanishing vertical conductivity is expected unless electron dispersion exists. When the Fermi energy exceeds the miniband width, the vertical conductivity is completely determined by the contributions of the electron states that belong to the open Fermi surface of the SL (which has the topology of an undulating cylinder oriented along the SL axis) and it is independent of the electron density while the
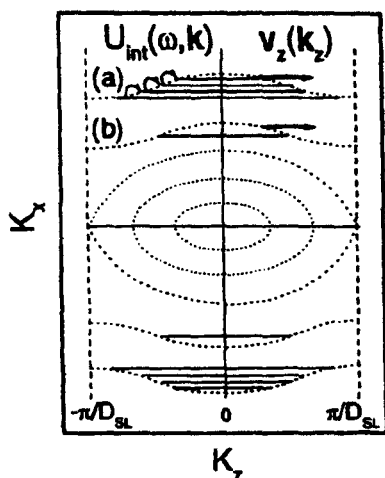
FIG. 1. Schematic cross section of the Fermi surfaces in a superlattice (dotted lines). Solid lines show the modification of open Fermi surfaces under a magnetic field in the cases when $\hbar\omega_c < W_{SL}$ (a) and $\hbar\omega_c > W_{SL}$ (b). Thin arrows show the electron interlevel transitions caused by the perturbation potential $U_{int}(\omega, k)$ that contribute to the vertical conductivity. The vertical components of the velocity of electrons occupying the open Fermi surfaces in the absence of the magnetic field are depicted by thick arrows.

Fermi level is located in a minigap (when the Fermi surface remains unchanged). Such behavior of the vertical conductivity was experimentally observed in SL's in Ref. 16. A modification of the Fermi surface of a SL is shown schematically in Fig. 1, where the closed Fermi surfaces are associated with the positions of the Fermi level inside a miniband, while the open Fermi surfaces correspond to the case when the Fermi level enters a minigap.

If now a strong enough magnetic field is applied along the superlattice axis, the in-plane motion of electrons becomes quantized into a series of Landau levels without affecting the miniband dispersion along the superlattice axis; then the energy dispersion becomes

$$E(\mathbf{k}) = E_z(k_z) + (n + \tfrac{1}{2})\hbar\omega_c, \tag{4}$$

where $\hbar\omega_c$ denotes the cyclotron energy and $n = 0,1,2,\ldots$.

For a magnetic field B such that $\hbar\omega_c > \hbar/\tau$ (where τ is the relaxation time) the vertical motion of an electron has purely one-dimensional character. In this case, for the open Fermi surfaces $v_z(\mathbf{k}) = 0$ and the conductivity of the SL vanishes. Therefore, a magnetic field induced metal-to-insulator transition is predicted to occur for the vertical conductivity when the increasing Fermi energy crosses the top of a miniband at a fixed magnetic field exceeding a critical value B_c, or when a varying magnetic field passes through this critical value in a SL with the Fermi level located in a minigap. The critical magnetic field is associated with the relation

$$B_c = \frac{\hbar m}{e\tau}. \tag{5}$$

These considerations allow us to conclude that at an appropriate magnetic field $(B > B_c)$ the value of the VLMR could be even larger than that of the vertical transverse mag-

netoresistance (VTMR)—the magnetoresistance associated with magnetic field perpendicular to the vertical current.

We developed a model to account for the observed VLMR. In this model the conductivity is determined by the number of broadened electron states at the Fermi surface that belong to different Landau levels and are mutually coupled by the scattering mechanism. In the following, we consider the electron transitions caused by elastic scattering of electrons by impurities in the presence of the external electric field E_0. The conductivity can be calculated by means of the matrix density method as proposed in Ref. 17. Following this method, the Hamiltonian can be written in the form

$$\hat{H}_{int} = CU_{int}(\mathbf{r})E_0 \exp(-i\omega t), \tag{6}$$

where $U_{int}(\mathbf{r}) = Ze^2 \sum_{j=1}^{N_j} [\exp(-\varkappa|\mathbf{r} - \mathbf{r}_j|)/|\mathbf{r} - \mathbf{r}_j|]$ is the potential of the interaction, N_j is the number of impurities, $\varkappa$ is the reciprocal screening length, and C is the coefficient of proportionality satisfying the necessary dimensionality.

In a linear approximation the average value of any operator is determined as

$$\langle \hat{\Phi} \rangle = \mathrm{Sp}(\rho_0 \hat{\Phi}) + C \sum_{\mathbf{k}'\alpha',\mathbf{k}\alpha} \frac{[f_0(\varepsilon_{\mathbf{k}'\alpha'}) - f_0(\varepsilon_{\mathbf{k}\alpha})]}{\varepsilon_{\mathbf{k}'\alpha'} - \varepsilon_{\mathbf{k}\alpha} - i\hbar/\tau} E_0$$

$$\times \exp(-i\omega t), \tag{7}$$

where the equilibrium value of the density matrix $\rho_0 = \rho(-\infty)$ and $f_0(\varepsilon_{\mathbf{k}\alpha}) = [\exp(\varepsilon_{\mathbf{k}\alpha} - \xi)/kT]^{-1}$ is the Fermi function, which defines the probability of finding an electron in the state $|\mathbf{k}\alpha\rangle$ with energy $\varepsilon_{\mathbf{k}\alpha}$, ξ is the chemical potential, and τ is the relaxation time. Thus, the generalized susceptibility can be calculated according to the formula[17]

$$\chi = \sum_{\mathbf{k}'\alpha',\mathbf{k}\alpha} \frac{[f_0(\varepsilon_{\mathbf{k}'\alpha'}) - f_0(\varepsilon_{\mathbf{k}\alpha})]}{\varepsilon_{\mathbf{k}'\alpha'} - \varepsilon_{\mathbf{k}\alpha} - i\hbar/\tau} (\hat{H}_{int})_{\mathbf{k}'\alpha',\mathbf{k}\alpha} \hat{\Phi}_{\mathbf{k}'\alpha',\mathbf{k}\alpha}. \tag{8}$$

The conductivity can be obtained by assuming that $\hat{\Phi}$ is the operator of the current density $\hat{j}_z = (e/mV)\hat{p}_z$ (where V is the crystal volume):

$$\sigma = \mathrm{Re}\left\{ C \sum_{\mathbf{k}'\alpha',\mathbf{k}\alpha} \frac{[f_0(\varepsilon_{\mathbf{k}'\alpha'}) - f_0(\varepsilon_{\mathbf{k}\alpha})]}{\varepsilon_{\mathbf{k}'\alpha'} - \varepsilon_{\mathbf{k}\alpha} - i\hbar/\tau} \right.$$

$$\left. \times \langle \mathbf{k}'\alpha'|\hat{U}_{int}|\mathbf{k}\alpha\rangle\langle \mathbf{k}\alpha|\hat{j}_z|\mathbf{k}'\alpha'\rangle \right\}. \tag{9}$$

In the calculations of the matrix elements of the interaction with impurities we can set $|\mathbf{k}\alpha\rangle = (1/\sqrt{V})\exp(i\mathbf{k}\cdot\mathbf{r})$ because the rapidly oscillating part of the Bloch function does not contribute significantly to the matrix element calculated over large distances $\varkappa^{-1} \gg a$, where a is the lattice constant. The result is

$$\langle \mathbf{k}'\alpha'|\hat{U}_{int}|\mathbf{k}\alpha\rangle = \frac{4\pi Ze^2}{V[\varkappa^2 + |\mathbf{k}' - \mathbf{k}|^2]} \sum_{j=1}^{N_j} e^{-i(\mathbf{k}' - \mathbf{k})\cdot\mathbf{r}_j}. \tag{10}$$

However, the full Bloch function

$$|k\alpha\rangle = (1/\sqrt{V})\exp(i\mathbf{k}\cdot\mathbf{r})u_{k\alpha}(\mathbf{r})$$

should be used when calculating the matrix element of the current density.[17] Then, taking into account that $\hat{j}_z = (e/mV)\hat{p}_z = -(e/mV)i\hbar\,\partial/\partial z$ we obtain

$$\langle k\alpha|\hat{j}_z|k'\alpha'\rangle = \frac{1}{N}\delta_{k'k}a_{\alpha\alpha'}(k), \tag{11}$$

where N is the number of electrons and $a_{\alpha\alpha'}(k) = (e/mv)\int_v u_{k\alpha}(r)(\hbar k_z - i\hbar\,\partial/\partial z)u_{k'\alpha'}(r)d^3r$ with v being the volume of the unit cell. Thus, the conductivity can be obtained as

$$\sigma_{zz} = \mathrm{Re}\left\{C\sum_{k'\alpha',k\alpha}\frac{[f_0(\varepsilon_{k'\alpha'})-f_0(\varepsilon_{k\alpha})]}{\varepsilon_{k'\alpha'}-\varepsilon_{k\alpha}-i\hbar/\tau}\right.$$
$$\left.\times\frac{4\pi Ze^2}{\varkappa^2 N_e}N_{imp}a_{\alpha\alpha'}(k_z)\right\}, \tag{12}$$

where N_e and N_{imp} are the concentrations of impurities and electrons, respectively.

Supposing $\varepsilon_{k'\alpha'}-\varepsilon_{k\alpha}=\hbar\omega_c$, at $k_z=k_{zF}$ (where k_{zF} is the Fermi wave number) we finally obtain

$$\sigma_{zz}=C\frac{2\pi Ze^2 N_{imp}}{\varkappa^2}a_{\alpha\alpha'}(k_{zF})\frac{\tau}{1+\omega_c^2\tau^2}\tanh\frac{\hbar\omega_c}{2kT}. \tag{13}$$

This model possesses all the essential features of the electron system considered here. Clearly, the conductivity decreases with increase of the magnetic field due to the increase of the inter-Landau-level separation ($\hbar\omega_c$). Moreover, as follows from Eq. (13), at $N_{imp}=N_e$ the conductivity increases with increasing electron density as $N_e^{2/3}$.

III. CHARACTERIZATION OF THE SAMPLES

In order to find the VLMR predicted above, we investigated structures consisting of a 20-period SL with 224 Å [80 monolayers (ML)] of GaAs wells and 8.4 Å (3 ML) of $Al_{0.3}Ga_{0.7}As$ barriers grown by molecular-beam epitaxy on a (100) n^+-type GaAs substrate. The SL's were doped with Si to achieve a desirable position of the Fermi level (above a miniband); they were sandwiched between two highly Si-doped 1000 Å thick GaAs contact layers. One high mobility undoped SL with the intrinsic electron concentration $N_e \sim 5\times10^{15}$ cm^{-3} was studied as well. The resulting structures were etched to yield mesas with a diameter of 0.5 mm. The Ohmic contacts were prepared by depositing Au-Ge-Ni alloy annealed at 450 °C for 120 s. In order to measure the thermostimulated current, a Schottky contact was formed at the top of the superlattices by the deposition of a 100 nm thick gold layer; these structures were used to control the electron concentration by CV measurements.

In addition, a structure consisting of a doped GaAs/$Al_{0.3}Ga_{0.7}As$ 40-period SL with the thicknesses of the wells and barriers equal to 210 Å (75 ML) and 8.4 Å (3 ML), respectively, grown on a semi-insulating (100) GaAs substrate without a highly doped cap layer was used to fabricate

a Hall bar in order to measure the effect of a magnetic field on the in-plane transport. This superlattice was doped up to $N=5\times10^{17}$ cm^{-3}, which corresponds to a Fermi level position well above the miniband, and it revealed a Hall mobility measured at $T=10$ K of about 1500 cm^2/V s, which corresponds to the value $\hbar/\tau \approx 10$ meV. Therefore, low field conditions ($\omega_c\tau\lesssim1$) hold in the doped superlattices with electron concentrations $N_e=(1-5)\times10^{17}$ cm^{-3}, while the high field condition ($\omega_c\tau>1$) is expected in the undoped superlattice.

Calculations made using the envelope function approximation including the effect of nonparabolicity showed that the SL's under investigation have a 4 meV wide lowest miniband. In all these narrow miniband SL's the Fermi levels were located in the minigap: well above the miniband in the doped SL's and close to the top of the miniband in the undoped SL. Measurements of the magnetoresistance were carried out at temperatures 1.5–4.2 K in magnetic fields up to 12 T.

Differently doped wide miniband (GaAs)$_{17}$(AlAs)$_2$ and (GaAs)$_{17}$(Al$_{0.3}$Ga$_{0.7}$As)$_6$ superlattices (with the width of the miniband $W_{SL}\approx65$ meV) grown without the contact layers, where partially and completely occupied minibands (which correspond to closed and open Fermi surfaces, respectively) can easily be achieved, were studied in order to confirm the influence of the shape of the Fermi surface on the VLMR.

As mentioned above, the peculiar shape of the Fermi surface of a SL is responsible for the VLMR discussed here. In order to confirm that there were no contributions of the effects of the localization of electrons to the measured VLMR (similar to those observed in Ref. 12), we explored the temperature dependence of the current across the SL's. Contrary to the activation character of the transport found in Ref. 12, a decrease of the current with increasing temperature caused by the scattering of electrons by phonons was observed in all the samples studied here. In addition, measurements of the thermostimulated current (TSC), a well-known method for detecting localization of carriers in semiconductors, revealed no presence of trapping. The results of these measurements are plotted in Fig. 2; they allowed us to conclude that in the samples under investigation the transport of electrons has Bloch miniband character. Therefore, in a strong enough magnetic field we expected to find VLMR caused by the quantization of the electron energy along the layers in the SL with an open Fermi surface.

In order to confirm the shape of the Fermi surface of the SL's studied here, we measured the transverse magnetoresistance, which is known to exhibit a strong variation when the orientation of the magnetic field is changed relative to the axis of the undulating cylinder (the SL axis). In the case of a strong magnetic field the magnetoresistance for such a Fermi surface was calculated in Ref. 18 and it takes the form

$$\rho=\frac{\beta_1 B^2\cos^2\varphi}{\theta^2 B^2+\lambda^2 B_0^2}C(\eta)+A, \tag{14}$$

where φ and θ are the angles between the current direction and the x axis (which lies in the plane of the magnetic field) and between the cylinder axis and the plane of the magnetic
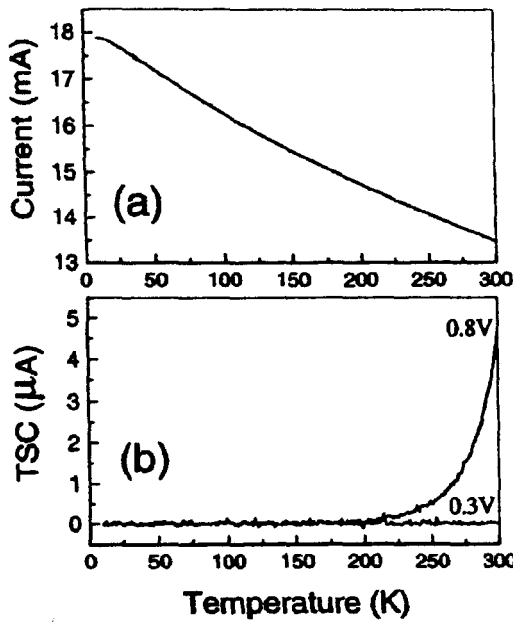
FIG. 2. Temperature dependence of the current across the $(GaAs)_{80}(Al_{0.3}Ga_{0.7}As)_3$ superlattice measured at the voltage $V = 1$ V (a) and of the thermostimulated current (b). The thermostimulated current was measured at different values of the reverse voltage (shown in the figure) applied to the Schottky contact fabricated at the top of the superlattice.

field, respectively, A, β_1, and λ are smooth functions of the angles, $C(\eta)$ is a smooth function of its argument $\eta = (\omega_c \tau \theta)^{-1}$, with $C(0) = C(\infty) = 1$, and the magnetic field B_0 is associated with the condition $\omega_c \tau = 1$. According to the formula (14), in the singular direction $\theta = 0$ (open orbits) the resistivity depends on the magnetic field as B^2, whereas in all other directions (closed orbits) it saturates at the field $B \approx B_0/\theta$.

The vertical magnetoresistances measured in the undoped superlattice with different orientations of the magnetic field are shown in Fig. 3. In this case, even at relatively weak magnetic fields, the high field conditions hold $(B > B_0)$ and the quadratic dependence of the transverse magnetoresis-
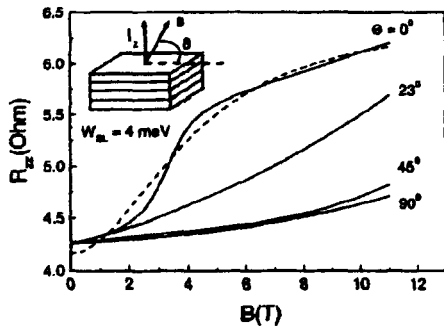

FIG. 3. Dependence of the resistance R_{zz} across the undoped $(GaAs)_{80}(Al_{0.3}Ga_{0.7}As)_3$ superlattice on magnetic fields with different orientations relative to the superlattice surface measured at $T = 1.5$ K. The dashed line shows the resistance calculated according to Eq. (14) for $\theta = 30°$.
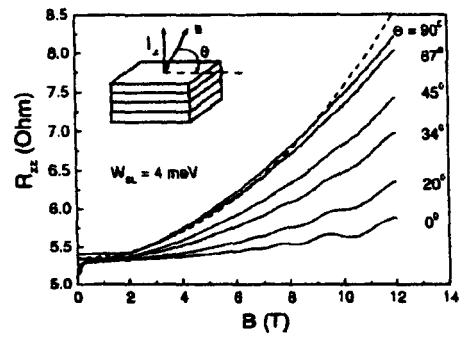
FIG. 4. Dependence of the resistance R_{zz} across the doped $(GaAs)_{80}(Al_{0.3}Ga_{0.7}As)_3$ superlattice with $N_e = 1.4 \times 10^{16}$ cm^{-3} on magnetic fields with different orientations relative to the superlattice surface measured at $T = 1.5$ K. The dashed line shows the calculated VLMR.

tance (the curve with $\theta = 0°$) is revealed. However, a small but finite electron scattering actually results in $\theta \neq 0$, which causes the saturation of the transverse magnetoresistance observed experimentally. The dashed line in Fig. 3 shows the best fit obtained from the formula (14) with the scattering angle $\theta = 30°$. This result confirms that the shape of the Fermi surface in the superlattices studied here is of the undulating cylinder type considered above.

IV. RESULTS AND DISCUSSION

A typical dependence of the resistance measured across the doped SL as a function of an applied magnetic field with different orientations is shown in Fig. 4. In a transverse magnetic field (normal to the z direction) we observed a weak positive VTMR. The Shubnikov–de Haas oscillations are clearly seen in this case. Their period did not depend on the doping of the SL's; therefore, they were attributed to the highly doped contact layers. Thus, we conclude that both the SL and the contacts contribute to the observed VTMR.

An increase of the positive vertical magnetoresistance was observed on increasing the angle θ between the direction of the applied magnetic field and the surface of the SL. This increase of the magnetoresistance was accompanied by a decrease of the amplitude of the Shubnikov–de Haas oscilla-

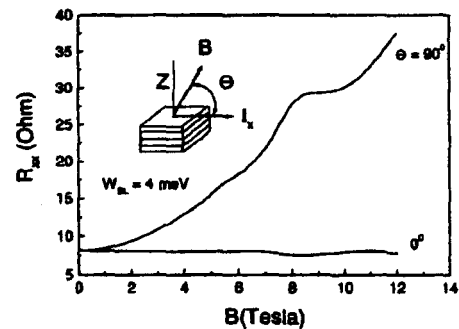FIG. 5. Dependence of the resistance R_{xx} along the layers of the doped $(GaAs)_{75}(Al_{0.3}Ga_{0.7}As)_3$ superlattice with $N_e = 2 \times 10^{17}$ cm^{-3} on magnetic fields parallel and perpendicular to the growth direction measured at $T = 1.5$ K.
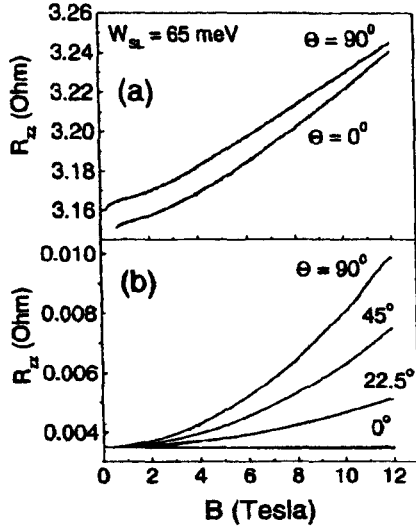
FIG. 6. Dependence of the resistance R_{zz} across the doped wide miniband superlattices GaAs/Al$_x$Ga$_{1-x}$As with $N_e = 5.0 \times 10^{17}$ cm^{-3} (closed Fermi surface) (a) and $N_e = 1.7 \times 10^{18}$ cm^{-3} (open Fermi surface) (b) on magnetic field measured at $T = 1.5$ K.

tions, which disappeared with the magnetic field parallel to the growth direction, when the measured VLMR originated completely from the SL, while the contact regions did not contribute. In this case the longitudinal magnetic field, quantizing the motion of electrons parallel to the layers, eliminates the contribution of the open Fermi surface to the vertical conductivity. The dependence of the resistance presented in Fig. 4 by the dashed line was calculated according to Eq. (13) as a value equal to σ_{zz}^{-1} with $\hbar/\tau = 12$ meV, and it agrees well with the experimental data.

The effect of the magnetic field on the in-plane motion of electrons occupying the open Fermi surface of a SL is demonstrated in Fig. 5. As expected, the longitudinal magnetic field revealed no significant effect on the in-plane transport, while the transverse magnetic field caused a strong positive magnetoresistance accompanied by Shubnikov–de Haas oscillations, now originating from the SL.

The dependence of the VLMR on the shape of the Fermi surface was explored in the wide miniband SL's where $W_{SL} > \hbar/\tau$ and therefore the SL with Fermi level located inside the miniband (closed Fermi surface) can be easily distinguished from the SL with Fermi level above the miniband (open Fermi surface). The experimental results plotted in Fig. 6 clearly show the absence of the VLMR in the SL with the closed Fermi surface and a strong VLMR in the case of the open Fermi surface. These SL's were grown without the contact layers, which therefore did not contribute to the measured magnetoresistance.

Good agreement was found between the experimental (data points) and calculated (solid line) dependencies of the
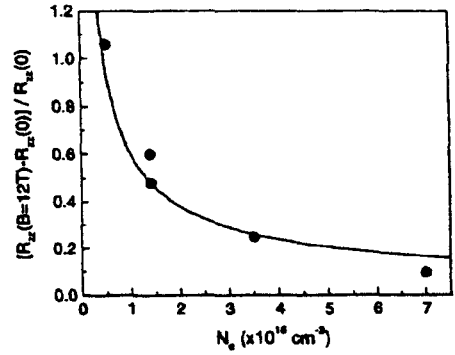
FIG. 7. Dependence of the relative vertical longitudinal magnetoresistance in the (GaAs)$_{90}$(Al$_{0.3}$Ga$_{0.7}$As)$_3$ superlattices on the electron concentration measured at $T = 1.5$ K.

relative vertical longitudinal magnetoresistance $[R_{zz}(B = 12$ T$) - R_{zz}(0)]/R_{zz}(0)$ on the concentration of the electrons, plotted in Fig. 7.

As a matter of fact, in a SL subject to a strong enough magnetic field perpendicular to the surface (such as $\hbar \omega_c > \hbar/\tau$), as a consequence of the vanishing vertical conductivity, the state of the three-dimensional electron gas resembles the quantized Hall state of a two-dimensional electron gas. This means that in appropriate conditions such a magnetic field forces the three-dimensional electron system, where it is not possible to observe the QHE, to acquire a state favorable for the observation of the QHE. It should to be stressed that, although the nature of the VLMR observed here seems to be similar to that of the QHE, there is an essential difference: the quantization of the in-plane electron energy is responsible for the QHE, while both the quantization and the specific shape of the Fermi surface of the superlattice determine the VLMR. As we observed, the VLMR does not depend as strongly on temperature as do the QHE and the conductivity caused by chiral surface states; therefore, it was detected at rather high temperatures when no signs of the QHE or surface states were found.

V. CONCLUSIONS

To conclude, we found vertical longitudinal magnetoresistance originating from the unusual shape of the Fermi surface of a semiconductor superlattice. It was shown that the quantization of the in-plane motion of electrons is responsible for the observed effect. The absence of the VLMR in superlattices with closed Fermi surfaces and when the current was measured parallel to the layers confirmed this conclusion.

ACKNOWLEDGMENTS

[1] H. L. Störmer, J. P. Eisenstein, A. C. Gossard, W. Wiegmann, and K. Baldwin, Phys. Rev. Lett. **56**, 85 (1986).

[2] H. L. Störmer, J. P. Eisenstein, A. C. Gossard, K. W. Baldwin, and J. H. English, in *Proceedings of the 18th International Conference on Physics of Semiconductors, Stockholm, 1986,* edited by O. Engström (World Scientific, Singapore, 1987), p. 385.

[3] D. P. Druist, P. J. Turley, K. D. Maranowski, E. G. Gwinn, and A. C. Gossard, Phys. Rev. Lett. **80**, 365 (1998).

[4] J. T. Chalker and S. L. Sondhi, Phys. Rev. B **59**, 4999 (1999).

[5] B. Zhang, J. Brooks, Z. Wang, J. Simmons, J. Reno, N. Lumpkin, J. O'Brien, and R. Clark, Phys. Rev. B **60**, 8743 (1999).

[6] K. K. Choi, B. F. Levine, N. Jarosik, J. Walker, and R. Malik, Phys. Rev. B **38**, 12 362 (1988).

[7] T. H. H. Vuong, D. C. Tsui, and W. T. Tsang, J. Appl. Phys. **66**, 3688 (1989).

[8] H. J. Hutchinson, A. W. Higgs, D. C. Herbert, and G. W. Smith, J. Appl. Phys. **75**, 320 (1994).

[9] A. E. Datars and J. E. Sipe, Phys. Rev. B **51**, 4312 (1995).

[10] B. Laikhtman and D. Menashe, Phys. Rev. B **52**, 8974 (1995).

[11] J. Q. You, Lide Zhang, and Q. B. Yang, Phys. Rev. B **55**, 15 757 (1997).

[12] M. Lee, N. S. Wingreen, S. A. Solin, and P. A. Wolff, Solid State Commun. **89**, 687 (1994).

[13] D. L. Miller and B. Laikhtman, Phys. Rev. B **54**, 10 669 (1996).

[14] S.-R. E. Yang and S. Das Sarma, Phys. Rev. B **37**, 10 090 (1988).

[15] R. Enderlein, L. M. R. Scolfaro, and J. R. Leite, Phys. Rev. B **50**, 18 312 (1994).

[16] Yu. A. Pusep, M. T. O. Silva, J. C. Galzerani, S. C. P. Rodrigues, L. M. R. Scolfaro, A. P. Lima, A. A. Quivy, J. R. Leite, N. T. Moshegov, and P. Basmaji, J. Appl. Phys. **87**, 1825 (1999).

[17] A. S. Davydov, *Solid State Theory* (Nauka, Moscow, 1976).

[18] I. M. Lifshitz and V. G. Peschanskii, Zh. Éksp. Teor. Fiz. **35**, 1251 (1958); [Sov. Phys. JETP **35**, 875 (1959)].

PUSEP, Y. A.; SOKOLOV, S. S.; FORTUNATO, W.; GALZERANI, J. C.; LEITE, J. R. Raman probing of spatial extents of collective excitations in AlGaAs alloys. **Journal of Physics:** condensed matter, Bristol, v. 13, p. 10165-10174, 2001.

Quantum interference in intentionally disordered doped GaAs/Al$_x$Ga$_{1-x}$As superlattices

A. J. Chiquito,[1] Yu. A. Pusep,[1] G. M. Gusev,[2] and A. I. Toropov[3]

[1]Instituto de Física de São Carlos. Universidade de São Paulo. 13560-970 São Carlos, SP. Brazil

[2]Instituto de Física da Universidade. São Paulo. 05315-970 São Paulo, SP. Brazil

[3]Institute of Semiconductor Physics. 630090 Novosibirsk, Russia

The processes of quantum interference are studied in intentionally disordered doped short-period GaAs Al$_x$Ga$_{1-x}$As superlattices where the conductivity can be controlled by the artificial disorder. We found that the usual formula for the weak localization correction to the classical conductivity of superlattices obtained in the propagative Fermi-surface approximation [W. Szott, C. Jedrzejek, and W.P. Kirk, Phys. Rev. Lett. 63, 1980 (1989)] does not allow to one explain the observed negative magnetoresistance. An excelent agreement was obtained between our results and recently published calculations of the quantum interference correction to the conductivity of the strongly disordered superlattices, where the transport regime corresponding to the diffusive Fermi surface was considered [A. Cassam-Chenai and D. Mailly, Phys. Rev. B 52, 1984 (1995)]. We found a tendency toward a propagative regime with an increase of the electron concentration, when the influence of disorder was weakened. The decrease of the dephasing of the electron wave function was observed with an increase of both the doping concentration and the disorder strength. The observed temperature dependence of the dephasing time manifested that the process of the dephasing is modified in the presence of strong disorder.

I. INTRODUCTION

Quantum interference corrections to conductivity cause a negative magnetoresistance of weakly disordered semiconductors.[1,2] In such materials transport is accompanied by the quantum interference between the electron wave functions, which is known as a weak localization of electrons. Weak-localization corrections determine the magnetoresistance in weak magnetic fields $\omega_c \tau \ll 1$. when the electron-electron interaction can be neglected.[3] Disorder plays a considerable role in the weak localization, providing two coherent scattering processes that contribute to the quantum interference. Early perturbative theories of weak localization were developed in the limit of weak disorder,[4] when the mean free path of electron (λ) is much larger than the Fermi wavelength, i.e., $k_F\lambda \gg 1$, where k_F is the Fermi momentum. As mentioned in Refs. 5 and 6, in the case of strong disorder the quantum corrections to the conductivity become even more relevant. At high disorder, when $k_F\lambda \lesssim 1$, different approaches were used to account for the quantum interference. In the first publication[7] the interference effects were considered among various paths associated with hopping between localized sites; then a negative magnetoresistance linear in the magnetic field was obtained. A theory of the magnetoresistance in the variable-range-hopping regime employing the critical percolation path picture yielded the quadratic field dependence.[8] More recent calculations, based on a self-consistent approach of Anderson localization, revealed a similar quadratic dependence for small magnetic fields.[6,9–11]

In the presence of strong localization and in the regime of the variable-range hopping the negative magnetoresistance associated with the quantum interference effects was observed in highly disordered In$_2$O$_{3-x}$ films[5,12] and in compensated GaAs.[13] The publications relevant to the experimental

study of weak localization in doped semiconductors can also be found in Refs. 14 and 15. It is clear that quantum interference depends on both electron density and disorder. However, in doped semiconductors, where disorder is produced by a random impurity potential, a variation of disorder is always accompanied by a corresponding variation of the electron concentration. Therefore, in this case a careful analysis of the temperature and magnetic-field dependencies of the conductivity are indispensable in order to separate the effects of the interaction and disorder on the quantum interference.[16,17] On the other hand, semiconductor superlattices present an electron system where disorder can be controlled independently of the electron concentration. In the so-called intentionally disordered superlattices firstly considered in Ref. 18, disorder is introduced during the growth by a random variation of the periodicity. At not very high doping concentrations this artificial disorder can dominate the disorder due to impurities. In this case the disorder strength can be completely controlled by a superlattice structure, while impurities supply the carriers. In such electron systems the weak localization can be studied in a wide range of disorder strengths—from almost perfectly ordered superlattices, where the transport is due to the extended electron states, to structures where the strong disorder induces spatially localized electron levels. The first observation of the electron localization in the intentionally disordered GaAs/Al$_x$Ga$_{1-x}$As superlattices was presented in Ref. 19.

Weak-localization corrections to the conductivity of the disordered semiconductor superlattices were recently considered in Ref. 20 in two limits: a strong disorder along the growth direction z, when $t_z\tau < \hbar$ (where t_z is the coupling energy along z and τ is the elastic scattering time). and a weak scattering with $t_z\tau > \hbar$. In both cases a weak in-plane disorder ($E_F\tau \gg \hbar$) was supposed. In the first case an electron experiences many scatterings before leaving a layer.

This is the diffusive Fermi-surface (DFS) regime, opposite to the second case of the weak scattering regime characterized by the usual propagative Fermi surface (PFS). It was shown that the strong vertical disorder modifies the parallel transport resulting in a very different shape of the magnetoconductivity caused by the quantum corrections than that one corresponding to the PFS regime.

In the regime of the propagative Fermi surface the weak localization effects were studied in the GaAs/$Al_xGa_{1-x}As$ superlattices in Refs. 21 and 22, while the anisotropy of the negative magnetoresistance was investigated in relatively high doped GaAs/$Al_xGa_{1-x}As$ superlattices in a regime close to the DFS one in Ref. 23.

Intentionally disordered superlattices, where disorder is introduced by a controlled random variation of well thicknesses, are excellent candidates to model the electron system considered in Ref. 20 and thus, to study the effects of the vertical disorder on the parallel transport. In such superlattices the disorder reveals the anisotropic character when the electrons can be localized along the growth direction, while moving freely in the plane of the wells.

In this paper we explore the weak localization in intentionally disordered short-period doped GaAs/$Al_xGa_{1-x}As$ superlattices in wide ranges of the disorder strengths and doping levels. In all the samples we found the characteristic features of the DFS regime with a tendency toward the PFS one observed with the increase of the electron density.

The paper is organized as follows. The theory is considered in Sec. II. The electronic properties of the samples are characterized in Sec. III. The experimental results and discussion are given in Sec. IV, while conclusions are outlined in Sec. V.

II. THEORY

Following Ref. 20, we will consider the transport properties of a superlattice in a weak-field regime ($\omega_c \tau \ll 1$). The vertical motion (parallel to the growth direction) is coherent when the elastic time $\tau \gg \hbar/t_z$. On the other hand, the coherent motion breaks down when $\tau \ll \hbar/t_z$, which corresponds to a localization of an electron on a length scale smaller than the period of a superlattice. In the first case the electrons propagatively move in a coherent band, and the use of a quasiclassical formalism is justified. However, in the second case the electron transport may occur as a hopping process between the neighboring wells, which is a diffusive process. In the later case the broadening of the Fermi surface along the z direction is larger than the width of the energy dispersion t_z. Consequently, one distinguishes two regimes: the regime of the propagative Fermi surface and the regime when the Fermi surface becomes diffusive—the DFS one. In the regime of a PFS a formula for the quantum correction to the classical conductivity was obtained,[24]

$$\delta\sigma_\parallel(H) - \delta\sigma_\parallel(0) = \frac{e^2}{2\pi^2\hbar l_H}\alpha F(\delta), \qquad (1)$$

where $l_H = \sqrt{\hbar c/eH}$ is the magnetic length, $\alpha = \sqrt{D_\parallel/D_\perp}$ is the coefficient of the anisotropy, $D_\parallel$ and $D_\perp$ are the diffu-
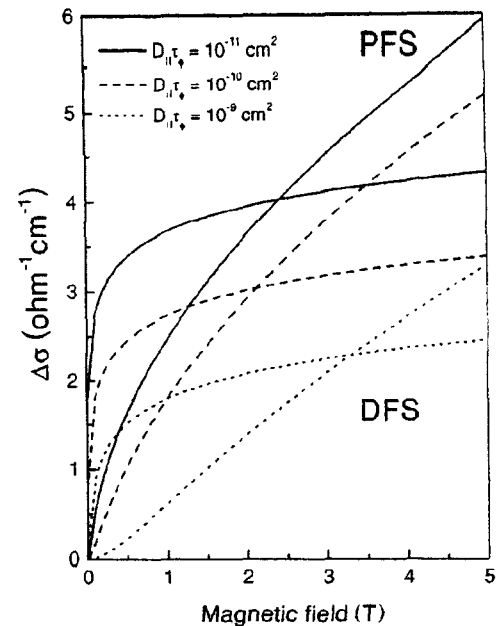
FIG. 1. Quantum corrections to the classical conductivity calculated in two transport regimes (PFS and DFS) according to Eqs. (1) and (2), with different values $D_\parallel\tau_\varphi$.

sion coefficients parallel and perpendicular to the layers respectively, $F(\delta) = \sum_{n=0}^\infty 2[(n+1+\delta)^{1/2} - (n+\delta)^{1/2}] - (n+\frac{1}{2}+\delta)^{-1/2}$ is the Kawabata function[25] with $\delta = l_H^2/4D_\parallel\tau_\varphi$, and τ_φ is the electron wave-function dephasing time.

In the case of a strongly DFS another formula was obtained,[20]

$$\delta\sigma_\parallel(H) - \delta\sigma_\parallel(0) = -\frac{e^2}{2\pi^2\hbar d_{SL}}F(\delta,\delta'). \qquad (2)$$

where d_{SL} is the period of a superlattice,

$$F(\delta,\delta') = \sum_{n=0}^\infty \frac{1}{\sqrt{n+\frac{1}{2}+\delta}\sqrt{n+\frac{1}{2}+\delta'}}$$
$$- 2\ln(\sqrt{n+1+\delta} + \sqrt{n+1+\delta'}) + 2\ln(\sqrt{n+\delta}$$
$$+ \sqrt{n+\delta'}).$$

with

$$\delta' = \frac{l_H^2}{4D_\parallel}\left(\frac{1}{\tau_\varphi} + 2\frac{l_z^2\tau}{\hbar^2}\right).$$

The essential difference between Eqs. (1) and (2) is in the prefactors multiplying the functions $F(\delta)$ and $F(\delta,\delta')$. It includes the magnetic length l_H or the superlattice period d_{SL} in the PFS or DFS regimes, respectively. This produces very different shapes of the weak-localization magnetoresistance in both regimes, as shown in Fig. 1, where the weak-localization corrections were calculated with different pa-

rameters $D_\perp \tau_\varphi$ entering Eqs. (1) and (2). Contrary to the PFS regime, the magnetoresistance calculated in the DFS regime reveals a much stronger dependence at very weak magnetic fields with a tendency to saturate with the increase of the magnetic field.

In the presence of vertical localization the coupling energy $t_\perp$ is replaced by the tunneling rate. Estimates show that in this case $1/\tau_\varphi \gg 2(t_\perp \tau/h^2)$, and therefore a good approximation is $\delta' \approx \delta$.

III. CHARACTERIZATION OF THE SAMPLES

In order to control the disorder strength, the $(GaAs)_m(Al_{0.3}Ga_{0.6}As)_6$:Si superlattices were prepared with a fixed doping. The vertical disorder was produced by a controlled random variation of the GaAs well thicknesses around the nominal value $m = 17$ ML, corresponding to a Gaussian distribution of the lowest levels of noninteracting electrons forming the conduction miniband. The barrier thicknesses were unchanged.

According to the calculations made by the Kronig-Penney model including the potential nonparabolicity, the width of the lowest Γ miniband of the nominal superlattice $(GaAs)_{17}(Al_{0.3}Ga_{0.6}As)_6$ is $W = 55$ meV. The doping concentrations were chosen in order to obtain the samples with a partial occupation of the miniband ($E_F = 32$ meV at $N = 6.0 \times 10^{17}$ cm^{-3}) and with a completely full miniband ($E_F = 52$ meV at $N = 1.7 \times 10^{17}$ cm^{-3}). The samples were grown by molecular beam epitaxy on (100)-oriented GaAs substrates. In order to avoid the short-range in-plane fluctuations, the growth of the superlattices was interrupted for 20 sec at the normal interface and for 3–5 sec at the inverted one. The total number of 50 periods was grown. The disorder strength was uniquely characterized by the disorder parameter $\delta = \Delta/W$, where Δ is the full width at half maximum of a Gaussian distribution of the electron energy calculated in the isolated quantum well, and W is the miniband width of the nominal superlattice in the absence of disorder. Even in the nominal superlattices the unavoidable monolayer fluctuations produce the vertical disorder strength $\delta \approx 0.18$. One expect that at $\delta \approx 1$ majority of the electrons moving in the miniband perpendicular to the layers should be localized. The localization of the vertically moving electrons was detected in the studied here superlattices by Raman scattering in Ref. 26.

The samples were patterned into Hall bars prepared by standard lithography and chemical etching. The Ohmic contacts were fabricated by depositing an Au-Ge-Ni alloy. A conventional ac four-probe method was used to measure resistivity. The values of the Hall in-plane mobilities measured at $T = 4.2$ K were found in the interval from 600 to 1500 cm^2/Vs, which results in the values $k_F\lambda \approx 3–9$. This implies in a quasi-metallic character of the in-plane conductivity, as supposed in Ref. 20. The parallel magnetoresistance measurements were performed in the "Oxford Instruments" superconducting magnet system at $T = 1.7$ K. The magnetic field was directed along the growth direction (z) of the superlattices.
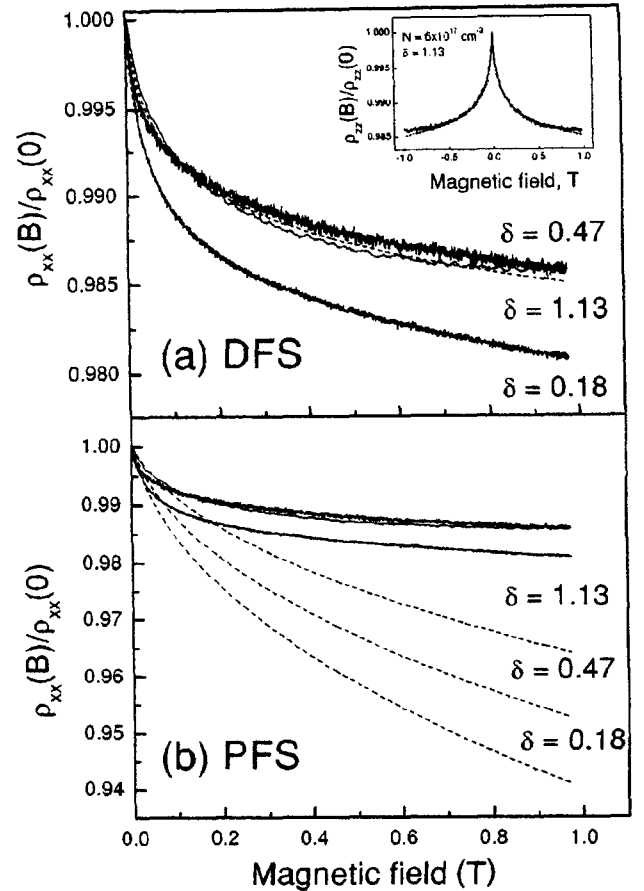
FIG. 2. Magnetoresistances measured in the disordered $GaAs/Al_xGa_{1-x}As$ superlattices with a fixed doping concentration $N = 6.0 \times 10^{17}$ cm^{-3} and different disorder strengths. A comparison is shown with the magnetoresistance calculated in a DFS (a) and in a PFS (b) transport regimes (dashed lines). The inset shows the magnetoresistance measured in the magnetic fields of the opposite orientations.

IV. RESULTS AND DISCUSSION

The magnetoresistances measured in the intentionally disordered $GaAs/Al_xGa_{1-x}As$ superlattices with different doping concentrations and disorder strengths are shown for some of the samples in Figs. 2 and 3. The observed symmetry of the low-field negative magnetoresistance caused by the quantum interference, shown in the insertion in Fig. 2(a) for one of the superlattices with the highest disorder strength, gives a proof of the macroscopic in-plane homogeneity of the samples.[27]

In the all here studied superlattices we found the best agreement with the magnetoresistance calculated in a DFS regime [Eq. (1)] than in a PFS one [Eq. (2)]. The dependences calculated for a PFS regime shown in Fig. 2(b) were fitted in the low-field range and then extrapolated to the high magnetic fields. As it was mentioned in Sec. II, the observed difference in the magnetoresistance mainly comes from the prefactor of Eqs. (1) and (2). In the PFS regime it depends on the magnetic field through the magnetic length l_H, while in the case of strong disorder the magnetic length is substituted
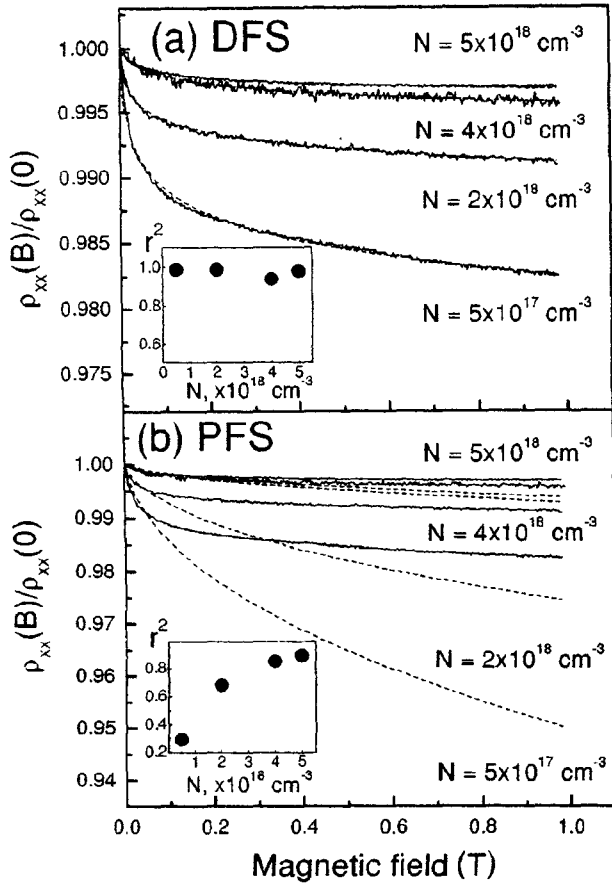
FIG. 3. Magnetoresistances measured in the disordered GaAs $Al_xGa_{1-x}As$ superlattices with a fixed disorder strength δ = 0.18 and different doping concentrations. A comparison is shown with the magnetoresistance calculated in DFS (a) and PFS (b) transport regimes (dashed lines). The insets show the concentration dependence of the coefficient of determination thus far achieved during the least-squares fitting (r^2).

by the superlattice period d_{SL}. Therefore, the magnetoresistance of the strongly disordered superlattices is completely associated with the function $F(\delta, \delta')$.

It is clear that the effect of disorder on the magnetoresistance should decrease with increasing electron density. This is because with the increase of the electron concentration, when $E_F > \Delta$, the condition $\hbar/\tau > l_z$ changes to $\hbar/\tau < l_z$. Therefore, we expect that an increase of the electron concentration should result in a transition from a DFS regime to a PFS one. As a consequence, the magnetoresistance measured in the highly doped disordered superlattices, instead following the magnetoresistance calculated with Eq. (2), should approximate the value calculated according to Eq. (1). Indeed, as is shown in Fig. 3(b), the better fitting of the calculated according to the PFS formula magnetoresistance can be obtained with increasing electron concentration, while no improvement of the fitting made by the PFS formula was obtained with the variation of the disorder strength [Fig. 2(b)]. The inset to Fig. 3(b) exhibits the values of the coefficient of determination thus far achieved during the least-squares fitting (r^2), which significantly increases with the
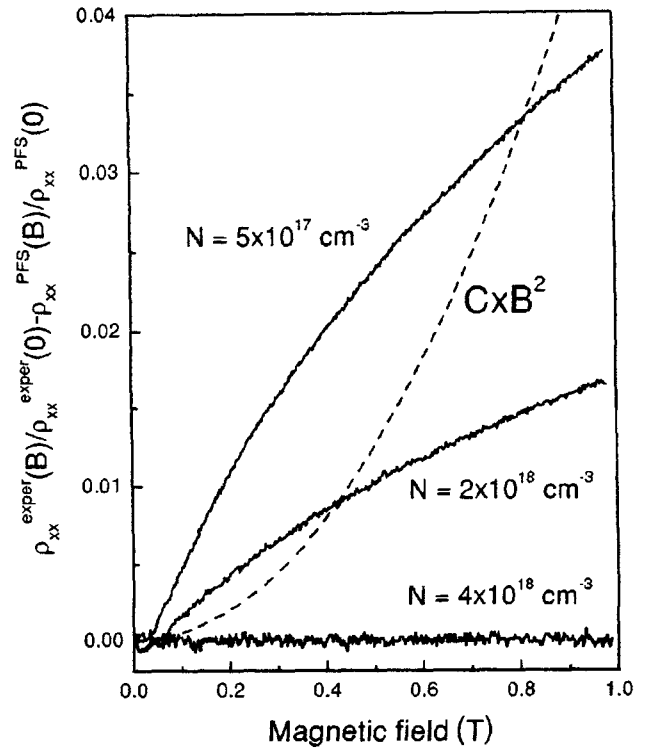
FIG. 4. Differences between the magnetoresistances measured in the differently doped superlattices $(GaAs)_{17}(Al_{0.3}Ga_{0.7}As)_6$ with $\delta = 0.18$ and the magnetoresistances calculated in a PFS regime. The dashed line shows the quadratic field dependence (C is the constant).

concentration showing the improvement of the fitting. Conversely, good fittings obtained with the DFS formula for all the samples independently of the concentration are demonstrated in the inset to Fig. 3(a). A better suitability of Eq. (1) in highly doped superlattices is also presented in Fig. 4, where the differences between the measured magnetoresistances and the magnetoresistances calculated according to the PFS formula revealed clear decrease with increasing concentration.

The ratios of the relative resistivities calculated in a PFS regime at $B = 1$ T to the lateral resistivities measured at the same magnetic field (ρ_{PFS}/ρ_{exp}) presented in Fig. 5 again show a better accordance between them obtained with the increase of the electron concentration [Fig. 5(a)]. While, an opposite behavior of the ratios ρ_{PFS}/ρ_{exp} revealed the slight enhancement of the disagreement between the PFS formula and the experimental data with increasing disorder [Fig. 5(b)].

It is worth mentioning that the differences between the measured magnetoresistances and that ones calculated according to the formula for a PFS regime [Eq. (2)], which are plotted in Fig. 4, do not reveal a quadratic dependence and therefore, cannot be assigned to the contribution of the positive classical magnetoresistance. Thus we concluded that the DFS transport regime was undoubtedly found in all the low-doped disordered superlattices under investigation with no signatures of the PFS regime. In highly doped superlattices

FIG. 5. Ratios of the relative resistivities calculated in a PFS regime at $B = 1$ T (ρ_{PFS}) to the relative resistivities measured at the same magnetic field (ρ_{expt}), obtained in the superlattices with a fixed disorder ($\delta = 0.18$) and different doping concentrations (a) and with fixed doping concentration ($N = 6.0 \times 10^{17}$ cm^{-3}) and various disorder strengths (b).
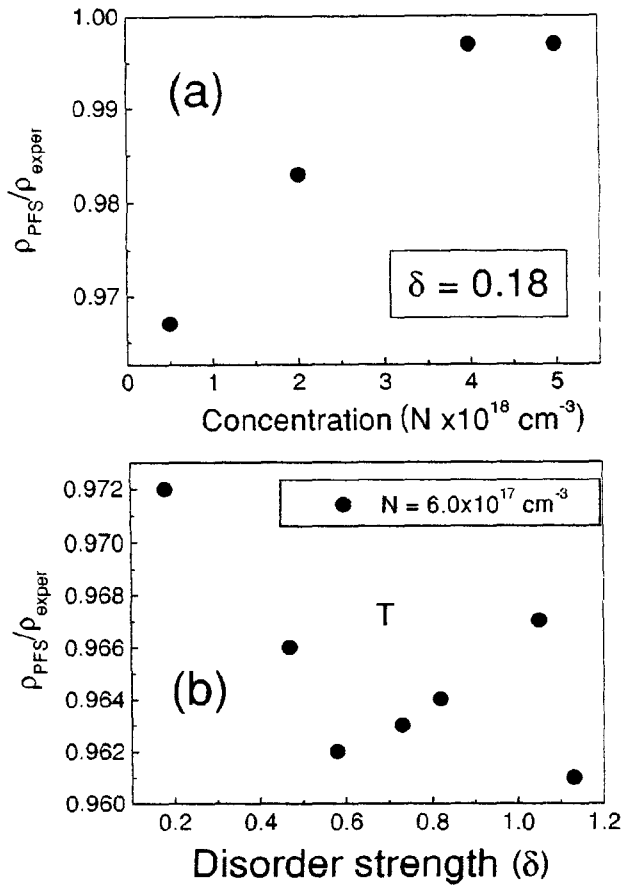
with relatively weak disorder, a tendency to the PFS regime was observed.

It also ought to be stressed that calculations of the quantum correction to the classical conductivity in the hopping conductivity regime, mentioned in Sec. I, yield a quadratic dependence for small magnetic fields, which does not account for the negative magnetoresistance observed here. Probably, this is caused by different characters of conductivities: the variable-range hopping transport considered in Refs. 6, 8, and 11 and the quasimetallic in-plane conductivity found in the studied here disordered doped superlattices.

The fitting of the magnetoresistance calculated in the DFS regime [Eq. (2) with $\delta' = \delta$, as explained in the end of Sec. II] to the experimental curves allowed us to obtain the decoherence time (τ_φ). The weak-localization parameters $D_\parallel \tau_\varphi$ corresponding to the best fitting were used to extract τ_φ when the diffusion coefficient $D_\parallel$ was determined by the measurements of the resistivity ρ_{xx} according to the Einstein relation for the degenerate electron gas. The values of the decoherence time measured as a function of the disorder strength and the doping concentration are shown in Figs. 6(a)
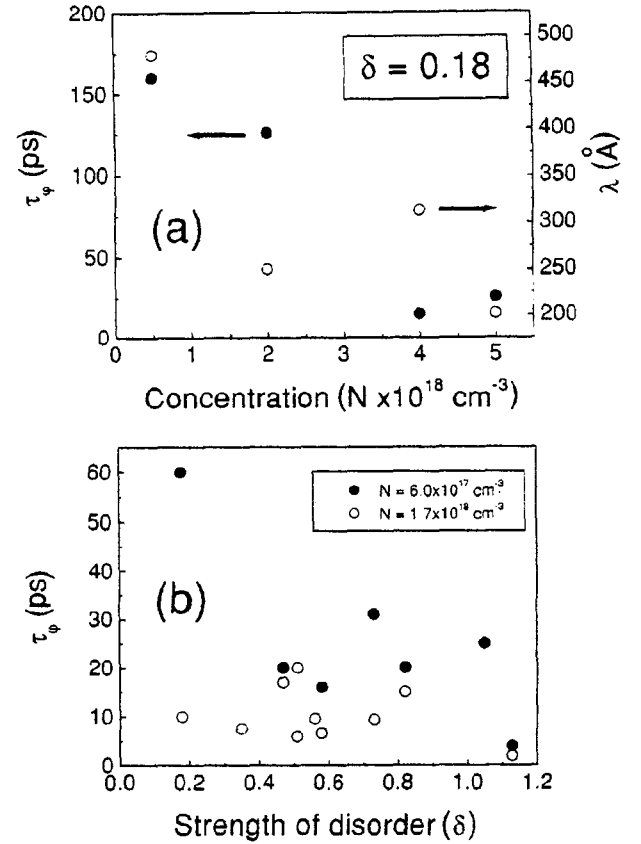
FIG. 6. Dephasing times obtained by the fitting of the magnetoresistance calculated in the DFS regime to the experimental magnetoresistances measured in the superlattices with a fixed disorder ($\delta = 0.18$) and different doping concentrations: (a) and with fixed doping concentrations ($N = 6.0 \times 10^{17}$ and 1.7×10^{18} cm^{-3}) and various disorder strengths (b). Open circles in (a) show the values of the electron mean free paths (λ) obtained by means of the conductivity measurements.

and 6(b). It is worth mentioning, that according to Ref. 28 expressions (1) and (2) obtained in the diffusion approximation overestimate the value of the weak-localization correction and therefore, the true values of the dephasing times is expected to be somewhat smaller than those obtained by the fitting. However, the qualitative behavior of the dephasing time will not change by this systematic error.

Usually, two contributions to the electron wave-function dephasing are considered: one due to the electron-electron interaction (τ_{ee}) and another one due to the electron-phonon interaction (τ_{ph}).[14,15] However, as is known, at low temperatures the electron-electron interaction produces the dominant contribution to the electron wave-function dephasing in the superlattices (see Ref. 29, and references therein). In accordance with Ref. 30, the rate of the electron-electron collisions depends on the value of momentum transfer. In the case of small momentum transfer $k \ll k_s$ (where k_s is the inverse screening length),

$$\frac{\hbar}{\tau_{ee,s}} = \left(\frac{k_B T}{k_F \lambda} \right)^{3/2} \frac{\sqrt{3}}{4\sqrt{E_F}}, \qquad (3)$$

FIG. 7. Relative magnetoresistances measured at various temperatures in the superlattices $(GaAs)_{17}(Al_{0.3}Ga_{0.7}As)_6$ with the electron concentration $N = 6.0 \times 10^{17}$ cm^{-3} and the disorder strength $\delta = 0.18$. The dashed lines were calculated in the DFS regime.

FIG. 8. Temperature dependencies of the dephasing time τ_φ measured in the disordered superlattices $(GaAs)_m(Al_{0.3}Ga_{0.7}As)_6$ with the electron concentration 6.0×10^{17} cm^{-3} and with different disorder strengths $\delta = 0.18$ (open circles) and $\delta = 1.05$ (closed circles).
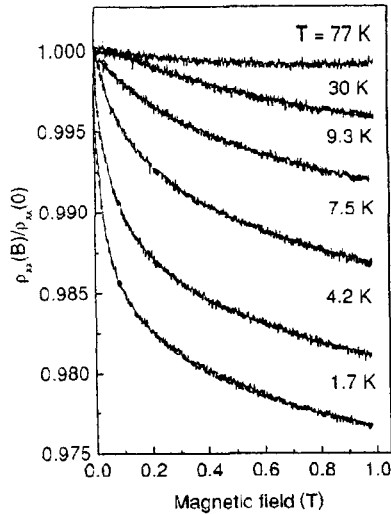
while processes with a large momentum transfer yield a scattering rate

$$\frac{\hbar}{\tau_{ee,L}} = \frac{(k_B T)^2}{\hbar E_F} \frac{k_\cdot}{k_F}. \qquad (4)$$

As follows from these expressions, the increase of the electron density should result in an increase of the dephasing time. Conversely, our experimental data presented in Fig. 6(a) exhibit the decrease of the dephasing time with an increase of the doping concentration. The observed decrease of the dephasing time can be associated with the dominant decrease of the mean free path in Eq. (4) with doping. The values of the electron mean free paths obtained by means of the parallel conductivity measurements, which are shown in Fig. 6(a) by open circles, indeed reveal a decrease with the increase of the doping. This shows that in weakly disordered superlattices collisions with small momentum transfers dominate. The same processes with the small momentum transfer probably govern the dependence of the dephasing time with the disorder strength found in the low-doped superlattices [closed circles in Fig. 6(b)], where the electron density is fixed while the mean free path decreases with increasing disorder. With an increase of the electron density the screening effects become stronger, resulting in a limitation of the momentum transfers. Therefore, the collisions with a large momentum transfer mainly contribute to the electron-electron scattering rate in the highly doped disordered superlattices where, according to Eq. (4), the dephasing time depends only on the electron concentration and the temperature which were fixed; therefore, $\tau_{ee,L}$ should not be influenced by disorder.

The temperature dependence of the magnetoresistance measured in the studied superlattices is shown in Fig. 7. An excellent accordance between the experimental data and the
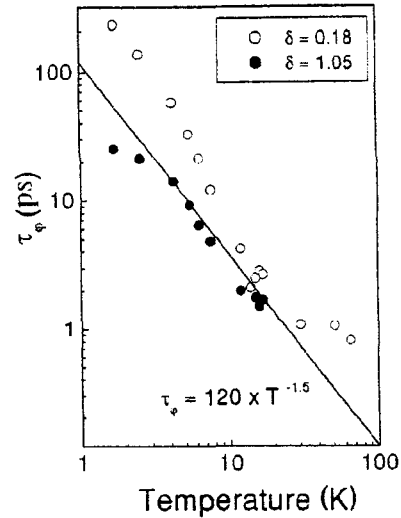
magnetoresistance calculated in the DFS regime [Eq. (2)] was found up to rather high temperatures. The values of the dephasing time τ_φ obtained at different temperatures by the fitting of the calculated magnetoresistance to the measured one are plotted in Fig. 8. At such temperatures the electron-electron interaction is expected to dominate in the dephasing process, yielding power dependencies (4) and (5) of the dephasing time on the temperature predicted theoretically in Ref. 30. In the relevant temperature range (between 1 and 10 K) the dependence corresponding to the small momentum transfers [Eq. (4)] was found in the regular GaAs/Al$_x$Ga$_{1-x}$As superlattices in Ref. 29. Our data do not clearly reveal such a power dependence; this implies that the dephasing processes in the presence of the strong localization and without it are probably different. The dependence of the dephasing time corresponding to Eq. (4) is shown in Fig. 8 as a reference.

We would like to point out that the effects of the diffusive Fermi surface observed here can influence the quantum interference even in the nominally regular superlattices where either the monolayer fluctuations or the interface roughnesses may provide the disorder. It is not clear whether or not such effects could be found in the superlattices studied in Ref. 29, where the measurements were presented in very weak magnetic fields. An indication of the discrepancy between the experiment and the theory can be found in Ref. 23, where the magnetoresistance of the short-period superlattices was studied in the magnetic fields up to 1 T.

Finally, we would like to discuss briefly a problem of the electron-electron interaction. An exhaustive analysis of the contributions from the interaction corrections to the conductivity of the superlattices was performed in Ref. 29. It was demonstrated that the electron-electron interaction effects cannot account for the negative magnetoresistance in superlattices at magnetic fields much lower than the elastic field

$B_{\perp} = \hbar/4eD_{\parallel}\tau_{\varphi}$, which in our case of the low-mobility samples is estimated to be equal to 7–12 T. A relatively small positive magnetoresistance superimposed on a large negative magnetoresistance can stem from the spin effects at fields much higher than $B_s = kT g^* \mu_B$, which is around 0.1 T in our case, while the orbital effects result in an insignificant contribution at low temperatures. Therefore, in the here studied superlattices we do not expect an appreciable influence of the electron-electron interaction effects to the measured negative magnetoresistance.

V. CONCLUSIONS

The processes of weak localization were studied in the intentionally disordered doped short-period GaAs/Al_xGa_{1-x}As superlattices where the disorder strength and the electron density can be controlled independently. Two different transport regimes were considered: the regime of weak disorder characterized by the propagative Fermi surface and the regime of strong disorder with the corresponding diffusive Fermi surface. For the low-doped disordered superlattices we found the diffusive transport regime, while a tendency to the propagative regime was observed with the increase of the electron concentration. This result manifests to itself in the influence of the vertical disorder on the quantum corrections to the in-plane conductivity of the semiconductor superlattices predicted in Ref. 20.

The decrease of the dephasing of the electron wavefunction was observed with the increase of both the doping concentration and the disorder strength, which suggests the importance of the electron-electron collisions with small momentum transfer. We did not find any significant influence of disorder on the dephasing process in the heavily doped superlattices, where the Fermi energy exceeded the random potential fluctuations. The temperature dependence of the dephasing time implies that the dephasing process observed in disordered GaAs/Al_xGa_{1-x}As superlattices is different from that found in regular superlattices.

[1] E. Abrahams, P.W. Anderson, D.C. Licciardello, and T.V. Ramakrishnan. Phys. Rev. Lett. **42**, 673 (1979).

[2] B.L. Al'tshuler and A.G. Aronov, Zh. Éksp. Teor. Fiz. **77**, 2028 (1979) [Sov. Phys. JETP **50**, 968 (1979)].

[3] B.L. Al'tshuler and A.G. Aronov, in *Electron-electron Interaction in Disordered Conductors*, edited by A.L. Efros and M. Pollak (North-Holland, Amsterdam, 1985).

[4] P.A. Lee and T.V. Ramakrishnan, Rev. Mod. Phys. **57**, 287 (1985).

[5] O. Farah and Z. Ovadyahu, Phys. Rev. B **38**, 5457 (1988).

[6] P. Kleinert and V.V. Bryksin, Phys. Rev. B **55**, 1469 (1997).

[7] V.I. Nguyen, B.Z. Spivak, and B.I. Shklovskii, Pis'ma Zh. Éksp. Teor. Fiz. **41**, 35 (1985) [JETP Lett. **41**, 42 (1985)].

[8] U. Sivan, O. Entin-Wohlman, and Y. Imry, Phys. Rev. Lett. **60**, 1566 (1988).

[9] D. Vollhardt and P. Wölfle, Phys. Rev. B **22**, 4666 (1980).

[10] V.V. Bryksin and P. Kleinert, Z. Phys. B: Condens. Matter **101**, 91 (1996).

[11] O. Bleibaum, H. Böttger, and V.V. Bryksin, Phys. Rev. B **64**, 104204 (2001).

[12] Z. Ovadyahu, Phys. Rev. B **33**, 6552 (1986).

[13] M. Benzaquen, D. Walsh, and K. Mazuruk, Phys. Rev. B **38**, 10 933 (1988).

[14] G. Bergmann, Phys. Rep. **107**, 1 (1984).

[15] T.A. Polyanskaya and Yu. V. Shmartsev, Fiz. Tekh. Poluprovodn. **23**, 3 (1989) [Sov. Phys. Semicond. **23**, 1 (1989)].

[16] G.M. Minkov, O.E. Rut, A.V. Germanenko, A.A. Sherstobitov,

V.I. Shashkin, O.I. Krohin, and V.M. Daniltsev, Phys. Rev. B **64**, 235327 (2001).

[17] P.T. Coleridge, A.S. Sachrajda, and P. Zawadzki, Phys. Rev. B **65**, 125328 (2001).

[18] J.D. Dow, S.Y. Ren, and K. Hess, Phys. Rev. B **25**, 6218 (1986).

[19] A. Chomette, B. Deveaud, A. Regreny, and G. Bastard, Phys. Rev. Lett. **57**, 1464 (1986).

[20] A. Cassam-Chenai and D. Mailly, Phys. Rev. B **52**, 1984 (1995).

[21] W. Szott, C. Jedrzejek, and W.P. Kirk, Phys. Rev. Lett. **63**, 1980 (1989).

[22] A.B. Gougam, J. Sicart, and J.L. Robert, J. Phys. III (France) **7**, 133 (1997).

[23] A.B. Gougam, J. Sicart, J.L. Robert, and B. Etienne, Phys. Rev. B **59**, 15 308 (1999).

[24] W. Szott, C. Jedrzejek, and W.P. Kirk, Phys. Rev. B **40**, 1790 (1989).

[25] A. Kawabata, J. Phys. Soc. Jpn. **49**, 628 (1980).

[26] Yu.A. Pusep, W. Fortunato, P.P. Gonzalez-Borrero, A.I. Toropov, and J.C. Galzerani, Phys. Rev. B **63**, 115311 (2001).

[27] W. Szott, E. Palm, and W.P. Kirk, Bull. Am. Phys. Soc. **33**, 821 (1988).

[28] G.M. Minkov, A.V. Germanenko, V.A. Larionova, S.A. Negashev, and I.V. Gornyi, Phys. Rev. B **61**, 13 164 (2000).

[29] W. Szott, C. Jedrzejek, and W.P. Kirk, Phys. Rev. B **48**, 8963 (1993).

[30] B.L. Al'tshuler and A.G. Aronov, Pis'ma Zh. Éksp. Teor. Fiz. **30**, 514 (1979) [JETP Lett. **30**, 482 (1979)].

PUSEP, Y. A.; CHIQUITO, A. J.; MERGULHAO, S.; TOROPOV, A. I. Parallel conductivity of random GaAs/AlGaAs superlattices in regime of controlled vertical disorder. **Journal of Applied Physics**, College Park, v.92, n.7, p.3830-3834, Oct. 2002.

Anisotropy of quantum interference in disordered GaAs/Al$_x$Ga$_{1-x}$As superlattices

Yu. A. Pusep,[1] M. B. Ribeiro,[1] H. Arakaki,[1] C. A. de Souza,[1] P. A. Zanello,[1] A. J. Chiquito,[2] S. Malzer,[3] and G. H. Döhler[3]

[1]*Instituto de Física de São Carlos, Universidade de São Paulo, 13560-970 São Carlos, São Paulo, Brazil*

[2]*Departamento de Física, Universidade Federal de São Carlos, Caixa Postal 676, 13565-905 São Carlos, Brazil*

[3]*Institut für Technische Physik I, Universität Erlangen, D-91058 Erlangen, Germany*

(Received 23 May 2003; revised manuscript received 22 August 2003; published 19 November 2003)

The influence of the anisotropic disorder on quantum interference was studied in the intentionally disordered GaAs/Al$_x$Ga$_{1-x}$As superlattices. In the case of sufficiently strong disorder the quantum interference exhibited a structural dependence resulting in the anisotropy of the phase-breaking time, which was found shorter in the direction of the disorder. The anisotropy effects were shown stronger in the insulating transport regime than in the metallic one. The weak-localization negative magnetoresistance was used to obtain the vertical coupling constant in the disordered superlattices.

I. INTRODUCTION

The disorder plays a considerable role in quantum interference processes of the conduction electrons providing the random potential responsible for their coherent scattering. In this way, the localization of the electrons can be represented as a product of the interference between two probability amplitudes for electrons propagating in opposite directions.[1] In the limit of weak disorder (when $k_F l \gg 1$, where k_F and l are the Fermi wave number and the mean free path, respectively) the quantum interference results in the weak localization giving the correction to the classical conductivity of the order of 1%. In this case the quantum interference was found noteworthy dependent on the strength of the scattering potential ensuing in a decrease of the phase-breaking time τ_φ with the decreasing elastic-scattering time τ (Ref. 2 and references therein).

When the disorder is strong such that diffusion vanishes, the interference of scattered electrons becomes even more essential resulting in the conductivity correction approaching the classical conductivity.[3] In such a case the quantum interference has to be strongly sensitive to the microscopic features of the localization potential, thus revealing the structural dependence of such an important characteristic parameter of the quantum interference as the phase-breaking time τ_φ.

The artificially structured multilayer semiconductor systems such as superlattices (SL's) are excellent candidates to verify an effect of the material arrangement on the quantum interference. The influence of the microscopic material features of periodic SL's, such as the width of the barriers, on the quantum interference effects was already studied in Refs. 4 and 5. In the present work, in order to investigate the influence of the material structure on the quantum interference, we examined intentionally disordered GaAs/Al$_x$Ga$_{1-x}$As SL's. In this case the vertical disorder potential (parallel to the growth direction) was provided by the controlled random variation of the well thicknesses. The essential microscopic feature of such a disorder is its one dimensionality and consequently, anisotropy. In this case the control of the coherency of the electron states along the growth direction is possible. In the structures with suffi-

ciently strong vertical disorder the corresponding anisotropy of the quantum interference is expected.

The SL's considered above present the properties of the three-dimensional anisotropic electron system with the coefficient of the anisotropy $\alpha = \sqrt{D_\parallel / D_z}$, where $D_\parallel$ and D_z are the diffusion coefficients parallel and perpendicular to the layers, respectively. In such an anisotropic electron system, in the limit of weak localization, the anisotropy of the negative magnetoresistance is anticipated due to the different coherent surfaces enclosing the magnetic-field fluxes at different orientations of the magnetic field. We demonstrate that in the metallic weak-localization regime both the diffusion coefficient and the phase-breaking time contribute to the disorder dependence of the quantum interference. Furthermore, the anisotropy of the quantum interference was found much stronger in the insulating regime than in the metallic one.

II. THEORY

Depending on the structure of a SL, three different regimes of the quantum transport can be distinguished. Two weak-localization regimes (in the notation of Ref. 6), when $k_F l > 1$: (i) the propagative Fermi-surface (PFS) regime when $t_z \tau > \hbar$ (with t_z being the vertical coupling energy, which in a regular SL is equal to the miniband width) and (ii) the diffusive Fermi surface (DFS) one, when $t_z \tau < \hbar$, and (iii) the regime of strong localization, when $k_F l < 1$. The DFS transport regime corresponds to the quasi-two-dimensional electron system formed in the SL with the open Fermi surface. The vertical disorder decreasing the vertical coupling energy also favors the DFS regime.

In a weak magnetic field orthogonal to the plane of the layers the weak-localization corrections to the parallel conductivity are determined by the following expressions. In the PFS regime[7]

$$\Delta \sigma_{PFS}(H) = \frac{e^2}{2\pi^2 \hbar l_H} \alpha F(\delta) \qquad (1)$$

and in the DFS regime[6]

$$\Delta\sigma_{DFS}(H) = -\frac{e^2}{2\pi^2\hbar d_{SL}}F(\delta,\delta'), \qquad (2)$$

where $l_H = \sqrt{\hbar/eH}$ is the magnetic length, d_{SL} is the superlattice period, $F(\delta) = \Sigma_{n=0}^{\infty}2[(n+1+\delta)^{1/2} - (n+\delta)^{1/2}] - (n+\frac{1}{2}+\delta)^{-1/2}$ is the Kawabata function,[8] $F(\delta,\delta') = \Sigma_{n=0}^{\infty}1/\sqrt{n+\frac{1}{2}} + \delta\sqrt{n+\frac{1}{2}+\delta'} - 2\ln(\sqrt{n+1+\delta} + \sqrt{n+1+\delta'}) + 2\ln(\sqrt{n+\delta} + \sqrt{n+\delta'})$, with $\delta = l_H^2/4D_\parallel\tau_\varphi$ and $\delta' = (l_H^2/4D_\parallel)(1/\tau_\varphi + 2/\tau_0)$ with $\tau_0 = \hbar^2/t_z^2\tau$ being the time an electron needs to change a layer. Thus, two characteristic times (τ_φ and τ_0) determine DFS regime and the relationship between them establishes the transport regime coherency of a SL. In the coherent regime, when $\tau_\varphi > \tau_0$ an electron coherently changes a plane, while in the incoherent regime when $\tau_\varphi < \tau_0$ the SL behaves as a set of independent planes.

In both the cases (PFS and DFS) the conductivity corrections in the magnetic field parallel to the layers can be obtained by scaling the field according to the relation

$$B_\parallel = B_z/\alpha, \qquad (3)$$

which corresponds to a decrease of a magnetic-field flux quantum piercing the coherent surface ($L_{\varphi\parallel}^2$ in the case of the field perpendicular to the layers and $L_{\varphi\parallel}L_{\varphi z} = L_{\varphi\parallel}^2/\alpha$ for the parallel field). The corrections to the vertical conductivity can be calculated using the scaling relation[7,9]

$$\frac{\sigma_\parallel(B)}{\sigma_\parallel(0)} = \frac{\sigma_z(B)}{\sigma_z(0)}, \qquad (4)$$

which should be valid as long as the coherence relations $\tau_\varphi \gg \tau, \tau_0$ hold.

On the other hand, at a strong disorder ($k_F l \lesssim 1$) and in a weak magnetic field the self-consistent approach gives[10]

$$\Delta\sigma(H) = \frac{e^2\delta^{-3/2}(\cos^2\varphi + \alpha^2\sin^2\varphi)}{192\pi^2\hbar\alpha l_H}, \qquad (5)$$

where φ is the angle between the magnetic-field direction and the growth direction. In this case the quantum correction arises due to the interference between the probability amplitudes for direct hopping transitions involving the localized states caused by disorder.

As we have already shown,[11] the metallic regime (DFS or PFS) exhibits a very different weak-field magnetoresistance than that of the insulating one; they are characterized by the negative and positive concavities, respectively. Moreover, the much weaker temperature dependence of the dephasing time was found in the insulating regime in contrast to what was detected in the weak-localization metallic regime. The different magnetoresistances and different temperature behaviors of the dephasing times observed in the metallic and insulating electron systems are manifestations of the different character of the quantum interferences.

In this work we prove the effects of the anisotropy of the weak-field magnetoresistance in the SL's in different quantum transport regimes. According to Eqs. (3) and (4), such an anisotropy follows from the directional dependence of the

diffusion coefficient and from the anisotropy of the phase-breaking time. The diffusion coefficient determines the conductivity, while both the diffusion coefficient and the phase-breaking time influence the coherent length L_φ. Our purpose was (i) to verify the scaling relations (3) and (4) in SL's—the electron systems where the anisotropy of the energy and disorder can be controlled and (ii) to distinguish the effect of the anisotropy on the quantum interference.

In order to determine the character of the transport regime, the resistances as functions of the temperature were studied. The insulating case is described by the exponential activation-type temperature dependence. As it was shown in Ref. 11, in the disordered SL's it corresponds to the Mott's law for variable-range hopping:[12]

$$\rho(T) = \rho_0 \exp\left[\left(\frac{T_0}{T}\right)^{1/4}\right], \qquad (6)$$

where T_0 is the characteristic temperature.

While, in the metallic SL's different contributions to the temperature behavior of conductivity can be distinguished depending on which regime (PFS or DFS) is relevant.[6]

The weak increase of the conductivity with the increasing temperature caused by the temperature destruction of the quantum interference is predicted in the PFS regime[1]

$$\sigma^{PFS}(T) = \sigma_0 + \frac{\alpha e^2}{2\pi^2\hbar a}T^{p/2}, \qquad (7)$$

where σ_0 is the Drude classical conductivity, a is the coefficient in the temperature dependence of the phase-breaking length $L_\varphi = aT^{-p/2}$, and p is the index depending on the scattering mechanism.

In the coherent DFS regime[6]

$$\sigma^{DFS}(T) = \sigma_0 - \frac{\alpha e^2}{2\pi^2\hbar d_{SL}}\ln\left(\frac{\tau_0}{\tau}\right) - \frac{\alpha e^2\ln 2}{2\pi^2\hbar}\frac{1}{l_0} + \frac{\alpha e^2}{2\pi^2\hbar}\frac{1}{L_\varphi}, \qquad (8)$$

where at low temperatures the temperature dependence of the quantum correction to the conductivity may emerge from the terms containing τ_0 (or l_0) and L_φ.

Whereas, the logarithmic temperature behavior characteristic for the two-dimensional electron system is expected in the incoherent DFS limit.

In addition, in both metallic regimes the semiclassical contribution discussed in Ref. 13 may also account for the observed temperature dependence of the conductivity. This semiclassical correction to the conductivity arises in metallic electron system due to the deviation of the chemical potential from the Fermi energy:[14]

$$\Delta\sigma^{sc}(T) = \frac{\pi^2 e^2\tau}{6m^*}(k_B T)^2 g'(E_F), \qquad (9)$$

where m^* is the effective mass. This part of the conductivity depends on the position of the Fermi level. It may significantly contribute at the edges of the relevant miniband, while it is zero for the SL with the open Fermi surface where the Fermi energy is located in the gap.

TABLE I. Parameters of disordered superattices measured at $T = 1.6$ K.

Samples	δ_{SL}	$n_H(cm)^{-3}$	$\mu_H(cm^2/Vs)$	$k_F l$
DSL198	0.18	6.9×10^{17}	600	2.2
DSL192	0.47	6.7×10^{17}	1400	5.1
DSL197	0.73	6.4×10^{17}	946	3.4
DSL194	0.82	7.0×10^{17}	1340	4.9
DSL196	1.05	2.9×10^{17}	4067	14.8
DSL193	1.13	3.9×10^{16}	1500	5.4
DSL865	0.35	1.3×10^{18}	1660	8.9
DSL866	0.59	1.2×10^{18}	1710	9.2
DSL871	0.82	1.2×10^{18}	1980	10.7
DSL873	1.13	9.9×10^{17}	2040	11.0
SL2102		5.1×10^{17}	2510	10.2
SL2702		7.1×10^{16}	450	0.42

III. EXPERIMENT

The samples here studied were the $(GaAs)_m(Al_{0.3}Ga_{0.7}As)_6$ SL's (where the thickness of the layers is expressed in monolayers) grown by molecular-beam epitaxy simultaneously on semi-insulating and doped (001) GaAs substrates. In order to form the degenerate electron system all the samples were homogeneously doped with Si. The samples with the nominal doping 7.0×10^{17} cm^{-3} (DSL192-198) and 1.2×10^{18} cm^{-3} (DSL865-873) were studied. According to the calculations, the low and high dopings result in the closed and open Fermi surfaces, respectively. The disorder was introduced by a random variation of the well thicknesses m around the nominal value 17 ML (monolayer). The disorder strength was characterized by the disorder parameter $\delta_{SL} = \Delta/W$, where Δ is the full width at half maximum of a Gaussian distribution of the electron energy calculated in the isolated quantum wells and W is the miniband width of the nominal SL in the absence of disorder. Details of the sample growth and characterization can be found in Ref. 15.

In order to study the anisotropy of the quantum transport we measured the parallel and vertical magnetoresistances with different orientations of the magnetic field. The samples were patterned into Hall bars or square shaped mesa structures with areas 1×1 mm^2, both prepared by standard lithography and chemical etching. The Ohmic contacts were fabricated by depositing In or an Au-Ge-Ni alloy. Parallel transport measurements were performed using standard four-probe low-frequency (5 Hz) lock-in technique in a pumped liquid-He cryostat in magnetic fields directed perpendicular and parallel to the layers at the temperatures from 1.6 K to 15 K. The vertical transport was measured in the low doped samples using two terminals. The parameters of the samples are listed in Table I where all the data relate to the parallel transport measurements. According to these data the characteristic magnetic fields when $\omega_c \tau = 1$ were found in the interval $2 - 21$ T in all the samples under investigation and hence, the weak-field condition $\omega_c \tau \ll 1$ holds at the magnetic fields used. Therefore, no negative magnetoresistance due to the electron-electron interaction effects is expected.
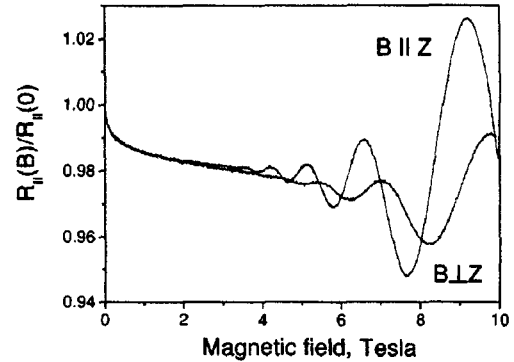

FIG. 1. High-field relative parallel magnetoresistances measured in the disordered superlattice $(GaAs)_m(Al_{0.3}Ga_{0.7}As)_6$ with $n_H = 6.7 \times 10^{17}$ cm^{-3}, $\delta_{SL} = 0.47$, $T = 1.6$ K with different orientations of the magnetic field.

The estimation of the appropriate characteristic magnetic field[1] shows that the spin effects also do not contribute to the magnetoresistances studied here. The orbital effects produce positive magnetoresistance in the magnetic fields $B_t > B > B_e$ there $B_t = \hbar D/ \pi k_B T$ and $B_e = \hbar/4eD\tau$ are the characteristic thermal and elastic fields, respectively. The corresponding characteristic magnetic fields are given in the figures for the samples where they fall into the interval of the experimental fields. In these samples the orbital effects are insignificant due to the narrowness of the magnetic-field intervals where they are anticipated.[13] The strong localization manifests itself in the decrease of the Hall electron concentration in the SL's with the highest disorder. In these SL's the interface roughness important in the thinnest wells may cause the localization effects observed in the parallel conductivity.

Basing on the Hall data, in all the SL's we found the ratio $t_z \tau/\hbar \approx 2 - 11$, with $t_z = W$. However, the vertical disorder destroys the coherency of the electrons in the neighboring wells and, consequently, decreases the coupling between them. Therefore, in the disordered SL's the coupling constant t_z is expected to be considerably smaller than the miniband width of the nominal regular SL. As we already found, in such disordered SL's the regime of the quantum transport corresponds to DFS, in fact implying in $t_z \tau/\hbar < 1$.[15]

In addition, two (regular) SL's exhibiting two extreme cases of the metallic PFS regime and the insulating one were studied. The PFS regime was observed in the $(GaAs)_{150}(Al_{0.7}Ga_{0.3}As)_6$ superlattice (SL2102) where the distances between the minibands were of the same order as $\hbar/\tau$ and hence, the bulklike electron energy spectrum emerges. While, the insulating behavior was found in the low doped $(GaAs)_{15}(Al_{0.7}Ga_{0.3}As)_6$ superlattice (SL2702) where the short-range scattering due to the interface roughness was responsible for the electron localization.[11] In spite of the regular structure of the insulating SL, the unavoidable monolayer fluctuations provided the vertical disorder with the strength $\delta_{SL} = 0.18$.

In all of the metallic samples we observed the Shubnikov–de Haas oscillations (shown in Fig. 1 for a selected SL) with both orientations of the magnetic field: parallel and perpendicular to the growth direction z. This con-
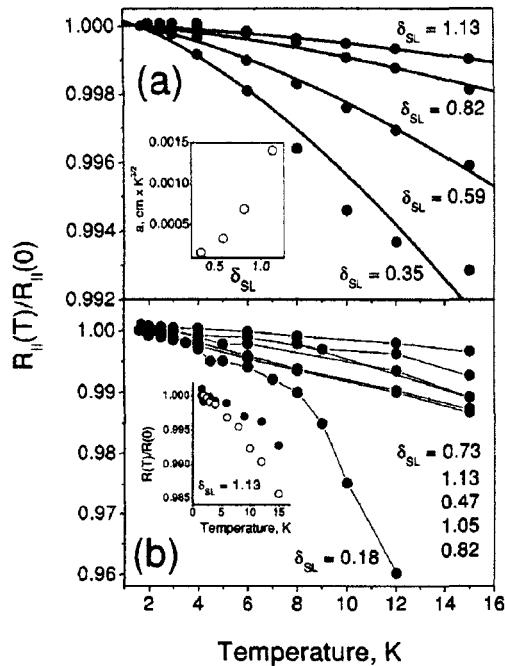
FIG. 2. Temperature dependences of the relative parallel resistances measured in the superlattices $(GaAs)_{n_i}(Al_{0.3}Ga_{0.7}As)_6$ with a nominal doping 1.2×10^{18} cm^{-3} (a) and 7.0×10^{17} cm^{-3} (b) and with different strengths of the vertical disorder δ_{SL}. The full lines in the panel (a) are the relative resistances calculated according to Eq. (7) with $p = 3$. While, lines in the panel (b) are the connections between the experimental points. Inset to the panel (a) demonstrates the variation of the fitting parameter a with the disorder strength while, inset to the panel (b) shows the parallel (closed circles) and vertical (open circles) relative resistances measured in the superlattices with the doping 7.0×10^{17} cm^{-3} and $\delta_{SL} = 1.13$, respectively.

firms three dimensionality of the samples and consequently, the coherency of the transport regimes implying in the condition $\tau_\varphi > \tau_0$.

IV. RESULTS AND DISCUSSION

An exhaustive analysis of the temperature effects on the zero-field conductivity of the periodic superlattices was presented in Ref. 13 . It was shown that in this case the electron-electron interaction is irrelevant because the observed positive variation of the conductivity with the increasing temperature was not accompanied by the corresponding decrease of the Hall constant. This implies that the contributions from exchange effects and from direct interactions, which enter the conductivity with opposite signs, nearly cancel one another. A similar behavior was found in the disordered SL's studied here, whence we concluded that the effect of the electron-electron interaction does not influence their zero-field conductivity.

The considerable effect of the disorder on the temperature behavior of the parallel resistances measured in the disordered SL's in the DFS transport regime is shown in Fig. 2. The disorder reduces the temperature dependence of the resistance in the highly doped SL's. While, no systematic in-

fluence of the disorder was found in the low doped SL's where only the SL with $\delta_{SL} = 0.18$ demonstrated a strong dependence at the temperatures higher than 8 K, probably caused by some intrinsic defects which also considerably decreased the Hall mobility measured in this SL.

The observed temperature dependences of the resistances show a weak decrease with the increasing temperature exhibiting the metallic behavior. In the SL's with the open Fermi surfaces the semiclassical correction vanishes and the quantum corrections contribute according to Eq. (8). At this, both characteristic times τ_φ and τ_0 can be responsible for the measured temperature dependences. However, the second and the third terms in Eq. (8) may partially compensate one another diminishing the effect of τ_0; then, the decoherence time dominates the temperature dependence of the quantum correction. The resistances calculated by Eq. (4) for the electron-phonon inelastic scattering ($p = 3$), shown in Fig. 2(a) by solid lines, demonstrate good agreement with the experimental data. The variation of the fitting parameter a with the disorder strength is illustrated in the inset to Fig. 2(a). The decrease of the quantum correction to the conductivity found with the increasing vertical disorder is consistent with the corresponding increase of the parallel mobility. Such effect of the enhancement of the parallel mobility in intentionally disordered SL's is caused by the effective suppression of the vertical disorder due to the redistribution of electrons over the vertical random potential.[16]

The interplay between all the considered contributions determines the temperature behavior of the quantum corrections in the low doped SL's with the closed Fermi surfaces [the data are shown in Fig. 2(b)]. A variety of these contributions, each of them depending on the disorder strength δ_{SL}, does not allowed us to distinguish which one is actually significant. Probably, in this case the semiclassical correction, which is absent in the highly doped SL's and which complicatedly depends on the disorder through the density of states, may cause the observed nonsystematic variation of the quantum correction with the disorder.

The inset in Fig. 2(b) shows the parallel (closed circles) and vertical (open circles) resistances as functions of the temperature measured in the equivalent SL's with the doping 7.0×10^{17} cm^{-3} and $\delta_{SL} = 1.13$. As expected, the vertical disorder influences the temperature dependence of the vertical resistance stronger than of the parallel one.

The temperature behavior of the SL's with the insulating and PFS regimes followed the corresponding theoretical dependences (6) and (7) with the characteristic temperature of the variable-range hopping $T_0 = 0.25$ K, and the index $p = 3$ implying in the electron-phonon interaction as a dominant mechanism for the dephasing in the weak-localization regime.

The weak-field magnetoresistances measured in the SL's with different disorder strengths are depicted in Fig. 3 where the parallel (a, b) and vertical (c) magnetoresistance traces are shown. In this case a noteworthy anisotropy of the magnetoresistance was detected. As it is seen, the vertical disorder does not significantly influence the parallel magnetoresistance. However, a suppression of the negative magnetoresistance by disorder implying in a decrease of the
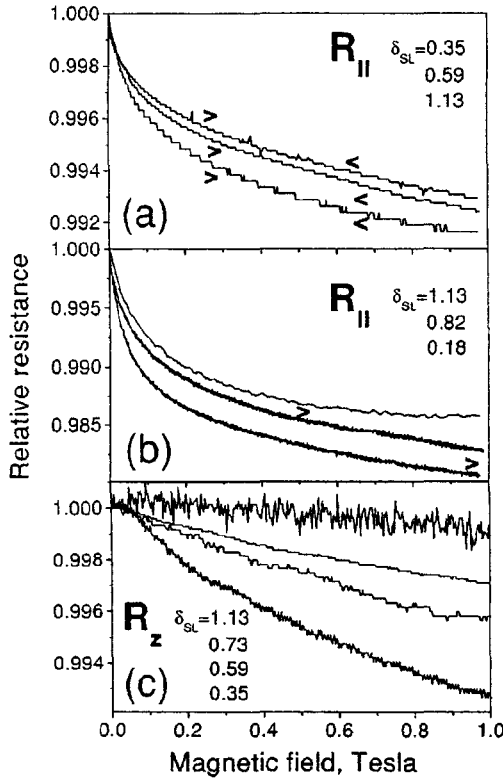
FIG. 3. Relative magnetoresistances measured parallel to the layers in the superlattices $(GaAs)_m(Al_{0.3}Ga_{0.7}As)_6$ with different disorder strengths: (a) with a nominal doping 1.2×10^{18} cm^{-3} and (b) - with a nominal doping 7.0×10^{17} cm^{-3}. The vertical magnetoresistances measured in similar disorder superlattices with a nominal doping 7.0×10^{17} cm^{-3} are depicted in (c). The marks "larger" and "smaller" indicate the characteristic fields B_l and B_e, respectively.

phase coherency length L_φ with the increasing disorder was found in the vertical magnetoresistances.

As it was mentioned above, the DFS regime governs quantum transport in the disordered SL's studied here. This entails the use of Eq. (2) for a fit to the experimental data. The coherency of the electron transport in the disordered SL's, which means $\tau_\varphi > \tau_0$, was confirmed by the Shubnikov–de Haas measurements. Therefore, the time τ_0 controls quantum interference in this case. The parallel magnetoresistances measured in one of the disordered SL's with different orientations of the magnetic field are depicted in Fig. 4. In agreement with the theory, the magnetoresistance measured with the magnetic field parallel to the layers was found weaker than that one with the perpendicular field. In this case the anisotropy is completely assigned to the anisotropy coefficient, because the time τ_0 may be considered independent of the weak magnetic field. In the fitting the parallel magnetic field was scaled with $\alpha = 2$, which is close to the anisotropy coefficient $\alpha_{calc} = 1.3$ calculated for the nominal superlattice with the same electron concentration as in the studied disordered SL. The best fittings of the magnetoresistance records were obtained at both orientations of the magnetic field with the same value $\tau_0 = 320$ fs, while the

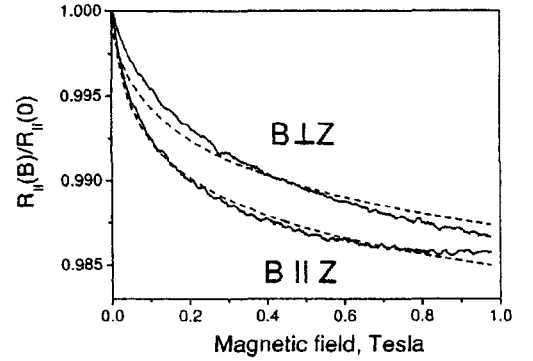FIG. 4. Relative parallel magnetoresistances measured in the superlattice $(GaAs)_m(Al_{0.3}Ga_{0.7}As)_6$ with $n_H = 3.9 \times 10^{17}$ cm^{-3} and $\delta_{SL} = 1.13$ at $T = 1.6$ K, with different orientations of the magnetic field. The dashed lines were calculated by Eq. (2) in the coherent limit $\tau_\varphi > \tau_0$ with $\tau_0 = 0.32$ ps. The parallel magnetic field was scaled with the anisotropy coefficient $\alpha = 2$.

value of the characteristic time τ_0 calculated with $l_z = W$ yields 2.3 fs, which is ≈ 140 times shorter. This indicates that the coupling constant is more than ten times smaller than the miniband width and demonstrates the influence of the vertical intentional disorder on the coupling between electrons in the neighboring quantum wells. Thus, the investigation of the weak-field magnetoresistance provides a way to measure the coupling constant in disordered SL's.

The influence of the orientation of the magnetic field on the vertical magnetoresistance is displayed in Fig. 5. Again, the observed anisotropy was found in qualitative accordance with the theory. However, as it is shown by dashed lines, in this case it was not possible to fit the experimental data with formula (2) in the coherent limit $\tau_\varphi > \tau_0$. On the other hand, a good fitting represented by full lines can be obtained with
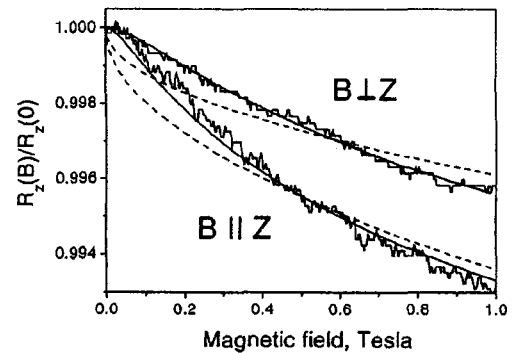
FIG. 5. Relative vertical magnetoresistances measured in the superlattice $(GaAs)_m(Al_{0.3}Ga_{0.7}As)_6$ with a nominal doping 7.0×10^{17} cm^{-3} and $\delta_{SL} = 0.59$, $T = 1.6$ K, with different orientations of the magnetic field. The dashed lines were calculated by Eq. (2) in the coherent limit with $D\tau_0 = 4.6 \times 10^{-12}$ cm^2 and $D\tau_0 = 8.6 \times 10^{-12}$ cm^2 for the magnetic field parallel and perpendicular to the layers, respectively. While, the full lines were calculated by Eq. (2) at $\tau_0 = \tau_\varphi$ with $D\tau_0 = 7.0 \times 10^{-11}$ cm^2 and $D\tau_0 = 1.0 \times 10^{-10}$ cm^2 at the magnetic field parallel and perpendicular to the layers, respectively. The parallel magnetic field was scaled with the calculated anisotropy coefficient $\alpha = 1.4$.
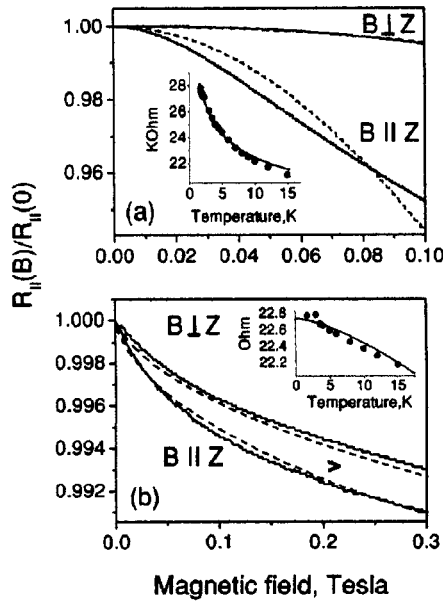
FIG. 6. Relative parallel magnetoresistances measured at T = 1.6 K with different orientations of the magnetic field in the insulating superlattice $(GaAs)_{15}(Al_{0.3}Ga_{0.7}As)_6$ (a) and in the metallic superlattice $(GaAs)_{150}(Al_{0.3}Ga_{0.7}As)_6$ with the PFS transport regime (b). The dashed lines are the dependences of the resistance on the magnetic field calculated with the following fit parameters: (a) $B{\perp}Z$—$\tau_\varphi = 1.5$ ps, $\alpha = 3$; $B{\parallel}Z$—$\tau_\varphi = 38$ ps and (b) $B{\perp}Z$—$\tau_\varphi = 60$ ps; $\alpha = 1.3$; $B{\parallel}Z$—$\tau_\varphi = 80$ ps, $\alpha = 1.4$. The mark "larger" indicates the characteristic field B_t. The insets show the corresponding temperature dependences of the parallel resistances.

$\tau_\varphi \approx \tau_0$. In such a case both of these times act in a similar way and therefore, Eq. (2) does not give a possibility to fix these two fit parameters. Nevertheless, this result indicates a possible anisotropy of the dephasing time in the intentionally disordered SL's: in the disorder direction τ_φ may be shorter than in the plane of the layers. Whereas, the time τ_0, which determines how long an electron move in the same layer before changing it, is directionally independent. Thus, while the coherence relation $\tau_\varphi > \tau_0$ holds for the parallel transport, it may fail for the vertical one—the effect found in the vertical magnetoresistance of the disordered SL in Fig. 5. The data shown in Fig. 3, which reveal a stronger effect of the vertical disorder on the vertical magnetoresistance than on the parallel one, are also consistent with this conclusion.

In order to provide an additional evidence of the influence of disorder on quantum interference, we measured the weak-field magnetoresistance in two SL's where the transport regimes correspond to two limiting cases: the metallic PFS transport regime and the insulating one. In the first case we do not expect that the anisotropy will strongly affect the dephasing time, while in the second one the anisotropic character of the disorder may result in the significant anisotropy of the phase-breaking time. The magnetoresistances measured in the metallic and insulating SL's with different orientations of the magnetic fields are shown in Figs. 6(a) and 6(b). The character of the transport (metallic or insulating) manifests itself in the temperature dependences of the resistances depicted in insertions. As it was mentioned above, the

fits of the temperature dependences of the resistances were performed with Eqs. (6) and (7) in the insulating and metallic SL's, respectively, while the fits of the magnetoresistance traces were achieved with the PFS formula (1) and with Eq. (5) in the metallic and insulating SL's, respectively. In the last case the coefficient of the anisotropy was fixed to the calculated value $\alpha = \sqrt{m_z/m_{\parallel}} \approx 3$. The obtained data exhibit no considerable anisotropy of the dephasing time in the metallic SL, while a strong anisotropy effect was observed in the insulating SL. This means that indeed, in the insulating superlattice the anisotropic vertical disorder results in a strong suppression of the quantum interference in the vertical direction.

As it was discussed in Ref. 2, in the presence of disorder the phase-breaking time reveals a dependence on the inelastic-scattering time. In the studied here disordered superlattices a possible anisotropy of the electron scattering might be responsible for the observed anisotropy of the quantum interference. Moreover, as it was pointed out in Ref. 6, in the DFS regime the weak-localization correction contains two contributions: one from the purely two-dimensional anisotropic loops in the planes of the layers and another is the usual three-dimensional anisotropic part. The strong disorder along the growth direction changes the dimensionality of the electron system thus, alternating the relative contributions of the two- and three-dimensional parts and resulting in the anisotropy of the quantum interference.

V. CONCLUSIONS

The quantum interference was studied in the intentionally disordered $GaAs/Al_xGa_{1-x}As$ SL's where the anisotropic disorder was produced along the growth direction by a random variation of the well thicknesses. Such a disorder determines a peculiar direction along which the coherency of the electron states can be controlled. The magnetotransport experiments were performed with the current parallel and vertical to the layers and with different orientations of the magnetic field. The presented results demonstrate validity of the scaling relations used to describe the magnetoresistance of the anisotropic electron system. The observed anisotropy of the weak-field magnetoresistance stems from the anisotropy of the phase coherency length L_φ which, in turn, is determined by the directional dependences of the diffusion coefficient and the phase-breaking time. The fitting of the vertical random superlattice potential allowed us to distinguish the influence of the disorder on the phase-breaking time and thus, on the quantum interference. The vertical coupling constant of the intentionally disordered superlattice, determined by the analysis of the weak-localization negative magnetoresistance, was found to be one order of magnitude smaller than the miniband width calculated in the periodic superlattice. Our results show that the vertical disorder suppresses quantum interference in the superlattices, reducing the quantum correction to the classical conductivity.

[1] P.A. Lee and T.V. Ramakrishnan, Rev. Mod. Phys. **57**, 287 (1985).

[2] R.A. Davies and M. Pepper, J. Phys. C **16**, L353 (1983).

[3] B.L. Al'tshuler and P.A. Lee, Phys. Today **41** (12), 36 (1988).

[4] W. Szott, C. Jedrzejek, and W.P. Kirk, Phys. Rev. Lett. **63**, 1980 (1989).

[5] A.B. Gougam, J. Sicart, J.L. Robert, and B. Etienne, Phys. Rev. B **59**, 15 308 (1999).

[6] A. Cassam-Chenai and D. Mailly, Phys. Rev. B **52**, 1984 (1995).

[7] W. Szott, C. Jedrzejek, and W.P. Kirk, Phys. Rev. B **40**, 1790 (1989).

[8] A. Kawabata, J. Phys. Soc. Jpn. **49**, 628 (1980).

[9] R.N. Bhatt, P. Wölfle, and T.V. Ramakrishnan, Phys. Rev. B **32**, 569 (1985).

[10] V.V. Bryksin and P. Kleinert, Z. Phys. B: Condens. Matter **101**, 91 (1996).

[11] Yu. A. Pusep, H. Arakaki, and C. A. de Souza (unpublished).

[12] N.F. Mott, J. Non-Cryst. Solids **1**, 1 (1968).

[13] W. Szott, C. Jedrzejek, and W.P. Kirk, Phys. Rev. B **48**, 8963 (1993).

[14] N. W. Ashcroft and N. D. Mermin, *Solid State Physics* (Holt, Rinehart and Winston, New York, 1976).

[15] A.J. Chiquito, Yu.A. Pusep, G.M. Gusev, and A.I. Toropov, Phys. Rev. B **66**, 035323 (2002).

[16] Yu.A. Pusep, A.J. Chiquito, S. Mergulhão, and A.I. Toropov, J. Appl. Phys. **92**, 3830 (2002).

Quantum interference in the presence of a metal-to-insulator transition

Yu. A. Pusep, H. Arakaki, and C. A. de Souza

Instituto de Física de São Carlos, Universidade de São Paulo, 13560-970 São Carlos, São Paulo, Brazil

The negative magnetoresistance related to the quantum interference was studied in the GaAs/AlGaAs doped superlattices as a function of the well thickness and consequently, the disorder induced by the interface roughness. As a result, the disorder driven metal-to-insulator transition was achieved. The qualitatively different magnetoresistances with the positive and negative concavities were observed in the metallic and insulating samples, respectively. Good agreements were found with the theories developed in the limits of the weak and strong disorder. Additionally, a modification of the phase-breaking mechanism was found when crossing from the metallic regime to the insulating one.

The insulating behavior of electron system is a consequence of disorder[1] and/or interaction.[2] One possible way to account for the disorder induced localization is to consider the quantum wave origin of conduction electrons. In this case the randomly distributed scattering centers provide the coherent backscattering of electrons which, interfering constructively, result in the Anderson kind localization. Such a localization due to the quantum interference does not require attractive potentials, but rather occurs by trapping of the conduction electrons at sufficiently high density of scattering centers. Perturbation approach of quantum interference, valid in the limit of small disorder when the elastic-scattering length l is bigger than the Fermi wavelength ($k_F l \gg 1$), gives the quantum correction to the classical conductivity which results in a weak localization. The weak localization is frequently considered of as a precursor of the complete localization.[3–5] Different approaches were developed to account for localization in the strong disorder limit ($k_F l \lesssim 1$) (see relevant references in Ref. 4); among them was the self-consistent theory of localization given in Ref. 6.

A very effective tool to study the localization problem is the measurement of the transport coefficients in the magnetic field. The magnetic field influences the phase coherence of the electrons suppressing their constructive interference, which gives rise to the negative magnetoresistance. The weak-localization theory provides the correct quantitative contribution of the quantum interference to the magnetoresistance. On the other hand, a consideration of the problem in the limit of the strong localization is a highly nontrivial problem. Nevertheless, the behavior of the magnetoresistance caused by the quantum interference was also considered in this case in Refs. 7–10.

The localized and conductive regimes can be experimentally distinguished by different temperature dependencies of the resistivity: the resistivity decreases with the temperature in the localized phase, while it remains unchanged for the Fermi system in the conductive one. On the other hand, the quantum interference is fundamentally determined by the disorder. Therefore, it is thought that also the magnetoresistance may reveal a signature of the metal-to-insulator transition (MIT).

The weak localization was extensively studied in different materials revealing properties of weakly disordered metal system (for instance, see Refs. 3 and 4). Furthermore, the quantum interference was explored in the strongly disordered insulating electron systems exhibiting the hopping conduction, where the characteristic quadratic dependence of the weak-field magnetoresistance was found (Ref. 11 and references therein). The crossover from weak to strong localization has been observed in 1D (one-dimensional) and 2D conductors in Ref. 12 and Refs. 13 and 14 respectively. However, to the best of our knowledge no consecutive investigation of the behavior of the quantum interference across the metal-to-insulator transition driven by disorder was presented to date in 3D electron system.

The disorder induced MIT can be realized in the semiconductor superlattices (SL) where the disorder can be controlled by managing the structure of a SL. The exhausting investigation of the weak localization in SL's was performed in a series of the papers.[15–18] At the same time the quantum interference effects were studied in the short-period GaAs/AlAs SL's with $k_F l \approx 1$ (Ref. 19) where, however, no connection to the MIT was presented. The weak-localization corrections to the conductivity were studied in the intentionally disordered GaAs/AlGaAs SL's in Ref. 20, where we demonstrated that in agreement with the theory, the vertical disorder influences the quantum corrections measured parallel to the layers. However, the disorder driven MIT could not be obtained in these SL's because of the suppression of the disordered superlattice potential due to the effect of the vertical screening. As a result, when increasing disorder, instead of being localized, the electron becomes redistributed over the vertical random potential increasing both the local Fermi energy and consequently, the parallel mobility.[21]

Another possibility to produce the electron scattering required for the quantum interference is given by the interface roughness always present in SL's. The effect of the interface imperfections dominates the parallel transport in the short-period SL's, while it vanishes with the increase of the SL period. Thus, the controlled variation of the well thicknesses should provide the disorder induced MIT. The roughness of the GaAs/AlGaAs interface is associated with smooth potential fluctuations which do not violate the homogeneity of the electron density while they generate necessary electron scattering.

TABLE I. Parameters of the $(GaAs)_m(Al_{0.3}Ga_{0.7}As)_6$ superlattices obtained at $T = 1.6$ K.

m (ML)	n_H (cm^{-3})	μ_H (cm^2/Vs)	$k_F l$	τ_φ ,ps	α
150	5.1×10^{17}	2513	10.2	506	1.4
50	8.3×10^{17}	2500	8.8	385	1.3
30	3.4×10^{17}	1027	2.1	110	2.4
15	7.1×10^{16}	446	0.42	35 (27)	3.1
10	1.0×10^{17}	64	0.084	48 (42)	3.2

In this work we report the investigation of the quantum interference effects in the short-period doped GaAs/AlGaAs superlattices where the disorder was provided with the interface roughness. The scattering due to the interface roughness strongly increases with the decreasing well thicknesses forcing the electrons into localized states when $k_F l < 1$ and thus, resulting in the insulating regime. We found that the quantum correction to the classical conductivity increased with the increasing disorder becoming even comparable with it in the insulating phase. The quantum interference was shown to be modified when passing from metal-to-insulator regime, manifesting itself in the qualitative alteration of the dependence of the resistance on the magnetic field. A good agreements were obtained with the weak-localization theory[15] in the weakly disordered metallic-type SL's and with the self-consistent theory of localization.[8]

The samples here studied were $(GaAs)_m(Al_{0.3}Ga_{0.7}As)_6$ superlattices homogeneously doped with Si. The total number of 30 periods were grown by molecular-beam epitaxy on the (001) semi-insulating GaAs substrates. The growth was interrupted for 30 sec at the normal interface. A variation of the thicknesses of the GaAs wells [m, expressed in monolayers (ML)] in the range 10–150 ML provided for the disorder driven MIT.

Transport measurements were performed using standard four-probe low-frequency (5 Hz) lock-in technique in a pumped liquid-He cryostat in the magnetic field directed perpendicular to the layers at the temperatures 1.6–15 K. The electric characteristics of the superlattices here studied related to their transport properties parallel to the layers are presented in Table I. All the samples were doped with the same nominal concentration of Si, which formed the Fermi gas of the conductive electrons. However, a significant decrease of the Hall concentrations and the mobilities were observed in the SL's with 15 and 10 ML of GaAs indicating the electron localization. The low mobilities obtained in these SL's are related to the interface roughness scattering, which is the dominant mechanism in the GaAs/AlAs quantum wells with a well thicknesses smaller than 60 Å.[22]

In the magnetic fields lower than 0.1 T we do not expect quantum corrections to the magnetoresistance caused by electron-electron interaction.[4] This is because in all of the samples the low-field condition $\omega_c \tau \ll 1$ was held. Moreover, the spin and orbital effects are expected to contribute at the magnetic fields higher than $H_s = kT/g^* \mu_B$ and $H_t = \pi kT/eD$, respectively (the formulas are written in nota-
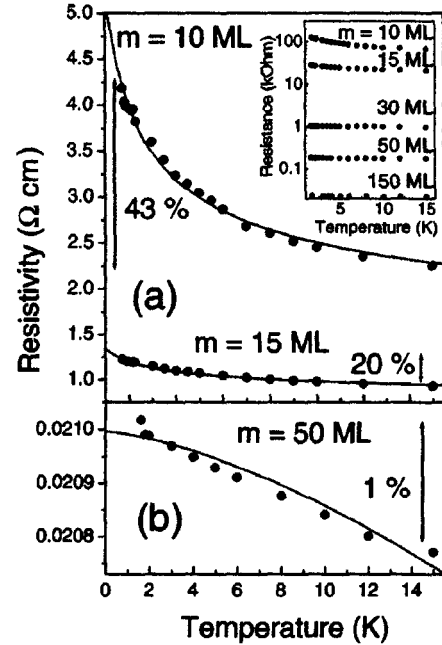

FIG. 1. Temperature dependences of the zero-field resistivities measured in the $(GaAs)_m(Al_{0.3}Ga_{0.7}As)_6$ superlattices with different well thicknesses. The full lines show the dependences calculated according to the Mott's law (a) and for the quantum correction to the classical conductivity (b). The arrow bars represent the magnitudes of the quantum corrections to the total resistivities. The insertion shows the data obtained in all the studied superlattices.

tions of Ref. 18), which are considerably higher than the experimental magnetic fields. Therefore, in the following we neglect the interaction effects.

The temperature dependences of the zero-field resistivities shown in Fig. 1 clearly demonstrate the strong localization of the electrons in the SL with the smallest well thickness (10 ML) where $k_F l \ll 1$, while the sample with 50 ML of GaAs where $k_F l \gg 1$ revealed the metallic behavior. The full lines in Fig. 1(a) were the resistivities calculated according to the Mott's law for variable-range hopping:[23]

$$\rho(T) = \rho_0 \exp\left[\left(\frac{T_0}{T}\right)^{1/4}\right], \quad (1)$$

where T_0 is the characteristic temperature. The best fits were obtained with $T_0 = 7.8$ K and 0.25 K for the SL's with $m = 10$ and 15 ML, respectively.

The weak decreases of the resistivities with the increasing temperature, caused by the quantum correction to the classical conductivity, were observed in the superlattices with $m = 150$ and 50 ML exhibiting the pronounced metallic-type behavior. In this case the temperature dependence of the conductivity is given by[4]

$$\sigma(T) = \sigma_0 + \frac{e^2}{\hbar \pi^3 a} T^{p/2}, \quad (2)$$

where σ_0 is the residual conductivity, a is the coefficient in the temperature dependence of the phase-breaking length,
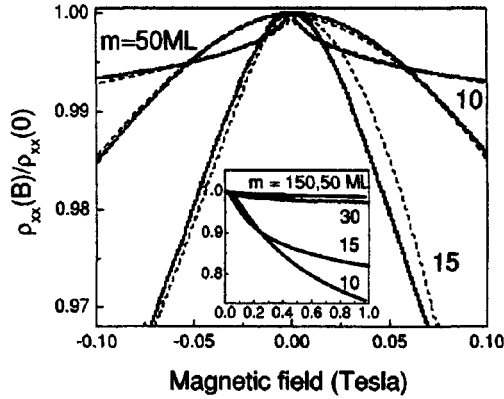
FIG. 2. Relative magnetoresistivities measured in the $(GaAs)_m(Al_{0.3}Ga_{0.7}As)_6$ superlattices with different well thicknesses at $T = 1.6$ K. The results of the fittings (as explained in the text) are shown by dashed lines for the two superlattices exhibiting extreme cases of the metallic and insulating behavior and for the one corresponding to the intermediate transitional regime. The insertion shows the high-field data obtained in all the studied superlattices.

and p is the index depending on scattering mechanism. The temperature dependence of the resistivity calculated by Eq. (2) for the electron-phonon inelastic scattering ($p = 3$), shown in Fig. 1(b) by solid line, demonstrates good agreement with the experimental data.

Thus, the temperature dependences of the resistances shown in Fig. 1 and the values of the localization parameter $k_F l$ manifest themselves to the character of the conductivity, revealing the metallic (roughly nontemperature dependent) and insulating (temperature-dependent, activation-type) behavior of the wide well and the short well superlattices, respectively.

The experimental results obtained in the weak-field conditions are depicted in Fig. 2. They reveal the qualitative modification of the magnetoresistance then crossing MIT. In all the metallic-type SL's ($m = 150$, 50, and 30 ML) the dependences of the parallel resistivities ρ_{xx} on the magnetic field H were characterized by the positive concavity ($d^2\rho_{xx}/dH^2 > 0$), while it changed the sign in the insulating samples ($m = 15$ and 10 ML). It is seen that the decreasing well thickness strongly increases the quantum interference correction confirming the principal role of the disorder in the quantum interference. In the metallic regime the correction was found smaller than 1% of the total resistivity. At the same time, the contribution of the quantum interference increased up to 30–40% in the insulating phase.

In the weak disorder limit ($k_F l \gg 1$) and in a weak magnetic field ($\omega_c \tau \ll 1$, where $\omega_c = eH/m_\parallel$) the weak-localization correction to the conductivity of a SL is determined by the expression[15]

$$\Delta\sigma_\parallel^{WL}(H) = \delta\sigma_\parallel(H) - \delta\sigma_\parallel(0) = \frac{e^2}{2\pi^2\hbar l_H}\alpha F(\delta), \quad (3)$$

where $l_H = \sqrt{\hbar/eH}$ is the magnetic length, $\alpha = \sqrt{D_\parallel/D_z}$ is the coefficient of the anisotropy, $D_\parallel$ and D_z are the diffusion

coefficients parallel and perpendicular to the layers, respectively, $F(\delta) = \Sigma_{n=0}^{\infty} 2[(n+1+\delta)^{1/2} - (n+\delta)^{1/2}] - (n+\frac{1}{2} + \delta)^{-1/2}$ is the Kawabata function[24] with $\delta = l_H^2/4D_\parallel\tau_\varphi$, and τ_φ is the electron wave-function dephasing time.

On the other hand, at the strong disorder ($k_F l \lesssim 1$) and in a weak magnetic field applied perpendicular to the layers the self-consistent approach gives[8]

$$\Delta\sigma_\parallel^{SL}(H) = \frac{e^2\delta^{-3/2}}{192\pi^2\hbar\alpha l_H}. \quad (4)$$

The self-consistent approach results in the parabolic dependence of the magnetoresistance. As a consequence, a qualitative modification of the magnetoresistance, similar to that one observed experimentally in Fig. 2, is expected during the crossover from weak to strong localization.

It ought to be mentioned that the self-consistent theories of localization[6,8] approach the metal-to-insulator transition from the metallic side and are not applicable deep in the insulator regime. However, the qualitatively similar result—the parabolic negative magnetoresistance—was also obtained in the localization limit using the calculations based on the critical path analysis in the model accounting for the interference during the hopping process in Refs. 9 and 10. Our data shown in Fig. 2 demonstrate that in the insulating regime the negative magnetoresistance indeed approaches the parabolic dependence predicted theoretically. Moreover, at least in the insulating sample with the well thickness of 15 ML, where $k_F l \approx 0.42$, we expect a validity of Eq. (4) and a reasonable precision in determination of the dephasing time. Already in this case we found the negative concavity of the magnetoresistance and the significant decrease of the dephasing time with respect to the one obtained in the metallic samples.

The best fittings obtained with the Eqs. (3) and (4) for the metallic-type ($m = 50$ ML) and insulating-type ($m = 10$ and 15 ML) SL's, respectively, are shown by the dashed lines in Fig. 2. The magnetoresistance traces measured in the metallic SL's were fitted with two fit parameters: the phase-breaking times τ_φ and the anisotropy coefficients α. The anisotropy coefficients of the metallic samples were found very close to the calculated values. The magnetoresistance data obtained in the isolating SL's were fitted with a single parameter τ_φ, while the anisotropy coefficients were fixed to their calculated magnitudes; in this case the best fits are shown in the range of the positive fields. The phase-breaking times obtained by the fits in all the samples are collected in Table I. It is seen that the dephasing time significantly drops when crossing MIT.

Furthermore, worth noticing is that although Eq. (3) is not valid in the case $k_F l \lesssim 1$, it may qualitatively explain the observed change of the concavity of the magnetoresistance across the metal-to-insulator transition. In the case of weak magnetic field ($\delta \gg 1$) $\Delta\sigma_\parallel^{WL}(H) \sim H^2$ (negative concavity), whereas in the opposite limit ($\delta \ll 1$): $\Delta\sigma_\parallel^{WL}(H) \sim \sqrt{H}$ (positive concavity) and the transition occurs at the critical field $H_c = \hbar/eD\tau_\varphi$. In the metallic SL's where the critical fields H_c are of the order of 10^{-4} T , the magnetoresistances were

measured in the fields much higher than H_c. However, in the insulating SL with the shortest wells the critical field is about 0.5 T and the data were taken in the fields lower than H_c where Eq. (3) provides the paraboliclike dependence of the conductivity correction on the magnetic field. The fits performed with Eq. (3) in the insulating SL's are shown in Fig. 2 for the magnetoresistance data obtained in the range of the negative fields. During the fits the coefficients of anisotropy were fixed to their calculated values, while the phase-breaking times and the zero field conductivity were varied. The best fits were obtained with the zero-field conductivities five to seven times higher than the measured magnitudes. The phase-breaking times obtained by the fits of Eq. (3) in the isolating SL's are shown in Table I in brackets and they match surprisingly well the values obtained by Eq. (4). This result agrees with that one obtained in the strongly localized two-dimensional electron gas (2DEG) in Ref. 14 and probably shows that even in this case the conductivity looks like a diffusive one.

As does the magnetic field, the inelastic scattering suppresses the backscattering quantum corrections at high temperatures. Indeed, the values of the conductivity corrections given by the temperature dependences of the resistivities, shown in Fig. 1 by the arrow bars, are consistent with the quantum corrections determined by the magnetoresistance measurements. This gives evidence of the mostly quantum origin of the conductivity corrections in all the samples studied here.

The temperature dependences of the dephasing times τ_φ obtained in the metallic and insulating SL's are displayed in Fig. 3. The metallic-type SL reveals the T^{-3} dependence which corresponds to the electron-phonon scattering.[4,18] While, a very weak variation of the magnetoresistance traces with the temperature, which resulted in a weak temperature variation of τ_φ proportional to $T^{-0.7}$, was observed in the insulating-type SL's. This demonstrates a change of the phase-breaking mechanism in the insulating regime. It is worth mentioning that a similar weak temperature dependence of the dephasing length $L_\varphi \sim T^{-0.4}$, where $L_\varphi = D\tau_\varphi$, was found in variable-range-hopping regime in n type of GaAs.[25] The weakness of the $\tau_\varphi(T)$ dependence with the increasing disorder was also observed in 2DEG.[14,26]

In summary, we studied the parallel magnetotransport in the short-period GaAs/AlGaAs SL's. It was shown that at
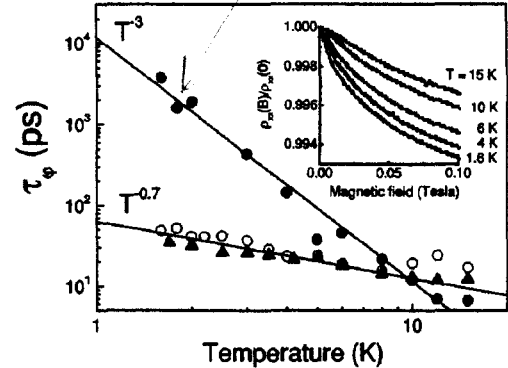

FIG. 3. Temperature dependences of the dephasing times τ_φ obtained in the metallic-type $(GaAs)_{50}(Al_{0.3}Ga_{0.7}As)_6$ superlattice (full circles) and in the insulating-type $(GaAs)_{15}(Al_{0.3}Ga_{0.7}As)_6$ (open circles) and $(GaAs)_{10}(Al_{0.3}Ga_{0.7}As)_6$ superlattices (triangles). The full lines were the dependences calculated as proportional to T^{-3} and to $T^{-0.7}$. The insertion shows the relative magnetoresistances measured at different temperatures in the metallic-type $(GaAs)_{50}(Al_{0.3}Ga_{0.7}As)_6$ superlattice.

low temperatures the transport properties of these SL's are governed by the quantum interference of conduction electrons experiencing the elastic scattering on interface imperfections. The variation of the thicknesses of the GaAs wells at a fixed doping allowed us to achieve the disorder driven MIT. The quantum interference was found to be responsible for the weak-field negative magnetoresistances observed on both sides of the transition. The dependences of the resistances on the magnetic field revealed different behavior on the metallic and insulating sides of the transition. It demonstrated the positive and negative concavities in the metallic-type and insulating-type samples, respectively, which were found in good agreements with the weak- and strong-localization theories. The different temperature dependences of the phase-breaking times were observed on different sides of the MIT reflecting dissimilar inelastic-scattering mechanisms. Thus, the metal-to-insulator transition was found to manifest itself in the corresponding modification of the quantum interference.

[1] P.W. Anderson, Phys. Rev. **109**, 1492 (1958).

[2] N. F. Mott, Metal-Insulator Transitions (Taylor and Francis, London, 1974).

[3] G. Bergmann, Phys. Rep. **107**, 1 (1984).

[4] P.A. Lee and T.V. Ramakrishnan, Rev. Mod. Phys. **57**, 287 (1985).

[5] H. Fukuyama, in Electron-Electron Interactions in Disordered Systems, edited by A. L. Efros and M. Pollak (Elsevier Science, Amsterdam, B.V., 1985).

[6] D. Vollhardt and P. Wölfle, Phys. Rev. B **22**, 4666 (1980).

[7] V.L. Nguyen, B.Z. Spivak, and B.I. Shklovskii, Zh. Exp. Teor.

Fiz. **89**, 1770 (1985) [Sov. Phys. JETP **62**, 1021 (1984)].

[8] V.V. Bryksin and P. Kleinert, Z. Phys. B: Condens. Matter **101**, 91 (1996).

[9] O. Entin-Wohlman, Y. Imry, and U. Sivan, Phys. Rev. B **40**, 8342 (1989).

[10] O. Entin-Wohlman and Y. Imry, Phys. Rev. Lett. **60**, 1566 (1988).

[11] Y. Zhang and M.P. Sarachik, Phys. Rev. B **43**, 7212 (1991).

[12] M.E. Gershenson, Yu.B. Khavin, A.G. Mikhalchuk, H.M. Bozler, and A.L. Bogdanov, Phys. Rev. Lett. **79**, 725 (1997).

[13] S.-Y. Hsu and J.M. Valles, Jr., Phys. Rev. Lett. **74**, 2331 (1995).

[14] G.M. Minkov, O.E. Rut, A.V. Germanenko, A.A. Sherstobitov,

B.N. Zvonkov, E.A. Uskova, and A.A. Birukov, Phys. Rev. B **65**, 235322 (2002).

[15] W. Szott, C. Jedrzejek, and W.P. Kirk, Phys. Rev. B **40**, 1790 (1989).

[16] W. Szott, C. Jedrzejek, and W.P. Kirk, Phys. Rev. Lett. **18**, 1980 (1989).

[17] W. Szott, C. Jedrzejek, and W.P. Kirk, Phys. Rev. B **45**, 3565 (1992).

[18] W. Szott, C. Jedrzejek, and W.P. Kirk, Phys. Rev. B **48**, 8963 (1993).

[19] A.B. Gougam, J. Sicart, J.L. Robert, and B. Etienne, Phys. Rev. B **59**, 15308 (1999).

[20] A.J. Chiquito, Yu.A. Pusep, G.M. Gusev, and A.I. Toropov, Phys. Rev. B **66**, 035323 (2002).

[21] Yu.A. Pusep, A.J. Chiquito, and A.I. Toropov, J. Appl. Phys. **92**, 3830 (2002).

[22] H. Sakaki, T. Noda, K. Hirakawa, M. Tanaka, and T. Matsusue, Appl. Phys. Lett. **51**, 1934 (1987).

[23] N.F. Mott, J. Non-Cryst. Solids **1**, 1 (1968).

[24] A. Kawabata, J. Phys. Soc. Jpn. **49**, 628 (1980).

[25] F. Tremblay, M. Pepper, D. Ritchie, D.C. Peacock, J.E.F. Frost, and G.A.C. Jones, Phys. Rev. B **39**, 8059 (1989).

[26] R.A. Davies and M. Pepper, J. Phys. C **16**, L353 (1983).

PUSEP, Y. A.; RIBEIRO, M. B.; ARAKAKI, H.; SOUZA, C. A.; ZANELLO, P. A.; MALZER, S.; DÖHLER, G. H. Regimes of quantum transport in superlattices in a weak magnetic field. **Journal of Physics:** condensed matter, Bristol, v. 16, n. 13, p. 2447-2453, Apr. 2004.

Effect of compensation of electron and hole scattering potentials on the optical band edge of heavily doped GaAs/Al$_x$Ga$_{1-x}$As superlattices

Yu. A. Pusep,[1] F. E. G. Guimarães,[1] M. B. Ribeiro,[1] H. Arakaki,[1] C. A. de Souza,[1] S. Malzer,[2] and G. H. Döhler[2]

[1]Instituto de Física de São Carlos, Universidade de São Paulo, 13560-970 São Carlos, SP, Brazil

[2]Institut für Technische Physik 1, Universität Erlangen, D-91058 Erlangen, Germany

The optical broadenings studied by the photoluminescence in the intentionally disordered GaAs/AlGaAs superlattices were compared with the broadenings of the individual electron states measured by the Shubnikov-de Haas oscillations. It was shown that the combined effect of the electron and hole energy blurrings is to decrease the optical broadening with respect to the individual state broadenings resulting in very sharp optical edges even in highly disordered superlattices. It was also found that the impurities almost equally influence the electron and hole scattering potentials, contrary to what happens due to the structural superlattice disorder.

The possibility to study disorder effects in semiconductor superlattices, where the disorder can be produced either by randomly varying layer thicknesses or by random layer compositions, was mentioned already in the first proposal of superstructured materials.[1] The great advantage of such random materials is a controlled nature of the disorder which allows us to distinguish the impact of the randomness on their properties.

The optical measurements, which are determined by the joint density of states, present a powerful method to study the disorder effects. The disorder affects the joint density of states through the modification of the energy and broadening of the electron conduction and valence band states. The renormalization of the electron energy and the broadening of the absorption edge in the presence of disorder were discussed in detail in Ref. 3. The first application of the photoluminescence (PL) to explore the localization of carriers in the intentionally disordered superlattices was performed in Ref. 2 where, however, no connections to the joint density of states and to the optical band edge were performed. In this communication we demonstrate that in disordered semiconductors the shape of the optical band edge drastically depends on the character of the optical transitions. According to Ref. 3, the indirect optical transitions form the broadened band edge, while, as we will show the direct transitions may lead to a sharp band edge, even in the presence of strong disorder.

The interaction of the carriers with imperfections causes the blurring of their energy:[4]

$$\frac{\hbar}{\tau_{e(h)}} = 2\pi u_{e(h)}^2 N_i \gamma. \tag{1}$$

where $\tau_{e(h)}$ is the electron (hole) single-particle relaxation time, $u_{e(h)}$ is the electron (hole) scattering potential, N_i is the concentration of imperfections and γ is the density of states on the Fermi surface. This blurring results in a broadening of the Landau levels which can be obtained by the magnetotransport measured in the range of the Shubnikov-de Haas oscillations.[5] Depending on the doping (n- or p-type) the

broadenings of the electron states of the conduction or valence bands can be obtained.

On the other hand, both the electron states of the valence and conduction bands contribute to the optical interband transitions. Therefore, the electron and hole blurrings (1) give rise to the broadening of the PL edge. In such a case, the intensity near the PL edge can be calculated according to[6]

$$I(\omega) = I_0 \left[\frac{1}{2} - \frac{1}{\pi} \arctan(2\tau \delta\Omega) \right]. \tag{2}$$

where I_0 is the PL intensity at the edge in the ideal (disorder-free) case. $\delta\Omega = \hbar\omega - 2E_F$, with E_F being the Fermi energy and τ the characteristic relaxation time which determines the absorption edge broadening. This relaxation time is defined by the formula

$$\frac{\hbar}{\tau} = 2\pi (u_e - u_h)^2 N_i \gamma. \tag{3}$$

This means that the broadening of the optical edge cannot be expressed in terms of the mean free times τ_e and τ_h. The formulas (2) and (3) were obtained in the limit $\hbar/\tau \ll E_F$ for the interaction of electrons with the short-range impurity potentials. These assumptions are also valid in our samples with a short-range structural disorder potential.

It is seen that the relaxation time τ in Eq. (3) depends on the difference of the electron and hole scattering potentials and, therefore, may be smaller than the individual broadenings. Moreover, the formula (3) means that in the case $u_e = u_h$ the optical edge is sharp even in the presence of the scattering by imperfections. This is because with the same scattering of electrons and holes and the same initial energy spectra, the electron and hole wave functions and energy eigenvalues modified by imperfections are exactly the same. In this case, as it is shown in Fig. 1, the optical transitions occur only between the like states and there are no transitions between the different states which are orthogonal. The energy deficits ΔE are identical for all the transitions which form the optical edge. This results in a sharp optical edge. Such an effect may cause the absorption or PL edge much
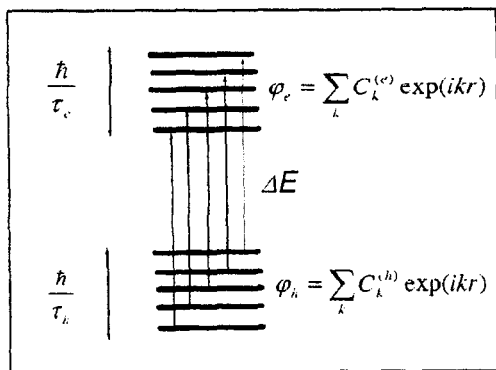
FIG. 1. Scheme of the optical transitions between the valence band states φ_e and the conduction band states φ_h which in the presence of disorder are represented by superpositions of states with different quasimomenta distributed in the energy intervals $\hbar/\tau_h$ and $\hbar/\tau_e$ respectively.

FIG. 2. Photoluminescence spectra measured at $T=4.2$ K in the $(GaAs)_m(Al_{0.3}Ga_{0.7}As)_6$ superlattices with different disorder strengths doped with $N=7.0\times10^{17}$ cm^{-3} (a), $N=1.2\times10^{18}$ cm^{-3} (b) and 1.7×10^{18} cm^{-3} (c). The full lines are the PL intensities calculated near the Moss-Burstein edges according to Eq. (2).

sharper than the expected from the transport measurements of the broadenings of the single electron states.

In this work we study the influence of the intentional disorder on the broadening of the PL edge of the doped GaAs/AlGaAs superlattices. In order to distinguish the effect of the individual states on the PL edge we compare the broadenings of the PL edges with the broadenings of the individual electron states obtained by the Shubnikov-de Haas oscillations, both measured in the superlattices with different disorder strengths.

The samples studied here were the $(GaAs)_m(Al_{0.3}Ga_{0.7}As)_6$ superlattices (where the thickness of the layers is expressed in monolayers, ML) grown by molecular beam epitaxy on (001) GaAs substrates. In order to form the degenerate electron system all the samples were doped with Si. The samples with the nominal doping concentrations 7.0×10^{17} cm^{-3}, 1.2×10^{18} cm^{-3}, and 1.7×10^{18} cm^{-3} were studied. The disorder was introduced by a random variation of the well thicknesses (m) around the nominal value 17 ML. The disorder strength was characterized by the disorder parameter $\delta-\Delta W$, where Δ is the full width at half maximum of a Gaussian distribution of the electron energies calculated in the isolated quantum wells and $W\approx55$ meV is the miniband width of the nominal superlattice in the absence of disorder. Details of the sample growth and characterization can be found in Ref. 7. In all the samples the low temperature ($T=1.7$ K) mobilities were found in the interval 1200–2000 cm^2/V s resulting in the parameter $k_Fl=7.5-14.2$, which corresponds to the metallic electron system. The PL measurements were performed at 4.2 K using a He-Cd laser line at 442 nm for excitation. The PL signal was detected in the lock-in mode by a GaAs photomultiplier mounted on a 0.5 m monochromator. Parallel magneto-transport measurements were carried out on the Hall bar samples using standard four probe low-frequency (5 Hz) lock-in technique in a pumped liquid He cryostat in the magnetic field directed parallel and perpendicular to the layers at the temperature 1.7 K.

It should be mentioned that the influence of disorder on the collective excitations (plasmons) was studied by Raman
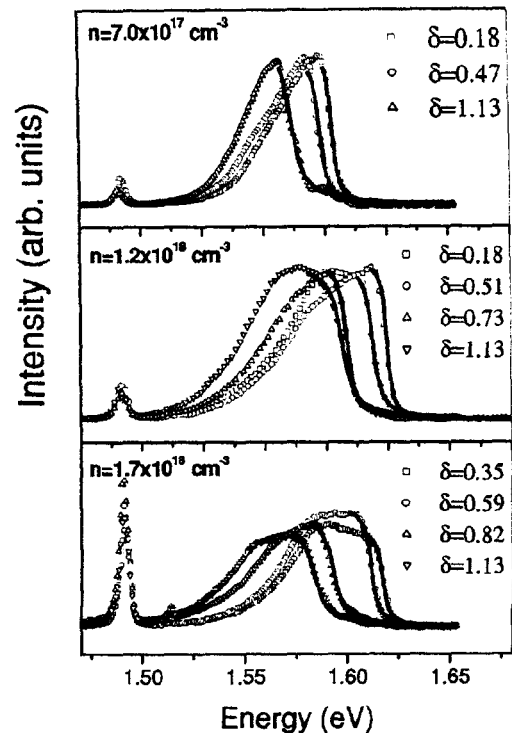
scattering in similar intentionally disordered superlattices in Ref. 7. Some of the samples used in this work were already characterized by the magneto-transport measurements in Refs. 8 and 9 where the anisotropic character of the intentional disorder was demonstrated and the weak-localization correction to the conductivity was explored. In all these cases clear consequences of the intentional structural disorder consistent with the theoretical predictions were found in the responses of electrons either to the field of radiation or to the electric field. Moreover, these data demonstrated that the disorder produced by random variation of the thicknesses of the layers provides well quantitatively controlled disorder strength.

Some of the PL spectra of the differently doped disordered superlattices are shown in Fig. 2. They show that the disorder leads to a significant red shift and broadening of the PL edge. The peaks at the energy 1.49 eV are due to the GaAs substrate. As it was shown in Ref. 3, in the presence of disorder, due to the redistribution of the electron density, the Fermi energy decreases by a value approximately equal to the amplitude of the fluctuations of the random potential. In the degenerate semiconductors the high frequency position of the PL edge is associated with the Fermi energy. Therefore, the red shift of the PL edge is related to a deviation of the Fermi energy from its value in a perfect crystal and, consequently, to the amplitude of the superlattice random potential which may be roughly estimated as a value of Δ - $W\delta$. The observed PL red shift ($\Delta\nu$) is depicted in Fig. 3 as
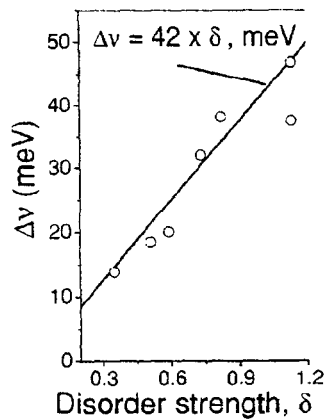
FIG. 3. Disorder induced red shifts of the PL edges measured in the closely doped random superlattices with $N=1.2 \times 10^{18}$ cm^{-3} and 1.7×10^{18} cm^{-3}. The full line represents the expected disorder induced shift of the Fermi energy.

FIG. 4. Relative magnetoresistances measured at $T=1.7$ K in the disordered $(GaAs)_m(Al_{0.3}Ga_{0.7}As)_6$ superlattices with $N=7.0 \times 10^{17}$ cm^{-3} with different orientations of the magnetic field, parallel (thick lines) and perpendicular (thin lines) to the growth direction z. Dashed lines are the calculated magnetoresistances.
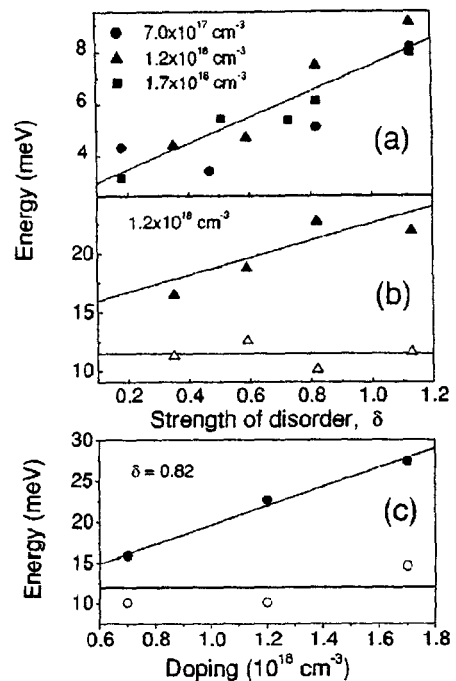
FIG. 5. Characteristic broadenings of the PL edge $\hbar/\tau$ (a) and the electron broadenings $\hbar/\tau_c$ (b), (c) obtained in the differently doped disordered superlattices $(GaAs)_m(Al_{0.3}Ga_{0.7}As)_6$. The open and full circles in panels (b), (c) correspond to the parallel and vertical electron energy broadenings, respectively. The lines are guides for eyes.
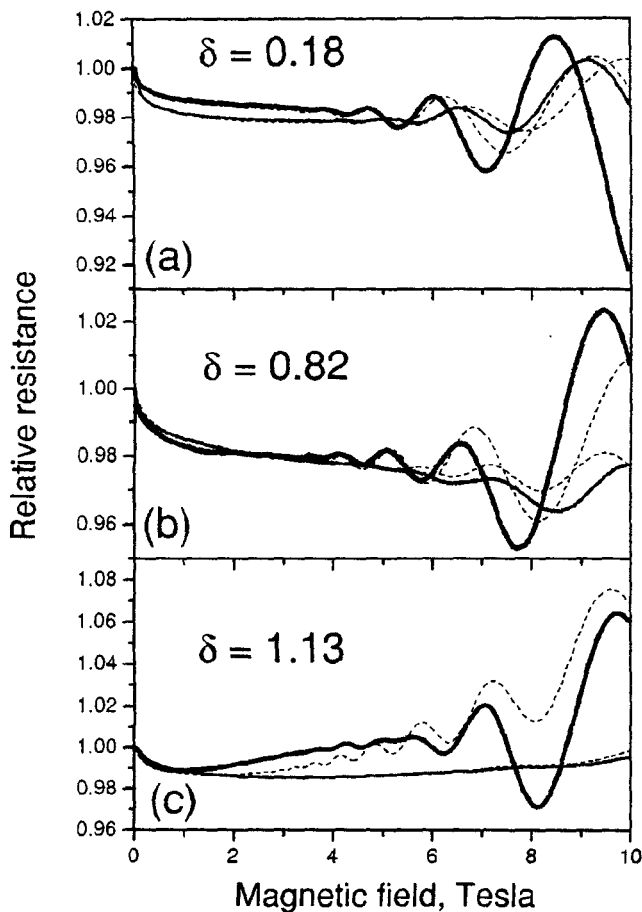
a function of the disorder strength. It is well described by the dependence $\Delta\nu=42\delta$. meV. where the linear coefficient was indeed found very close to the value of the nominal miniband width ($W=55$ meV). Thus, our data demonstrate good agreement with the theory.[3]

The magnetoresistance traces measured with different orientations of the magnetic field are shown for selected superlattices in Fig. 4. They reveal well developed Shubnikov-de Haas oscillations. The amplitudes of these oscillations were found smaller for the magnetic fields directed along the layers than for the fields perpendicular to the layers. This shows a strong anisotropy of the electron energy broadening, which correspondingly was found larger along the disorder direction (vertical broadening) than parallel to the layers (parallel broadening).

The characteristic broadenings of the PL edges $\hbar/\tau$ were determined in the superlattices with different disorder strengths by the fit of the PL spectra, calculated by Eq. (2), to the experimental spectra measured in the range of the Moss-Burstein edge (see Fig. 2, where the continuous lines are the spectra calculated near the edge). The values $\hbar/\tau$ obtained by this way are depicted in Fig. 5(a). In spite of the relatively strong randomization, the PL edges were found surprisingly sharp when compared to the transport data [Fig. 5(b)].

The electron energy broadenings $(\hbar/\tau_c)$ associated with the broadenings of the Landau levels were obtained by the fits of the magnetoresistances calculated according to Ref. 10 to the experimental magneto-transport data. The dependences of the vertical and parallel electron broadenings $\hbar/\tau_c$

on the disorder strengths obtained by the magneto-transport measurements in the differently doped superlattices are shown in Fig. 5(b) for the SL's with the doping 1.2 $\times 10^{18}$ cm^{-3}. The similar data obtained in other SL's are presented in Ref. 8. The vertical electron energy broadening and the optical broadening display similar behaviors—the noteworthy enhancement with the increasing disorder. While, as expected, the parallel electron energy broadenings were not affected by the vertical superlattice disorder. As it was mentioned above, the broadenings of the individual electron states were found considerably higher than the characteristic broadenings of the PL edges. This discrepancy is explained by the effect of the partial compensation of the electron scattering potential by the hole scattering potential, which is demonstrated by Eq. (3). This is evidence that the scattering potential of the holes is fairly comparable to that of the electrons.

Furthermore, as it is shown in Fig. 5(c), the vertical individual electron broadenings were found to increase with the increasing doping level, which represents a noticeable contribution of the impurity scattering. At the same time, the characteristic broadenings of the PL edge did not exhibit such an influence of the doping—the optical broadenings were found to depend only on the disorder strength and not on the doping level. This may happen because a random variation of the superlattice potential, which takes place in the presence of the intentional disorder, produces more difference between the scattering potentials u_e and u_h than do the impurities.

The anisotropy of the individual electron broadening increasing with the raising doping concentration is shown in Fig. 5(c). Obviously, this effect is due to the modulation of the doping concentration along the growth direction which consequently, generates the corresponding modulation of the impurity scattering potential. Such a modulation may take place because during the growth the flux of Si was kept constant while the growth rates of the GaAs and AlGaAs layers were different, 0.5 ML/s and 0.7 ML/s, respectively. Thus, a higher doping concentration is expected in the GaAs wells than in the AlGaAs barriers and the resulting difference between the impurity scattering potentials should increase with the increasing doping level.

Conclusion: The broadenings of the PL edges and of the Landau levels were studied and compared in the n-doped, intentionally disordered GaAs/AlGaAs superlattices. The first one is associated with the combined effect of the electron and hole energy blurrings, while the second one is due to the blurrings of the electron energy states of the conduction band. The broadenings of the PL edges were found to be considerably smaller than those of the electron states. It was shown that this is explained by the fact that the optical edge broadening is determined by the difference between the electron and hole scattering potentials. Therefore, in the case of their proximity, the resultant characteristic optical broadening may be much smaller than the individual electron (hole) energy broadening. Both, the intentional superlattice disorder and impurities enhance the individual electron and hole scattering potentials. However, according to our data, in contrast to the scattering due to the superlattice disorder, the impurity scattering almost does not influence the difference between them. This suggests similar electron and hole impurity scattering potentials.

[1] L. Esaki and R. Tsu, IBM J. Res. Dev. **14**, 61 (1970).

[2] A. Chomette, B. Deveaud, A. Regreny, and G. Bastard, Phys. Rev. Lett. **57**, 1464 (1986).

[3] B. I. Schklovskii and A. L. Efros, *Electron Properties of Doped Semiconductors* (Springer-Verlag, Berlin, 1984).

[4] A. A. Abrikosov, L. P. Gor'kov, and I. E. Dzyaloshinskii, *Quantum Field Theoretical Methods in Statistical Physics* (Pergamon, Oxford, 1965).

[5] A. Gold, Phys. Rev. B **38**, 10798 (1988).

[6] E. G. Batyev, Yu. A. Pusep, and M. P. Sinyukov, Sov. Phys. Solid State **27**, 708 (1985).

[7] Yu. A. Pusep, W. Fortunato, P. P. Gonzalez-Borrero, A. I. Toropov, and J. C. Galzerani, Phys. Rev. B **63**, 115311 (2001).

[8] Yu. Pusep, A. J. Chiquito, S. Mergulhão, and A. I. Toropov, J. Appl. Phys. **92**, 3830 (2002).

[9] A. J. Chiquito, Yu. A. Pusep, G. M. Gusev, and A. I. Toropov, Phys. Rev. B **66**, 035323 (2002).

[10] A. E. Stephens, D. G. Seiler, J. R. Sybert, and H. J. Mackey, Phys. Rev. B **11**, 4999 (1975).

Disorder-driven coherence-incoherence crossover in random GaAs/Al$_{0.3}$Ga$_{0.7}$As superlattices

Yu. A. Pusep,[1] M. B. Ribeiro,[1] H. Arakaki,[1] C. A. de Souza,[1] S. Malzer,[2] and G. H. Döhler[2]

[1]Instituto de Física de São Carlos, Universidade de São Paulo, 13560-970 São Carlos, SP, Brazil

[2]Institut für Technische Physik I, Universität Erlangen, D-91058 Erlangen, Germany

(Received 9 September 2004)

The crossover from interlayer coherent to interlayer incoherent transport was studied in intentionally disordered GaAs/Al$_{0.3}$Ga$_{0.7}$As superlattices as a function of the vertical interlayer coupling. Depending on the relation of the disorder energy and the Fermi energy, the coherent and incoherent diffusive transport regimes were distinguished. The vertical coupling energy, the vertical coherence length, and the in-plane phase-breaking time were obtained by magnetoresistance measurements in the coherent and incoherent regimes. All of them were found to decrease with increasing vertical disorder strength. This demonstrates the disorder-induced breakdown of the interlayer coherence of quasiparticles, which drastically affected their intralayer coherence.

I. INTRODUCTION

The electron systems comprising weakly coupled metallic layers exhibit many interesting properties due to their electric anisotropy when the conductivities perpendicular and along the layers are considerably different. The interplay between the interlayer and intralayer conductivities is essentially linked to the dimensionality of the system: the vanishing interlayer conductivity results in two-dimensionalization of the electronic properties. As it was recently shown, the interlayer transport is also linked to the coherence of quasiparticles responsible for the metallic conductivity.[1,2] It is worth mentioning that the existence of quasiparticles is a central problem of the conductivity of disordered electron systems.[3] The anisotropy of layered materials naturally sets two temporal scales: the decoherence time τ_φ and the time an electron needs to change a plane τ_0 (the diffusive interlayer time). When $\tau_\varphi \ll \tau_0$, the electron is scattered many times, losing its phase in one plane before changing to the next one; then the layered system behaves like a stack of incoherent two-dimensional metallic planes. In the opposite limit, when $\tau_\varphi \gg \tau_0$, an electron changes a layer without a significant loss of the phase, and hence the layers are coherently coupled. Thus, the relationship between these two characteristic times establishes the coherence-incoherence crossover in layered electron systems.

The coherent or incoherent character of the interlayer transport and the transition between them basically determine the electrical properties of the layered systems, including superconductivity.[4] The temperature-driven interlayer coherence-incoherence crossover has recently been detected in different layered metallic materials in Ref. 1 and was discussed in Ref. 5. In this case the conductivity perpendicular to the layers (along the c axis) reveals an insulating (incoherent) behavior at high temperatures but becomes metal-like (coherent) at low temperatures, whereas transport parallel to the layers remains metallic over the whole temperature range. Consequently, the temperature variation of the interlayer conductivity results in the observed coherence-incoherence transition. It was shown that the quasiparticles disappeared within the layers at approximately the same temperature at which the interplane conductivity crossed over from metallic to insulating behavior. However, the reason why the interplane conductivity exhibits the metal-to-insulator transition and how it couples to the in-plane coherence remain unclear. One possible explanation for this unusual temperature behavior of the interplane conductivity is the presence of disorder in the c-axis direction.[6,7]

Here we examine another layered electron system—intentionally disordered semiconductor superlattices (SL's) GaAs/Al$_{0.3}$Ga$_{0.7}$As where corresponding doping with Si provides for the metallic properties. The artificial disorder potential of a SL built in the growth direction (z) perpendicular to the layers (vertical disorder) controls the coupling between them. Therefore, the interlayer coherence-incoherence crossover can be achieved at a fixed temperature with variation of the vertical disorder strength. Accordingly, the purposely disordered SL's can be regarded as a model layered material where the coupling energy between the planes (t_z) can be easily monitored and the assumption about a possible role of the interlayer disorder can be proved.

The theory of the quantum transport of the weakly coupled SL's has been developed in Refs. 8–11. It was shown that in the weakly disordered limit, when $\hbar/\tau < t_z$, where τ is the elastic scattering time, an electron ballistically crosses the layers and the system exhibits the usual three-dimensional anisotropic behavior. While, when $\hbar/\tau > t_z$ the strong anisotropic (vertical) disorder changes the characteristic of the system into a mixture of two- and three-dimensional behavior with corresponding contributions to the quantum correction to the conductivity.[11] In this case the electron diffuses to the neighboring plane, and depending on the relationship between the phase-breaking time τ_φ and the time τ_0, the coherent and incoherent regimes can be distinguished.

The coherency of the electron excitations determined by the phase-breaking time is intrinsically linked to the quantum correction to the conductivity. The well known method to acquire the quantum correction and to measure the decoherence time is the weak-field magnetoresistance emerging when the magnetic field breaks coherency between two opposite electron trajectories.[12]

1-1

The weak-field magnetotransport was investigated in the semiconductor periodic GaAs/Al$_{0.3}$Ga$_{0.7}$As SL's in the ballistic regime in Refs. 13 and close to the localized regime in Ref. 14, where however, no conditions for the coherence-incoherence crossover were realized. Quantum interference in the presence of a metal-to-insulator transition induced by the interface roughness was recently studied in the short-period GaAs/Al$_{0.3}$Ga$_{0.7}$As SL's in Ref. 15. In this work we present the magnetotransport data obtained in the intentionally disordered GaAs/Al$_{0.3}$Ga$_{0.7}$As SL's. As it will be shown, the magnetoresistances measured in the studied random superlattices here revealed signatures of the coherence-incoherence transition induced by the interlayer vertical disorder. We demonstrated that the anisotropic vertical disorder produced in the growth direction reduces both the interlayer coupling and the interlayer coherency of electrons. Moreover, this vertical disorder resulted in a strong decrease of the in-plane electronic coherency. The paper is organized as follows. The sample characterization and the experimental conditions are given in Sec. II. The experimental results together with their discussion are considered in Secs. III and IV, while conclusions are outlined in Sec. V.

II. EXPERIMENT

In this work, in order to study the dimensionality and the coherence of the electron excitations, we performed the magnetoresistance measurements in the intentionally disordered (GaAs)$_m$(Al$_{0.3}$Ga$_{0.7}$As)$_6$ SL's with different disorder strengths where the thicknesses of the corresponding layers are expressed in monolayers (ML). The vertical disorder was produced by random variation of the well thicknesses (m) around the nominal value 17 ML, and the disorder strength was characterized by the disorder parameter $\delta_{SL}=\Delta/W$, where Δ and W are the disorder energy of the random SL and the width of the relevant miniband of the nominal periodic (GaAs)$_{17}$(Al$_{0.3}$Ga$_{0.7}$As)$_6$ SL, respectively. The values of the disorder energy were calculated as the widths at half maximum of the Gaussian distributions of the bound state energies of isolated quantum wells. The unavoidable monolayer fluctuations of the layer thicknesses resulted in $\delta_{SL}=0.18$ even in the nominally periodic SL. The growth details of these SL's can be found in Refs. 16 and 17. The influence of the disorder on the dynamic electron properties depends on the relation between the disorder energy and the Fermi energy (E_f). In order to increase the disorder effect we decreased the doping concentration. With decreasing doping level the effect of the vertical disorder on the phase-breaking time increases (reducing τ_φ), while the tunneling rate decreases, resulting in the corresponding increase of the time τ_0. In this way, the coherent and incoherent regimes were realized in the high-doped (the nominal doping concentrations 1.2×10^{18} cm^{-3} and 1.7×10^{18} cm^{-3}) and the low-doped (the nominal doping concentration 7.0×10^{17} cm^{-3}) disordered SL's, respectively. The dispersion of the electron energy calculated in the lowest miniband of the nominal periodic SL together with the positions of the Fermi energies measured by the Shubnikov–de Haas oscillations in the low- and high-doped disordered SL's are shown in Fig. 1. The
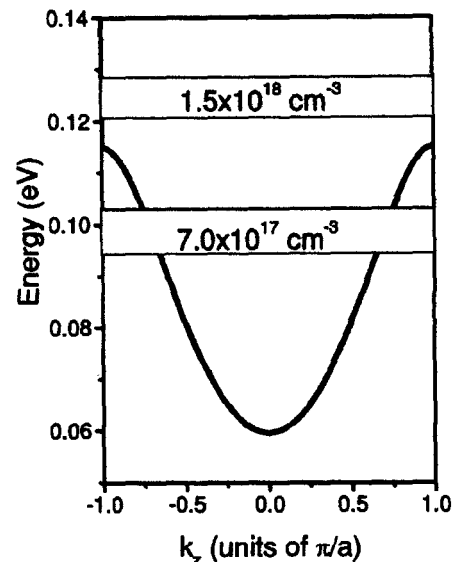

FIG. 1. Calculated dispersion of the electron energy in the lowest miniband of the periodic (GaAs)$_{17}$(Al$_{0.3}$Ga$_{0.7}$As)$_6$ superlattice. The shaded areas show positions of the Fermi energies measured by Shubnikov–de Haas oscillations in the low-doped disordered superlattices (nominal doping concentration 7.0×10^{17} cm^{-3}) and in the high-doped disordered superlattices (nominal concentrations 1.2×10^{17} cm^{-3} and 1.7×10^{17} cm^{-3}).

miniband structure was calculated by the envelope function approximation.[18]

Moreover, to determine the influence of the interlayer coupling on the negative weak-field magnetoresistance, the periodic (GaAs)$_{50}$(Al$_{0.3}$Ga$_{0.7}$As)$_n$ SL's with different barrier thicknesses (n) and with the nominal doping 7.0×10^{17} cm^{-3} were investigated.

In-plane magnetoresistance measurements were performed in the Hall bars using the standard four-probe low-frequency (5 Hz) lock-in technique. Vertical magnetoresistances were measured in the square-shaped mesa structures with areas 1×1 mm^2. The Hall bars and the mesa structures were prepared by standard lithography and chemical etching. The Ohmic contacts were fabricated by depositing either In or an Au-Ge-Ni alloy. In both the in-plane and the vertical geometries the transversal magnetoresistances (with the magnetic field perpendicular to the current direction) were measured in a pumped liquid-He cryostat.

It ought to be mentioned that the weak magnetic field condition $\omega_c \tau \ll 1$, where ω_c is the cyclotron frequency, held in the samples studied here in the range of the magnetic fields used to study the weak localization correction. Therefore, no negative magnetoresistance caused by the electron-electron interaction[19] is expected. The spin-orbital effects also are not anticipated.[17]

An additional aspect that must be taken into account when considering transport in SL's is the shape of the Fermi surface. As it is seen from Fig. 1, in the low-doped disordered SL's studied here $E_f < W$, which means that the Fermi levels are located inside the lowest miniband, resulting in a closed anisotropic Fermi surface. In contrast, the Fermi surfaces become open in the high-doped disordered SL's with $E_f > W$.
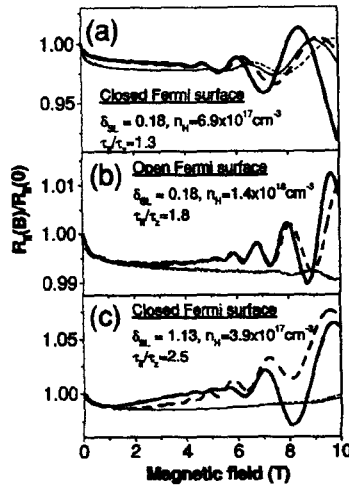
FIG. 2. High-field parallel magnetoresistances measured with different orientations of the magnetic fields at $T = 1.6$ K in the (a) low-doped and (b) high-doped periodic $(GaAs)_1$-$(Al_{0.3}Ga_{0.7}As)_6$ superlattices with the closed and open Fermi surfaces, respectively, and (c) in the low-doped (closed Fermi surface) disordered $(GaAs)_m(Al_{0.3}Ga_{0.7}As)_6$ superlattice with $\delta_{SL} = 1.13$. The thick (thin) lines correspond to the magnetic field perpendicular (parallel) to the layers. The broken lines were calculated as mentioned in the text.

The shape of the Fermi surface determines the dimensionality of the electron gas in SL's, which is three-dimensional anisotropic when the Fermi surface is closed and which is quasi-two-dimensional in the case of the open Fermi surface. In the SL with the open Fermi surface the magnetic field perpendicular to the layers, sufficiently strong to quantize the in-plane electron motion, results in the formation of a two-dimensional electron gas. This magnetic-field-induced two-dimensionalization was predicted in Ref. 10 and was observed in Ref. 20.

III. HIGH-MAGNETIC FIELD DATA: DISORDER-INDUCED TWO-DIMENSIONALIZATION OF ELECTRONS

The effect of the Fermi surface on the electron properties of SL's can be probed in high magnetic field. The Shubnikov–de Haas oscillations measured in the low-doped (closed Fermi surface) and high-doped (open Fermi surface) periodic $(GaAs)_1$-$(Al_{0.3}Ga_{0.7}As)_6$ SL's with different orientations of the magnetic fields studied here are shown in Figs. 2(a) and 2(b). The characteristic times $\tau_\parallel$ and $\tau_\perp$ related to the in-plane (measured with the magnetic field perpendicular to the layers) and vertical (the magnetic field along the layers) quantum-mechanical broadenings of the electron states on the Fermi surface, respectively, were obtained by the fits of the magnetoresistances calculated according to Ref. 21 to the experimental magnetoresistance traces. The disagreements **between the calculated and experimental magnetoresistances** observed at high magnetic **fields are caused by the magnetic "freezing" of the impurities.**[22] The observed increase of the ratio $\tau_\parallel/\tau_\perp$ in the SL with the open Fermi surface in Fig. 2(b)

is due to the above-mentioned effect of the magnetic-field-induced two-dimensionalization of the electron gas.

The vertical disorder violates the coherency between the electrons in the neighboring wells, thus favoring disorder-induced two-dimensionalization, which in analogy with the previous case can be demonstrated by the Shubnikov–de Haas oscillations measured with different orientations of the magnetic field. This effect is shown in Fig. 1(c) where we found the increase of the ratio $\tau_\parallel/\tau_\perp$ with increasing disorder strength in the low-doped SL's with the closed Fermi surfaces (where no magnetic-field-induced two-dimensionalization is expected). Consequently, the high-field data prove the decrease of the interlayer coupling with the increasing vertical disorder. Further evidence of the two-dimensionalization in SL's caused by the vertical disorder is the enhancement of the spatial modulation of the electron density along the growth direction found with the increasing vertical randomization in Ref. 23. This directly demonstrated that the effect of the vertical disorder is to distribute the electrons over the random potential such that the quasi-two-dimensional planes arise.

As discussed in the Introduction, the observed disorder-induced two-dimensionalization of the electron gas should lead to the interlayer coherent-incoherent crossover. Moreover, according to Ref. 11, the change of the dimensionality of the electronic system should break the scaling relation derived by Bhatt, Wölfle, and Ramakrishnan for anisotropic disordered electronic systems in Ref. 24:

$$\frac{\sigma_\parallel(0)}{\sigma_\perp(0)} = \frac{\Delta\sigma_\parallel(H)}{\Delta\sigma_\perp(H)} = \alpha^2. \qquad (1)$$

where $\sigma_{\parallel(\perp)}(0)$ and $\Delta\sigma_{\parallel(\perp)}(H)$ are the in-plane (vertical) zero-field conductivity and the in-plane (vertical) quantum corrections to the conductivity respectively, while α is the coefficient of anisotropy. In the next session we present the results of the investigation of the effects of the vertical disorder on tunneling and coherence of electrons, which indicate the predicted breakdown of this scaling relation.

IV. WEAK-MAGNETIC-FIELD DATA: VERTICAL TUNNELING AND DISORDER-INDUCED COHERENCE-INCOHERENCE CROSSOVER

The vertical magnetoresistance data (with the current parallel to the SL axis) obtained in the low-doped SL's with different disorder strengths are depicted in Fig. 3(a). As it was stated in Ref. 11, only the three-dimensional trajectories contribute to the vertical component of the conductivity tensor. Therefore, the usual anisotropic formula for the quantum correction can be used in this case:

$$\Delta\sigma_\perp(H) = \frac{e^2}{2\pi^2\hbar l_H\alpha}F(\delta). \qquad (2)$$

where $l_H = \sqrt{\hbar/eH}$ is the magnetic length, $F(\delta)$ is the Kawabata function,[25] and $\delta = l_H^2/4L_\varphi^2$, with L_φ being the electron phase coherency length.

The vertical coherence lengths obtained by the fits of the **vertical magnetoresistance data are shown in Fig. 3(b). It is**
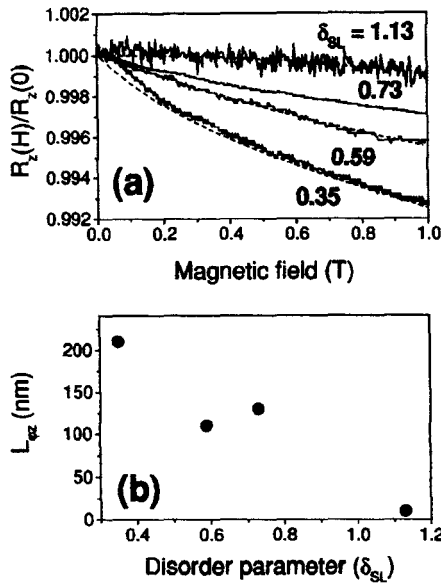
FIG. 3. (a) Vertical weak-field magnetoresistances and (b) the vertical coherence lengths measured at $T = 1.6$ K in the magnetic field parallel to the layers in the random low-doped $(GaAs)_m(Al_{0.3}Ga_{0.7}As)_6$ superlattices with different disorder strengths.

seen that the vertical disorder considerably affects the electron coherence length, resulting in the localization along the growth direction. In the following we shall demonstrate that the vertical disorder also significantly influences the coherence of the electrons moving parallel to the layers.

The weak-field in-plane magnetoresistance records are depicted for selected SL's in Fig. 4. As it was shown in Ref. 16, in the short-period GaAs/Al$_{0.3}$Ga$_{0.7}$As SL's the diffusive transport regime is responsible for the weak-field parallel magnetoresistance. The corresponding expression for the weak-localization correction to the parallel conductivity in the magnetic field perpendicular to the layers, which describes the coherence-incoherence transition, was obtained in Ref. 11:

$$\Delta\sigma_\parallel(H) = \Delta\sigma_\parallel(0) - \frac{e^2}{2\pi^2\hbar d_{SL}} F(\delta,\delta'),\qquad(3)$$

where d_{SL} is the superlattice period,

$$F(\delta,\delta') = \sum_{n=0}^{\infty} \frac{1}{\sqrt{n+\frac{1}{2}+\delta}\sqrt{n+\frac{1}{2}+\delta'}} - 2\ln(\sqrt{n+1}+\delta)$$
$$+ \sqrt{n+1+\delta'}) + 2\ln(\sqrt{n+\delta}+\sqrt{n+\delta'})$$

with

$$\delta = \frac{l_H^2}{4D_\parallel}\left(\frac{1}{\tau_\varphi}+\frac{2}{\tau_0}\right),$$

with $D_\parallel$ being the diffusion coefficient parallel to the layers. The time an electron wastes before changing a layer is given by:
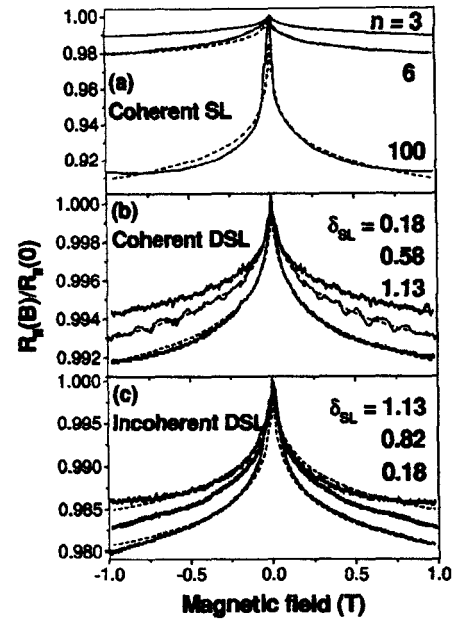

FIG. 4. Parallel weak-field magnetoresistances measured at $T = 1.6$ K: (a) in the periodic $(GaAs)_{50}(Al_{0.3}Ga_{0.7}As)_n$ superlattices with different barrier thicknesses in the coherent transport regime, (b) in the random high-doped (the coherent transport regime) and (c) low-doped (the incoherent transport regime) $(GaAs)_m(Al_{0.3}Ga_{0.7}As)_6$ superlattices with different disorder strengths. The broken lines were calculated as mentioned in the text.

$$\tau_0 = \frac{\hbar^2}{t_z^2\tau}.\qquad(4)$$

Thus, in the diffusive transport regime the quantum correction to the conductivity of a SL is determined by two characteristic times τ_0 and τ_φ. In the incoherent limit, when $\tau_\varphi \ll \tau_0$ the contribution of the diffusive interlayer time τ_0 is insignificant, while the quantum correction is mainly due to this time in the coherent limit, when $\tau_\varphi \gg \tau_0$. The last case means that the observation of electrons moving in the plane of the layers provides information how they move between them.

The behavior of the time characterizing the negative weak-field in-plane magnetoresistance with variation of the vertical disorder manifests as the type of the transport regime. Obviously, the magnetoresistance enhancing with increasing barrier thickness, observed in the periodic $(GaAs)_{50}(Al_{0.3}Ga_{0.7}As)_n$ SL's [shown in Fig. 4(a)], is characterized by the rising time τ_0. Physically this corresponds to the reducing coupling energy t_z. This occurs in the coherent transport regime when the effect of the interlayer time τ_0 dominates the effect of the phase-breaking time. The magnetoresistance increasing with the increasing vertical disorder was found in the high-doped random SL's [shown in Fig. 4(b)]. This also implies in the vanishing interlayer coupling, again indicating the coherent regime. In both these cases the diffusive interlayer times τ_0 and consequently the coupling energies t_z were obtained. However, in neither case may the
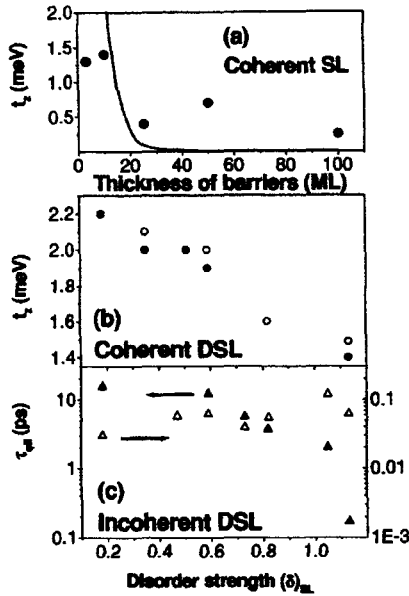
FIG. 5. Vertical coupling energies obtained in the coherent transport regime (a) in the periodic $(GaAs)_{50}(Al_{0.3}Ga_{0.7}As)_n$ superlattices with different barrier thicknesses and (b) in the random high-doped $(GaAs)_m(Al_{0.3}Ga_{0.7}As)_6$ superlattices with different disorder strengths. The width of the lowest miniband calculated in the $(GaAs)_{50}(Al_{0.3}Ga_{0.7}As)_n$ superlattice is shown by the solid line in panel (a) as a function of the barrier thickness. The open (closed) circles in panel (b) correspond to the doping concentration 1.2 $\times 10^{18}$ cm^{-3} (1.7$\times 10^{18}$ cm^{-3}). (c) The phase-breaking times obtained in the incoherent transport regime in the low-doped random $(GaAs)_m(Al_{0.3}Ga_{0.7}As)_6$ superlattices. The closed (open) triangles correspond to the in-plane phase-breaking (elastic scattering) times.

vertical disorder increase the interlayer coupling. Therefore, the same considerations do not apply to the case of the low-doped random SL's shown in Fig. 4(c) where the magnetoresistance decreased with increasing disorder. In fact, as mentioned above, the decrease of the Fermi energy makes the effect of disorder stronger. With this, the vertical coupling weakens (and as a consequence τ_0 increases) while the dephasing time decreases. This sets the electrons into the incoherent transport regime with $\tau_\varphi < \tau_0$. In this case the phase-breaking time determines the magnetoresistance and this time can be found by means of Eq. (3). The broken lines in Fig. 4 show the best fits obtained with the formula (3) in the corresponding transport regimes (coherent or incoherent).

In the SL's exhibiting the coherent diffusive regimes the interlayer coupling energies were calculated according to formula (4) with the times τ_0 and τ found by the magnetoresistance and by the Hall mobility measurements, respectively. They are shown in Fig. 5 as functions of the barrier thickness and the disorder strength in the periodic and random SL's, respectively. In the periodic SL's the interlayer coupling energies were compared with the widths of the lowest miniband, which represent the coupling energies in the ballistic regime. The variation of the interlayer coupling energy with the thickness of the barriers was found to be much weaker than the corresponding (exponential) dependence of the calculated miniband width. This signifies that the overlapping

of the electron wave functions, which determines the miniband structure of a regular SL in the ballistic transport regime, is irrelevant in the diffusive regime. In addition, although the increasing barrier thickness enhances the time τ_0, it does not lead to the incoherent transport regime, which was achieved in the low-doped SL's owing to the vertical randomization. Thus, a determinative role of the interlayer disorder in formation of the incoherent regime was established.

The decrease of the coupling energy obtained in the random SL's with open Fermi surfaces with increasing disorder [shown in Fig. 5(b)] reflects the breakdown of the coherency between neighboring layers already observed in Fig. 3(b). It is worth mentioning that the data obtained in these SL's do not depend on the doping level. This demonstrates the dominant effect of the artificial disorder and the unimportant role of the impurity scattering.

According to the Hall mobility measurements, in all of the SL's under investigation we found the values $\hbar/\tau$ in the interval 6–15 meV, which is significantly higher than the obtained interlayer coupling energies. This confirms the diffusive character of the electron transport.

The high-field magnetoresistance data presented in a previous section showed that the low-doped disordered SL's reveal the disorder-induced two-dimensionalization of the electron gas. As discussed above, such a separation of the electron planes should result in the incoherent diffusive transport regime. The phase-breaking times obtained in this case are due to the contribution of two-dimensional trajectories to the quantum correction.[11] Our results presented in Fig. 5(c) show that in the incoherent transport regime the vertical disorder strongly suppresses the in-plane phase-breaking time. Hence, even in the incoherent regime the parallel electron motions in the neighboring planes are correlated and the planes are not entirely independent. This is consistent with the results obtained in Ref. 2, where it was shown that the coherence of quasiparticles within the layer is affected by the interlayer transport. Namely, coherent quasiparticles are anticipated when their intralayer momentum is conserved during the interlayer tunneling process. The vertical disorder inhibits the conservation of the interlayer momentum. As a consequence, the in-plane dephasing time decreases and the quasiparticles disappear.

Furthermore, in Fig. 5(c) in addition to the phase-breaking times (which determines the in-plane quantum corrections) we show the in-plane elastic scattering times (which determines the zero-field in-plane conductivities) obtained by the mobility measurements. Opposite to the phase-breaking time, the in-plane elastic time does not demonstrate any significant influence of the vertical disorder. As it was shown in Fig. 3(b), the vertical coherence length (and thus, the vertical quantum correction) reveals a strong decrease with decreasing disorder. We were not able to measure the vertical zero-field conductivity without a noteworthy error. However, the indirect evidence of the strong decrease of the vertical conductivity with increasing vertical disorder was obtained in similar intentionally disordered SL's in Ref. 26. The same behavior of the vertical conductivity is expected in the random SL's studied here. Therefore, the different behavior of the in-plane elastic time and in-plane phase-breaking time

together with the supposed identical behavior of their vertical counterparts may indicate the breakdown of the scaling relation (1) in the incoherent diffusive regime predicted in Ref. 11.

V. CONCLUSIONS

Depending on the relation between the disorder energy and the Fermi energy, two different diffusive regimes of the quantum transport were distinguished in the short-period intentionally disordered $GaAs/Al_{0.3}Ga_{0.7}As$ SL's. They are the coherent/incoherent regimes when an electron changes layers without/with a considerable loss of the wave function phase, both found in the high-doped and low-doped disordered SL's, respectively. We demonstrated that the incoherent transport regime is linked to a noteworthy change of the effective dimensionality of the electron gas from three to two dimensions. It was shown that in the coherent regime the quantum correction to the conductivity is determined by the time an electron needs to change a layer, while in the incoherent one

the phase-breaking time is responsible for the quantum correction. Both the characteristic times were found dependent on the strength of the vertical disorder. The observed increase of the diffusive interlayer time with increasing disorder is caused by the evident decrease of the interlayer coupling. The decrease of the in-plane dephasing time with increasing vertical disorder requires a more sophisticated explanation and closely relates to the problem of the coherency of the quasiparticles in strongly correlated layered metals. Our results show that in accordance with theory, the interlayer tunneling controls the coherence of the carriers moving along the layers. In addition, we show an indication of the breakdown of the scaling relation that connects the zero-field conductivities to the quantum corrections to the conductivity in anisotropic disordered electronic systems.

[1] T. Valla, P. D. Johnson, Z. Yusof, B. Wells, Q. Li, S. M. Loureiro, R. J. Cava, M. Mikami, Y. Mori, M. Yoshimura, and T. Sakaki, Nature (London) 417, 627 (2002).

[2] U. Lundin and R. H. McKenzie, Phys. Rev. B 68, 081101 (2003).

[3] B. L. Altshuler and P. A. Lee, Phys. Today 41(■), 36 (1988).

[4] L. B. Ioffe and A. J. Millis, Science 285, 1241 (1999).

[5] A. J. Millis, Nature (London) 417, 599 (2002).

[6] A. G. Rojo and K. Levin, Phys. Rev. B 48, 16861 (1993).

[7] A. F. Ho and A. J. Schofield, cond-mat/0211675 (unpublished).

[8] W. Szott, C. Jedrzejek, and W. P. Kirk, Phys. Rev. B 40, 1790 (1989).

[9] N. Dupuis and G. Montambaux, Phys. Rev. Lett. 68, 357 (1992).

[10] N. Dupuis and G. Montambaux, Phys. Rev. B 46, 9603 (1992).

[11] A. Cassam-Chenai and D. Mailly, Phys. Rev. B 52, 1984 (1995).

[12] P. A. Lee and T. V. Ramakrishnan, Rev. Mod. Phys. 57, 287 (1985).

[13] W. Szott, C. Jedrzejek, and W. P. Kirk, Phys. Rev. Lett. 63, 1980 (1989); W. Szott, C. Jedrzejek, and W. P. Kirk, Phys. Rev. B 45, 3565 (1992); W. Szott, C. Jedrzejek, and W. P. Kirk, ibid. 48, 8963 (1993).

[14] A. B. Gougam, J. Sicart, J. L. Robert, and B. Etienne, Phys. Rev. B 59, 15308 (1999).

[15] Yu. A. Pusep, H. Arakaki, and C. A. de Souza, Phys. Rev. B 68,

205321 (2003).

[16] A. J. Chiquito, Yu. A. Pusep, G. M. Gusev, and A. I. Toropov, Phys. Rev. B 66, 035323 (2002).

[17] Yu. A. Pusep, M. B. Ribeiro, H. Arakaki, C. A. de Souza, P. A. Zanello, A. J. Chiquito, S. Malzer, and G. H. Döhler, Phys. Rev. B 68, 195207 (2003).

[18] G. Bastard, Phys. Rev. B 24, 5693 (1981).

[19] M. A. Paalanen, D. C. Tsui, and J. C. M. Hwang, Phys. Rev. Lett. 51, 2226 (1983).

[20] Yu. A. Pusep, G. M. Gusev, A. J. Chiquito, A. K. Bakarov, A. I. Toropov, and J. C. Leite, Phys. Rev. B 63, 165307 (2001).

[21] A. E. Stephens, D. G. Seiler, J. R. Sybert, and H. J. Mackey, Phys. Rev. B 11, 4999 (1975).

[22] B. M. Askerov, *Electron Transport Phenomena in Semiconductors* (World Scientific, Singapore, 1994).

[23] Yu. A. Pusep, A. J. Chiquito, S. Mergulhão, and A. I. Toropov, J. Appl. Phys. 92, 3830 (2002).

[24] R. N. Bhatt, P. Wölfle, and T. V. Ramakrishnan, Phys. Rev. B 32, 569 (1985).

[25] A. Kawabata, J. Phys. Soc. Jpn. 40, 628 (1980).

[26] A. Chomette, B. Deveaud, A. Regreny, and G. Bastard, Phys. Rev. Lett. 57, 1464 (1986).

Managing disorder in random GaAs/AlGaAs superlattices

Yu.A.Pusep

Instituto de Física de São Carlos, Universidade de São Paulo,
13560-970 São Carlos, SP, Brazil.
phone: ++55-16-33788076, fax: ++55-16-33739827, e-mail: pusep@if.sc.usp.br

(05/01/2005)

The artificial random Gaussian-type potential built in the GaAs/AlGaAs superlattices grown by molecular beam epitaxy was explored by various methods. The effect of the intentional disorder was shown to dominate intrinsic superlattice imperfections and its impact on the electronic properties was found in good agreement with the theoretical predictions. It was demonstrated that the modern state of the molecular beam epitaxy allows for a growth of the superstructured materials with well defined disorder strength.

PACS:71.55.Jv, 72.20.-i,73.61.Ey, 78.66.-w

Both, disorder and electronic correlations fundamentally determine behavior of the disordered electron systems undergoing the metal-to-insulator transition [1]. This has been established to radically complicate an investigation of such a transition. In order to maximally simplify the problem it is strongly desirable to separate the contributions of the disorder and interaction between electrons. However, in most of the experimental realizations of the disordered electron systems a variation of the disorder strength is accompanied by the consequent change of the electron density, which influences the interaction. This happens in such commonly used examples as doped semiconductors where the doping produces disorder together with excess electrons, semiconductor alloys where alloy concentration creates disorder and also considerably changes electron concentration and field effect devices where alteration of the thickness of the depletion layer influences both, the effect of the surface disorder and the electron density.

Meanwhile, a separate control of the disorder strength and the interaction energy can be obtained in the semiconductor superlattices (SL 's) which are formed by a periodic sequence of coupled quantum wells. In the periodic superlattice potential electron waves can propagate without attenuation because of the coherent constructive interference between the waves transmitted in opposite directions along the SL axis [2]. Deviations from the periodicity break down the coherency of the electron waves resulting in a formation of the localized electron states. Consequently, the disorder driven metal-to-insulator transition can be achieved. The possibility to study disorder effects in semiconductor SL 's was pointed out already in the first proposal of superstructured materials [3], where the disorder was suggested to produce either by randomly varying layer thicknesses or by random layer compositions. In turn, the interaction energy can be managed by variation of the doping level. At this, when the characteristic scale of the superlattice structural disorder is smaller when that of the impurity disorder, the former dominates the later. In spite of great potentiality of such intentionally disordered SLs to test important localization theories, a relatively small number of experimental works was done since that. The first observation of the disorder effects produced in the semiconductor SL 's by intrinsic imperfections was published in Ref. [4]. While, the first realization of the intentional disorder in SL's was demonstrated in Ref. [5]. The most important successive works there the SL 's with artificial disorder were used are listed in Ref. [6]. It is worth mentioning the recent publications in this field [7]. Between them are also our works [8–12].

The problem which often appears when investigating intentionally disordered SLs is linked to the quantitative characterization of the disorder strength. It is also important to prove that the built-in artificial disorder creates a dominant contribution to disorder effects. In a series of our articles we utilized different methods to confirm and to characterize the disorder effects produced by a random variation of the well thicknesses in the GaAs/AlGaAs SLs.

2

We demonstrated that the modern state of the molecular beam epitaxy allows for a fabrication of the superlattices with quantitatively controlled disorder. It is thought that some these data collected together may serve as a proof of the complete control of the disorder strength in the purposely disordered SLs and this can stimulate their further utilization in the study of the disorder effects. This work is addressed to experimenters who works in the field of the investigation of the properties of the electron disordered systems.

The results obtained in the $(GaAs)_m(Al_{0.3}Ga_{0.7}As)_6$ SLs grown by molecular beam epitaxy on (001) GaAs substrates are presented. Here the thicknesses of the corresponding layers are expressed in monolayers (ML). The vertical disorder was produced by the controlled random variation of the GaAs well thicknesses around the nominal value $m = 17$ ML corresponding to a Gauss distribution of the lowest levels of noninteracting electrons forming the conduction miniband, while the barrier thicknesses were unchanged. In order to avoid the short-range in-plane fluctuations, the growth was interrupted for 20 sec at the normal interface and for 3-5 sec at the inverted one. The total number of 50 periods was grown. In the case of such a Gaussian disorder the strength of disorder can be characterized by the unique disorder parameter $\delta_{SL} = \Delta/W$, where Δ is the full width at half maximum of a Gauss distribution of the energy of the noninteracting electrons calculated in the isolated quantum wells and W is the width of the nominal miniband in the absence of disorder. The miniband width calculated by the envelope function approximation [13] in the nominal $(GaAs)_{17}(Al_{0.3}Ga_{0.7}As)_6$ superlattice is equal to 55 meV. The schematic illustration of the energy structure of the here studied superlattices is shown in Fig.1. In the above mentioned superlattices the unavoidable monolayer fluctuations result in $\delta_{SL} \approx 0.18$. To form a degenerate electron gas the superlattices were homogeneously doped with Si.

In order to characterize the effect of the intentional vertical disorder on the electronic properties of the SLs under investigation we used the capacitance-voltage (C-V), photoluminescence (PL) and magnetotransport measurements. The PL measurements were carried out at 4.2 K using a He-Cd laser line at 441 nm for excitation. The PL signal was detected in the lock-in mode by a GaAs photomultiplier mounted on a 0.5 m monochromator. Parallel magneto-transport measurements were performed on the Hall bar samples using standard four probe low-frequency (5 Hz) lock-in technique in a pumped liquid He cryostat in the magnetic field directed parallel and perpendicular to the layers at the temperature 1.6 K. For the transport measurements the samples were patterned into Hall bars by standard lithography and chemical etching. The Ohmic contacts were fabricated by depositing of In. The C-V characteristics were measured on 1 mm diameter mesa structures at temperature $T = 10K$ using Al as a Schottky contact.

The spatial distribution of the electric charge along the direction of the applied voltage can be obtained by the

C-V measurements. In our case the voltage was applied along the growth direction thus, the vertical distributions of the electron density (the C-V profiles) were obtained. The distributions of the electron density obtained by the C-V measurements in the SLs with different disorder strengths are depicted in Fig.2 [10]. The modulation of the electron density along the growth direction significantly increases with the increasing disorder strength, directly exhibiting enhance of the localization effects caused by the intentional disorder.

The PL measurements probe the relative energy of the electrons. In the case of the degenerate electron gas the spectral position of the PL edge is determined by the electron Fermi energy (the Moss-Burstein effect [14]). As it was shown in Ref. [14], in the presence of disorder, due to the redistribution of the electron density, the Fermi energy decreases by a value approximately equal to the amplitude of the fluctuations of the random potential. The fluctuations of the amplitude of the superlattice random potential may be roughly estimated as a value of $\Delta = W \cdot \delta_{SL}$. Consequently, the disorder should result in a significant red shift of the PL edge $\Delta\nu \simeq \Delta$. The disorder induced red shifts of the PL edges, which according to the theory are related to the amplitude of the random potential, are depicted in Fig.3 as a function of the disorder parameter δ_{SL}. It was found that the experimental data are well described by the dependence $\Delta\nu = 42 \cdot \delta_{SL}$, meV, where the linear coefficient was indeed found very close to the value of the nominal miniband width ($W = 55\ meV$). Thus, our results demonstrate good agreement with the theory [14].

The amplitude of the Shubnikov-de Haas oscillations is proportional to the broadening of the electron energy levels in the disordered SLs. The vertical (perpendicular to the layers) broadening energy $\hbar/\tau_z$, associated with the vertical relaxation time τ_z, determines the amplitude of the oscillations measured in the magnetic field parallel to the layers. While, the parallel (parallel to the layers) broadening $\hbar/\tau_\parallel$ is responsible for the oscillations measured in the magnetic field along the growth direction. The results of these measurements are shown in Fig.4. In the range of high fields the stronger Shubnikov-de Haas oscillations were observed with the magnetic field parallel to the growth direction of the superlattice than with the magnetic field parallel to the layers, which manifests to the anisotropic disorder character. The corresponding electron broadening energies were obtained by the fit of the magnetoresistances calculated according to Ref. [15] to the experimental data. The disagreements between the experimental magnetoresistance traces and the calculated curves found at high magnetic fields are caused by the magnetic "freezing " of the impurities [16]. The electron energy broadenings determined by magnetoresistance measurements together with the calculated widths of the Gaussian distributions of the electron energies are shown in Fig.5 for the superlattices with different strengths of disorder. No influence of the vertical disorder was observed on the parallel broadenings. While, the noteworthy increase of the vertical broadening energies, although weaker than the calculated increase of the width of the Gaussian

distributions of the electron energies (Δ), was found with the increasing disorder strength. The discrepancies between the calculated random electron energy distributions and the measured values of the vertical broadenings are associated with the suppression of the disordered superlattice potential due to the Coulomb fields arising because of the electron redistribution over the quantum wells of the superlattice [17]. The value of the reduction factor $A = 3.2$, responsible for the effect of the narrowing of the level distribution in the disordered superattices was calculated in similar superlattices in Ref. [17]. This value is in a reasonable agreement with the observed here narrowing of the vertical electron energy characterized by the reduction factor $A = 2.4$.

In conclusion, the Gaussian-type intentional disorder was suggested to realize in the semiconductor SL's by a variation of the layer thicknesses. We proved that such a disorder can be quantitatively characterized by a single disorder parameter δ_{SL}. Different methods were applied to characterize the random potential and its influence on electron properties of the intentionally disordered GaAs/AlGaAs superlattices. It was demonstrated that the employment of the electrical measurements (the C-V and magnetotransport measurements) together with the spectroscopic measurements (photoluminescence) allowed for a quantitative characterization of the disorder strength. The effect of the disorder on the electron properties was found in good agreement with the theoretical predictions. The impact of the structural artificial randomization on the electronic properties of the studied here disordered doped superlattices was shown to dominate the impurity disorder and the intrinsic structural imperfections, such as interfacial broadening. This manifests itself to the comprehensive control of the intentional disorder achieved in the GaAs/AlGaAs superlattices. It is worth adding that the good quantitative agreement between the experimental and theoretical data obtained with the values of the disorder strengths calculated for the noninteracting electrons indicates the negligible effect of the interaction on transport and optical properties of disordered materials far from the metal-to-insulator transition.

[1] D.Belitz and T.R.Kirkpatrik, Rev.Mod.Phys., **66**, 261 (1994).

[2] P.Y.Yu and M.Cardona, Fundamentals of Semiconductors, Springer, Berlin, 2001.

[3] L.Esaki and R.Tsu, IBM J.Res.Dev. **14**, 61 (1970).

[4] F.Capasso, K.Mohammed, A.Y.Cho, R.Hull, and A.L.Hutchinson, Phys.Rev.Lett., **55**, 1152 (1985).

[5] A.Chomette, B.Deveaud, A.Regreny, and G.Bastard, Phys.Rev.Lett, **57**, 1464 (1986).

[6] E.Tuncel and L.Pavesi, Phil.Mag. B **65**, 213 (1992).

[7] A.A.Toropov, T.V.Shubina, S.V.Sorokin, A.V.Lebedev, R.N.Kyutt, S.V.Ivanov, M.Karlsteen, M.Willander, G.R.Pozina, J.P.Bergman, and B.Monemar, Phys.Rev. B, **59**, R2510 (1999); V.Bellani, E.Diez, R.Hey, L.Toni, L.Tarricone, G.B.Parravicini, F.Dominguez-Adame, and R.Gomez-Alcala, Phys.Rev.Lett. **82**, 2159 (1999); A.Parisini, L.Tarricone, V.Bellani, G.B.Parravicini, E.Diez, F.Dominguez-Adame, and R.Hey, Phys.Rev. B **63**, 165321 (2001)

[8] Yu.A.Pusep, W.Fortunato, P.P.Gonzalez-Borrero, A.I.Toropov, J.C.Galzerani, Phys. Rev.**B63**, 115311 (2001).

[9] A.J.Chiquito, Yu.A.Pusep, G.M.Gusev, A.I.Toropov, Phys.Rev.B **66**, 035323 (2002).

[10] Yu. A. Pusep, A. J. Chiquito, S. Mergulhão, A.I.Toropov, J. Appl.Phys **92**, 3830 (2002).

[11] Yu.A.Pusep, M.B.Ribeiro, H.Arakaki, C.A. de Souza, P.A.Zanello, A.J.Chiquito, S.Malzer, G.H.Döhler, Phys.Rev.B **68**, 195207 (2003).

[12] Yu.A.Pusep, H.Arakaki, C.A. de Souza, Phys.Rev.B **68**, 205321 (2003).

[13] G.Bastard, Phys.Rev. **24**, 5693 (1981).

[14] B.I.Schklovskii and A.L.Efros, Electron Properties of Doped Semiconductors, Springer-Verlag (1984).

[15] A.E.Stephens, D.G.Seiler, J.R.Sybert, and H.J.Mackey, Phys.Rev.B **11**, 4999 (1975)

[16] B.M.Askerov, Electron Transport Phenomena in Semiconductors, World Scientific, Singapore, 1994.

[17] G.Richter, W.Stolz, P.Thomas, S.W.Koch, K.Maschke, and I.P.Zvyagin, Superlattices and Microstructures, **22**, 475 (1997).

Figure captions:

Fig.1. Energy structure of the nominal periodic $(GaAs)_{17}(Al_{0.3}Ga_{0.7}As)_6$ superlattice and the disordered $(GaAs)_m(Al_{0.3}Ga_{0.7}As)_6$ superlattice. The dispersion of the electron energy and the energy distribution of the electron levels are shown in the periodic and disordered superlattices respectively.

Fig.2. C-V profiles measured along the growth direction (z) in the disordered $(GaAs)_m(Al_{0.3}Ga_{0.7}As)_6$ superlattices with the nominal doping concentration $N_{Si} = 6.0x10^{17}$ cm^{-3} and different disorder strengths at $T = 10K$ [10].

Fig.3. Disorder induced red shifts of the PL edges measured in the doped random $(GaAs)_m(Al_{0.3}Ga_{0.7}As)_6$ superlattices with the nominal doping concentrations $N_{Si}=1.2x10^{18}$ cm^{-3} and $1.7x10^{18}$ cm^{-3} and different disorder strengths at $T = 4.2K$. The full line represents the calculated disorder induced shift of the Fermi energy.

Fig.4. Relative parallel magnetoresistances measured in the magnetic fields parallel (thin lines) and perpendicular (thick lines) to the layers in the disordered $(GaAs)_m(Al_{0.3}Ga_{0.7}As)_6$ superlattices with the nominal doping concentration $N_{Si} = 6.0x10^{17}$ cm^{-3} and different disorder strengths at $T = 1.6$ K. The broken lines were calculated as mentioned in the text.

Fig.5. Vertical (closed circles) and parallel (open circles) broadenings of the electron energy obtained by the fit of the magnetoresistance traces in the disordered $(GaAs)_m(Al_{0.3}Ga_{0.7}As)_6$ superlattices with the nominal doping concentration $N_{Si} = 6.0x10^{17}$ cm^{-3} and different disorder strength at $T = 1.6$ K. The full line corresponds to the calculated widths of the Gaussian distribution of the electron energies (Δ), while broken lines are guides for eyes [10].
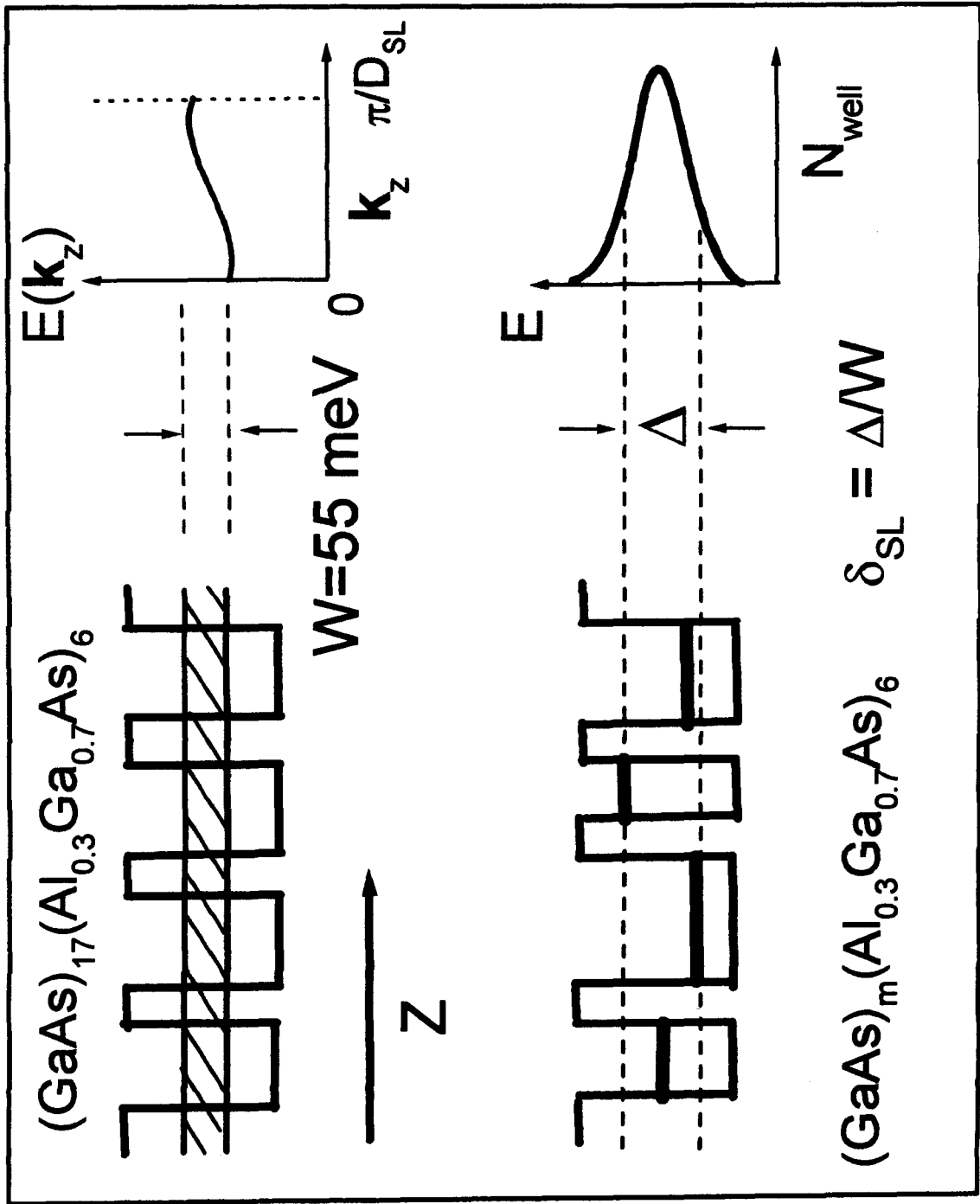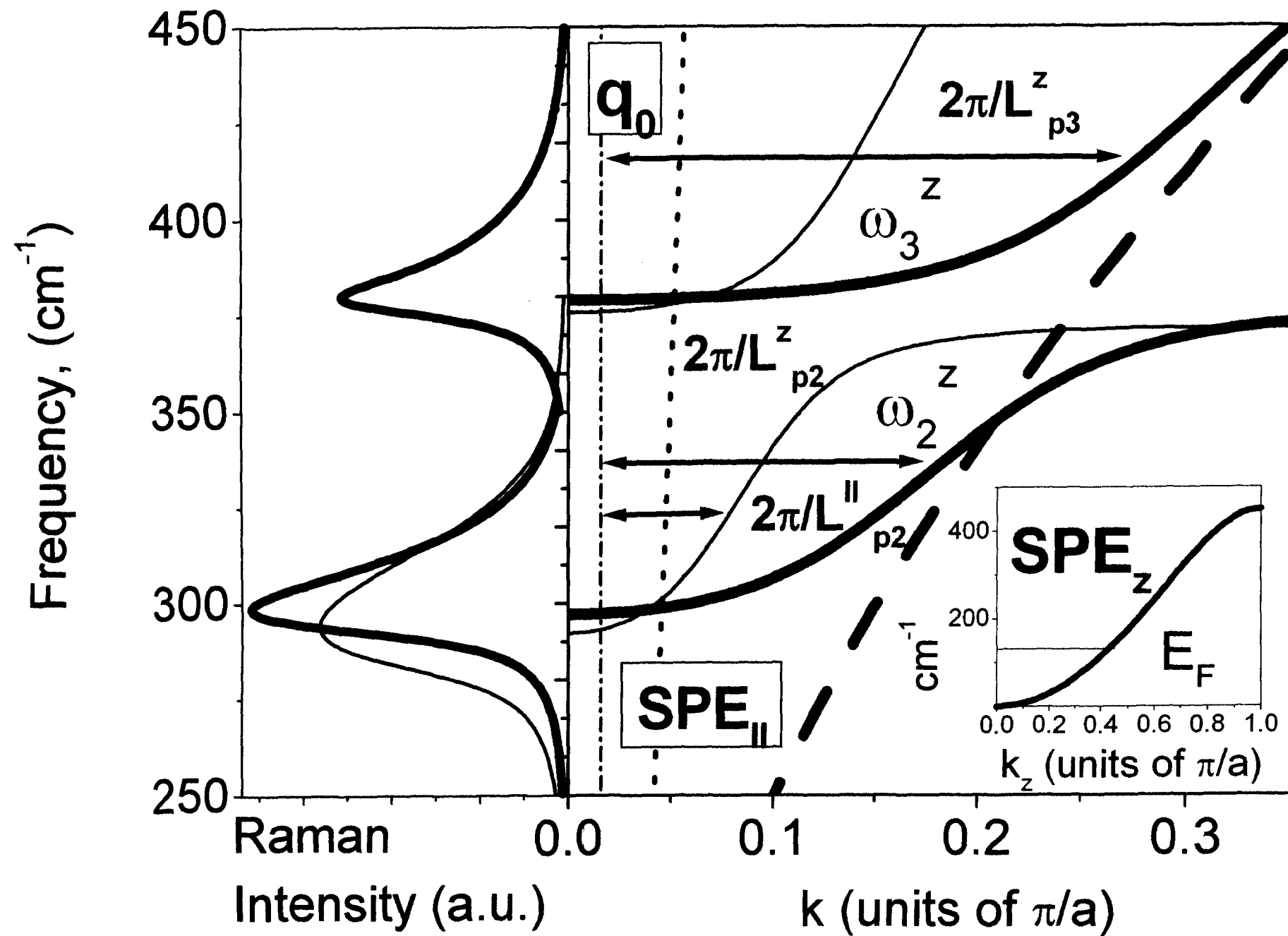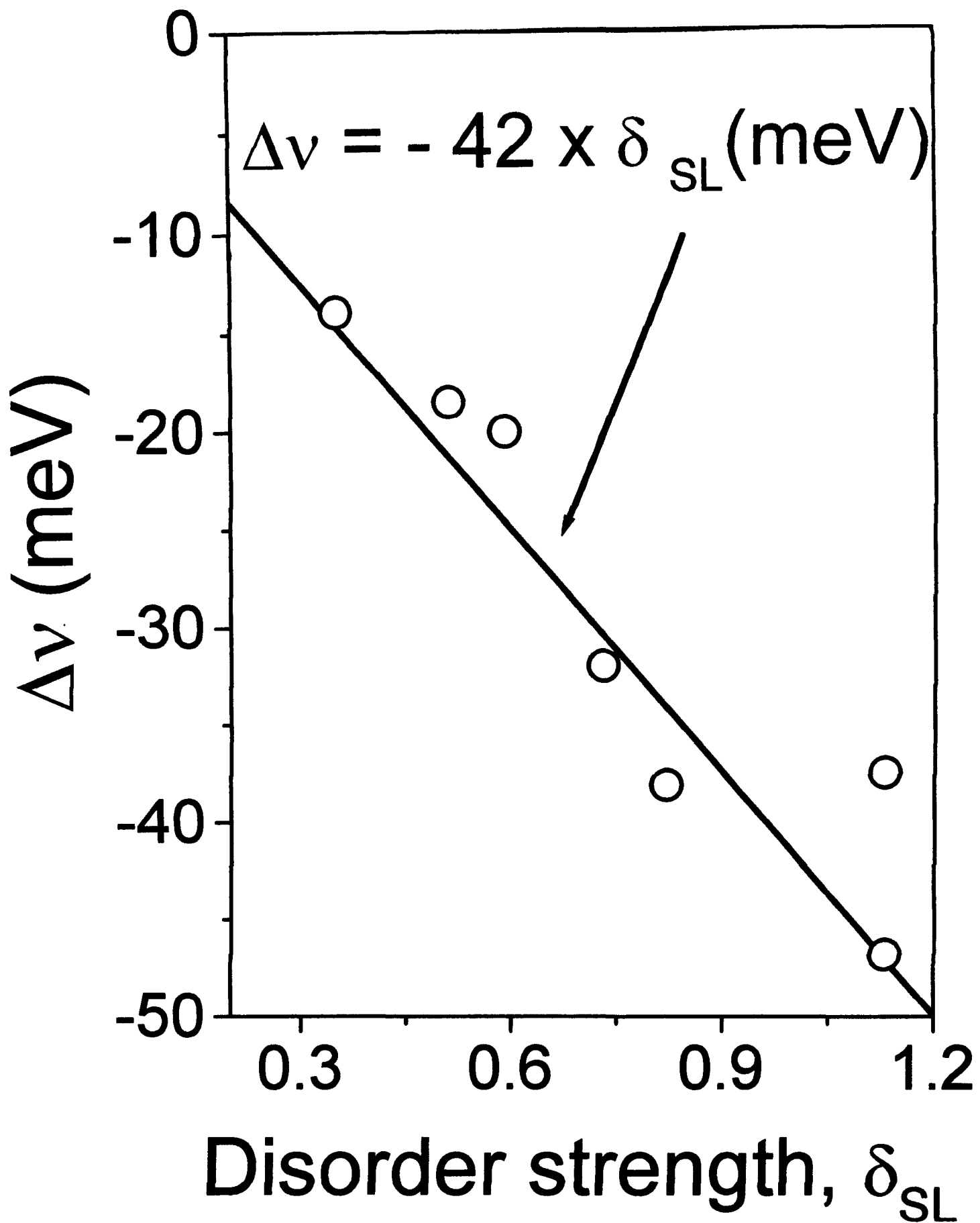
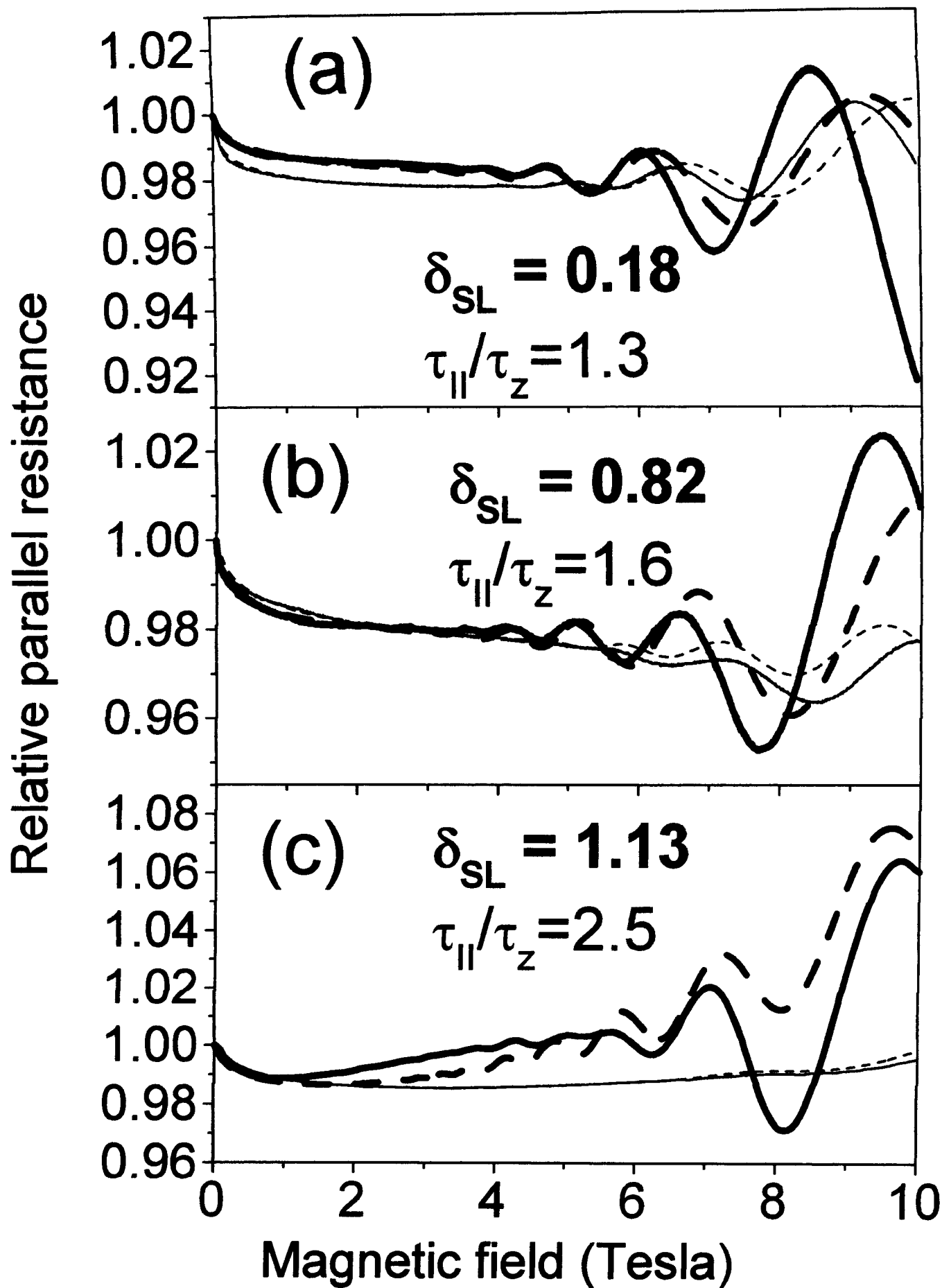Fig. 1

Fig.2

$\Delta \nu = - 42 \times \delta_{SL} \text{(meV)}$

Fig.4

(a) $\delta_{SL} = 0.18$ $\tau_{||}/\tau_z = 1.3$

(b) $\delta_{SL} = 0.82$ $\tau_{||}/\tau_z = 1.6$

(c) $\delta_{SL} = 1.13$ $\tau_{||}/\tau_z = 2.5$
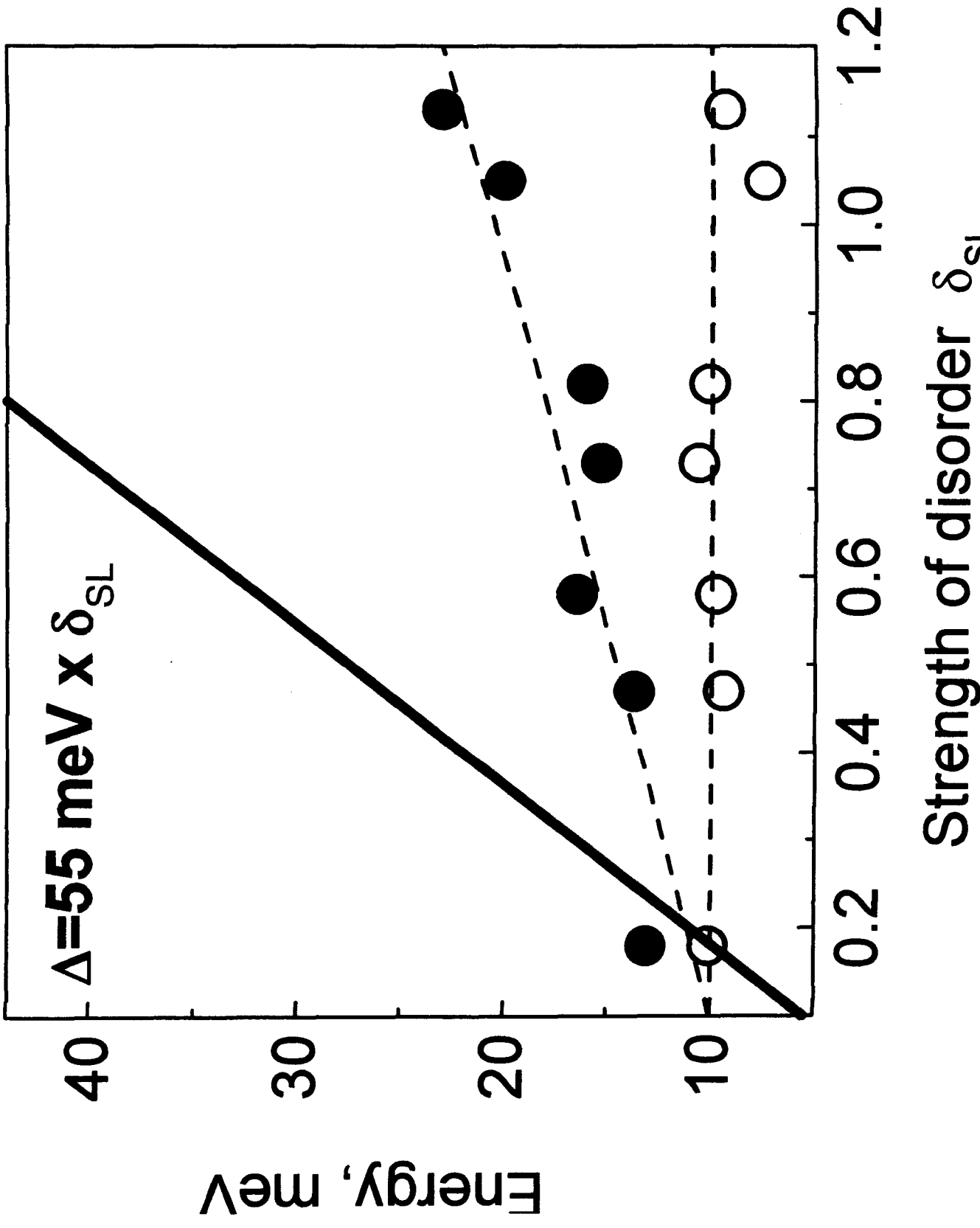
Relative parallel resistance

Magnetic field (Tesla)

Fig.

Coherency of Elementary Excitations in Disordered Electron Systems

Yu.A.Pusep[1], M.B.Ribeiro[1], V.E.Carrasco[2], G.Zanelato[2], J.C.Galzerani[2],

[1] *Instituto de Fisica de São Carlos, Universidade de São Paulo,*
13560-970 São Carlos, SP, Brazil
[2] *Departamento de Fisica, Universidade Federal de São Carlos, CP 676,*
13565-905, São Carlos, SP, Brazil
(21/12/2004)

The localization properties of the single-particle and collective electron excitations were investigated in the intentionally disordered $GaAs/AlGaAs$ superlattices by weak field magnetoresistance and Raman scattering. The Landau damping was found to limit the localization length of the collective excitations propagated along the layers. Meanwhile, the localization lengths of both, the single-particle and collective excitations propagated perpendicular to the layers were determined by the disorder. In this case the localization length of the individual electron was found to be considerably larger than that one of the collective excitations. This suggests that the disorder has weaker effect on the electrons than on their collective motion and that the interaction which gives rise to the collective effects increases localization.

According to W.Kohn [1], the electron localization occurs in the configuration space and therefore, rather relates to the wave nature of electron wave function than to the distribution of the electron charge density in the real space. Consequently, the insulating state, which results in a zero dc conductivity, is determined by the localization of the ground wave function. Therefore, a direct probe of the properties of the wave function is a central subject of the localization problem. Any elementary excitations having a wave origin reveal the same qualitative aspects of localization. However, their specific features may result in different characteristic performances. A generality of the localization in the cases of the individual electrons and their collective motions (plasmons) was firstly pointed out in Ref. [2], where the random semiconductor superlattices (SLs) were also proposed as a tool to control the strength of the disorder. The essential difference between electrons and plasmons is in the dynamic polarization which determines the collective electron motion. Hence, the interaction between electrons intrinsically determines features of their collective excitations (plasmons). Therefore, the comparison between the localization properties of the plasmons and the electrons may shed some light on the problem of how the interaction influences localization. It is pertinent mentioning that yet P.A.M.Dirac pointed out: "if we wish to make an observation on a system of interacting particles, the only effective method of procedure is to subject them to a field of electromagnetic radiation and see how they react" [3].

In this way the phase-breaking length of the individual electrons can be obtained by the weak-field magnetoresistance measurements [4]. As it was stated in Ref. [5], the phase-breaking length determines the minimum width of an electron wave packet and therefore, it may serve as the lower cutoff for the localization length. On the other hand, the localization length associated with the indetermination of the quasi-momentum of the plasmons can be measured by Raman scattering [6,7].

It is worth mentioning that a comprehensive analysis of the disorder effects induced by the unavoidable monolayer fluctuations on the vertical transport properties of $GaAs/AlGaAs$ SLs was presented in Ref. [8].

In this work we study and compare the localization properties of the single-particle and the collective electron excitations subjected to a random potential in the intentionally disordered $GaAs/AlGaAs$ SLs where the vertical (along the growth direction) disorder was produced by a random variation of the well thicknesses. Such a disorder let us to control the spatial extent of the wave functions of the elementary excitations propagating normal to the layers and to choose the structure of the samples where the localization properties of both the electrons and the plasmons can be measured concurrently. We showed that in good agreement with a theory, the Landau damping results in a restriction of the parallel quasi-momentum (along the layers) of the collective excitations by the single-

electron excitations. This demonstrates a precision and a reliability of the experimental method used to determine the localization length of the collective excitations. Afterwards, the vertical localization length (perpendicular to the layers) of the collective excitations was measured in the SL with the minigap set in the frequency range of the collective modes. In this case no Landau damping is anticipated and the disorder determines the localization length of the plasmons.

Two pairs of the $(GaAs)_m(Al_{0.3}Ga_{0.7}As)_6$ SLs (where the thicknesses of the layers are expressed in monolayers) with different disorder strengths and doping concentrations were grown on (001) $GaAs$ substrates. Each pair consisted of two identical SLs, one grown on semi-insulating substrate and another grown on doped one. They were used to measure the vertical and parallel magnetotransport respectively. The disorder strength was characterized by the disorder parameter $\delta_{SL} = \Delta/W$, where Δ is the width of a Gaussian distribution of the electron energy calculated in the isolated quantum wells and W is the miniband width of the nominal SL (with $m = 17ML$) in the absence of disorder. The samples with $\delta_{SL} = 0.4$ and $\delta_{SL} = 0.82$ and with the total thickness 0.3 μm (50 periods) and 0.9 μm (150 periods) respectively, were studied. A contact 0.4 μm thick highly doped $GaAs$ layer was deposited on the top of the SLs grown on doped substrate. This top layer was removed before the Raman measurements. In order to form the degenerate electron system the samples were homogeneously doped with Si.

The samples were patterned either into Hall bars or square shaped mesa structures with areas 1x1 mm^2, both prepared by standard lithography and chemical etching. The Ohmic contacts were fabricated by depositing either In (Hall bars) or an $Au : Ge : Ni$ alloy (mesas). All transport measurements were performed with the current 10^{-5}-$10^{-4}A$, when the contact resistances were confirmed to be ohmic, using standard low-frequency (1 Hz) lock-in technique in the temperature range from 1.6K to 80K. The vertical transversal magnetoresistances were acquired by two-probe measurements in a double mesa structures consisted of two identical mesas connected in series as it is shown in Fig.3(b). As in Ref. [8], a direct comparison with the four-probe vertical measurements did not reveal a significant contact resistances. The collective excitations propagated normal to the layers were examined with Raman scattering performed at $T = 10K$ with a "Instruments S.A. T64000 " triple grating spectrometer; the 5145 $\overset{o}{A}$ line of an Ar^+ laser was used for non-resonant excitation. Raman scattering of the collective excitations propagated along the layers was collected from the (110) side of the SL with the total thickness $d_{SL} = 0.9$ μm. In order to avoid scattered light coming from the substrate, the micro-Raman system which focused the light with the spot size smaller than 1 μm was used. In this case the Raman spectra were taken at $T = 80K$. The parameters of the studied disordered SLs are listed in Table 1.

In the recent articles [6,7] we have demonstrated that in the intentionally disordered $GaAs/AlGaAs$ SLs the observed asymmetry of the Raman lines associated to the plasmon-like collective excitations is due to the effect of their localization. In this case the magnitude of the localization length of the relevant collective excitations indicates the strength of the correlation effects (the longer localization length, the stronger electron correlation) and it can be determined using the formula [6]:

$$I(\omega) \sim \int \exp[-\frac{(q - q_0)^2 L_p^2}{4}] \frac{dq}{[\omega - \omega_p(q)]^2 + (\Gamma/2)^2} \tag{1}$$

where $q_0 = 4\pi n(\lambda)/\lambda$ is the wave number transferred by the laser light with the wave length λ used for excitation, $n(\lambda)$ is the refractive index, $\omega_p(q), L_p$ and Γ are the dispersion of the appropriate collective excitations, their localization length and their damping constant respectively. The dispersions of the collective modes were calculated in the direction of propagation of the light using the random phase approximation (RPA) as in Ref. [6]. In the absence of the Landau damping the validity of the RPA was confirmed in Ref. [9].

The high-field magnetoresistance data which display the distinct Shubnikov - de Haas oscillations (they were used to determine the Fermi energies given in Table 1) and the absence of the activation type temperature behaviors of resistances show that the electrons in the studied disordered SLs exhibit properties of metallic systems subjected to a weak anisotropic disorder.

In the weak localization regime ($k_F l \gg 1$) and in a weak magnetic field ($\omega_c \tau \ll 1$, where ω_c and τ are the cyclotron frequency and the elastic scattering time respectively) the magnetic field dependence of the conductivity is caused by the weak-localization correction. In the magnetic field $H_\perp$ orthogonal to the plane of layers the weak localization corrections to the parallel conductivity of a SL is determined by the following expression [10]:

$$\Delta\sigma^{\shortparallel}(H) = \frac{e^2}{2\pi^2 \hbar l_H} \alpha F(\delta) \tag{2}$$

where $l_H = \sqrt{\hbar/eH_\perp}$ is the magnetic length, $\alpha = \sqrt{m_z/m_{\shortparallel}}$ is the coefficient of anisotropy (in the studied here SLs the calculations give $\alpha = 1.4$), $F(\delta)$ is the Kawabata function and $\delta = \frac{l_H^2}{4L_\varphi^2}$ with L_φ being the electron phase-breaking length. The quantum correction to the vertical magnetoresistance of a SL subjected to the magnetic field parallel to the layers is given by the formula (2) divided by α^2 with the magnetic field determined by the scaling relation $H_{\shortparallel} = H_\perp/\alpha$ [11].

The Raman scattering intensities obtained at $T = 80K$ in the $z(x, x)\bar{z}$ and $x'(z, z)\bar{x}'$ back-scattering configuration (where z is the growth [001] direction and $x \parallel$ [100], $x' \parallel$ [110]) in the thick disordered SL are shown in Fig.1(a,b). According to the selection rules, in both these cases the longitudinal optic (LO) vibrations are active [12]. In the

$z(x,x)\bar{z}$ geometry we observed the intensive line at 294 cm^{-1} which consists of two components: one due to the unscreened LO $GaAs$-like phonon from the depletion surface layer and another is the ω_2^z coupled plasmon-LO phonon $GaAs$-like mode (the superscript means the direction of the mode propagation) which revealed the disorder induced asymmetry [6]. Also, the likely asymmetrical ω_3^z coupled $AlAs$-like mode was found around 380 cm^{-1}. The weak LO_1^z and at LO_2^z lines were assigned to the $GaAs$-like and $AlAs$-like LO phonons of the $Al_{0.3}Ga_{0.7}As$ barriers respectively revealed due to the depletion layer. In such an alloy these modes are expected at 282 cm^{-1} and at 375 cm^{-1} correspondingly [13]. Moreover, we observed the disorder induced TO_1^z and TO_2^z phonon lines attributed to the $GaAs$ well and to the $Al_{0.3}Ga_{0.7}As$ barriers respectively; their expected values are 272 cm^{-1} and 363 cm^{-1} correspondingly.

The Raman spectrum measured in the $x'(z,z)\bar{x}'$ geometry shows the same character as in Ref. [13,14]: the intensive forbidden TO phonons and the weaker LO phonons. Nevertheless, the asymmetry of the $\omega_2^{\parallel}$ mode is still well pronounced.

The fits of the Raman intensities calculated by Eq.(1) to the experimental spectra measured in different configurations allowed us to obtain the localization lengths of the plasmon-like excitations propagated in different directions. The results of the best fits are shown in Fig.1(a,b). At $T = 80K$ we found $L_{p2}^z \simeq 3.5nm$, $L_{p3}^z \simeq 2.1nm$ for the $GaAs$ and $AlAs$ plasmon-like excitations propagated normal to the layers respectively and $L_{p2}^{\parallel} \simeq 8.4nm$ for the $GaAs$ plasmon-like excitations propagated along the layers.

The energy spectra of both the single-particle and collective excitations calculated in different directions of the investigated above SL are depicted in Fig.2. For the parallel collective plasmon-like excitations the wave number cutoff caused by the localization effects $(2\pi/L_{p2}^{\parallel})$ was found in reasonable agreement with the limitation of the wave number of the collective excitations due to the Landau damping. At the same time, the Landau damping does not influence the localization of the collective excitations propagated perpendicular to the layers because of the significant difference between their energy and the energy of the lowest miniband of the single-particle excitations. Therefore, in this case the disorder induced localization length was extracted.

In order to compare the disorder induced localization length of the collective excitations with that of the electrons we measured Raman back-scattering from the (001) surface of the SL at $T = 10K$. The corresponding localization length of the $GaAs$ plasmon-like excitations together with the vertical phase-breaking length obtained at the same temperature are given in Table 1.

It should be mentioned that at low temperatures the electrons reveal strongly anisotropic negative magnetoresistance demonstrated in Fig.1(c). The phase-breaking length obtained at $T = 1.6K$ in the directions perpendicular and

5

parallel to the layers were 710 nm and 2200 nm respectively. However, while the parallel phase-breaking length strongly decreased with the temperature, no significant temperature variation of the vertical phase-breaking length was observed. As a result, already at $T = 10K$ the electrons expose isotropic localization.

Similar results were obtained in another SL with different disorder strength and higher doping concentration. The Raman intensity measured in this SL is depicted in Fig.3(a). In such a case we found the well pronounced plasmon-like asymmetry of the ω_3^- mode. While, the ω_2^- mode exhibited the opposite phonon-like asymmetry due to its phonon-like character, expected in highly doped SLs [6]. As in the previous case no effect of the Landau damping is anticipated and consequently disorder and the electron-electron interaction result in the localization length of the collective excitations shown in Fig.4. The weak field vertical magnetoresistance measured in the mesa structure prepared from this SL grown on doped substrate is shown in Fig.3(b) together with the data obtained in the mesa structure fabricated on the same doped substrate without the SL. The mesa-shaped $GaAs$ substrate revealed no considerable magnetoresistance. Consequently, the contribution from the substrate is negligible. The data obtained in this SL are given in Table 1.

Finally, it is worth adding that the weak-field magnetoresistance in the studied here disordered superlattices is due to the quantum interference processes and is not caused by the interaction effects [15]. Therefore, a comparison between the localization lengths of the vertical plasmon-like excitations and the vertical phase-breaking lengths of the noninteracting electrons provides arguments for understanding the influence of the interaction on localization effects. The localization length of the collective excitations was found considerably smaller than that of the individual electron. This means that the disorder affects the collective excitations in a stronger way than it does to the single-particle ones.

[1] W.Kohn, Phys.Rev. **133**, A171 (1964)
[2] S.Das Sarma, A.Kobayashi, and R.E.Prange, Phys.Rev.Lett. **56**, 1280 (1986)
[3] P.A.M.Dirac, Proceedings of the Royal Society of London, **A136**, 453 (1932)
[4] G.Bergmann, Physics Reports **107**, 1 (1984)
[5] B.L.Altshuler, A.G.Aronov, and D.E.Khmelnitsky, J.Phys.C **15**, 7367 (1982)
[6] Yu.A.Pusep, M.T.O.Silva, N.T.Moshegov, P.Basmaji, and J.C.Galzerani, Phys.Rev.B **61**, 4441 (2000)
[7] Yu. Pusep, W. Fortunato, P. P Gonzalez-Borrero, A. I. Toropov, J. C. Galzerani, Phys. Rev. B **63**, 115311-1 (2001)
[8] M.Lee, S.A.Solin, and D.R.Hines, Phys.Rev.B **48**, 11921 (1993)
[9] A.Pinczuk, G.Abstreiter, R.Trommer, and M.Cardona, Sol.St.Comm., **21**, 959 (1977)
[10] W.Szott, C.Jedrzejek and W.P.Kirk, Phys.Rev.B **40**, 1790 (1989)
[11] A.Cassam-Chenai, D.Mailly, Phys.Rev. B **52**, 1984 (1995)

[12] A.Feinstein, P.Etchegoin, M.P.Chamberlain, M.Cardona, K.Tötemeyer, and K.Eberl, Phys.Rev.B **51**, 14448 (1995)

[13] S.W.da Silva, Yu. Pusep, J. C. Galzerani, M.A.Pimenta, D.I.Lubyshev, P. P Gonzalez-Borrero, P.Basmaji, Phys. Rev. B **53**, 1927 (1996)

[14] R.Hessmer, A.Huber, T.Egeler, M.Haines, G.Tränkle, G.Weimann, and G.Abstreiter, Phys.Rev.B **46**, 4071 (1992)

[15] Yu.A.Pusep, H.Arakaki, C.A.de Souza, Phys.Rev.B **68**, 205321 (2003)

Figure captions:

Fig.1. Raman intensities of the collective modes propagated perpendicular (a) and parallel (b) to the layers measured at $T = 80 \ K$ in the $(GaAs)_m(Al_{0.3}Ga_{0.6}As)_6$ superlattice with the disorder strength $\delta_{SL} = 0.82$. The dash lines are the intensities calculated according to Eq.(1). The contributions of the asymmetrical plasmon-like peaks are shown by thick lines. Low panel (c) shows the parallel and vertical magnetoresistances measured in the same superlattice at $T = 1.6 \ K$; here the dash lines were calculated according to Eq.(2). Insets show the Hall bar and the double superlattice mesa used for the parallel and vertical transport measurements respectively.

Fig.2. Energy spectra of the vertically propagated single-particle (inset) and collective excitations calculated in the $(GaAs)_{17}(Al_{0.3}Ga_{0.6}As)_6$ superlattice with the electron concentration $n = 2.0x10^{17}cm^{-3}$. The dash and full lines represent the dispersions of the uncoupled plasmons and the plasmons coupled to the LO phonons respectively. Thin lines show the dispersions of the single-particle (dash line) and collective excitations (full lines) propagated parallel to the layers. The vertical dash-dotted line demonstrates the wave number transferred by the light used for excitation. The left panel shows the corresponding calculated Raman intensities obtained by the fits as explained in the text.
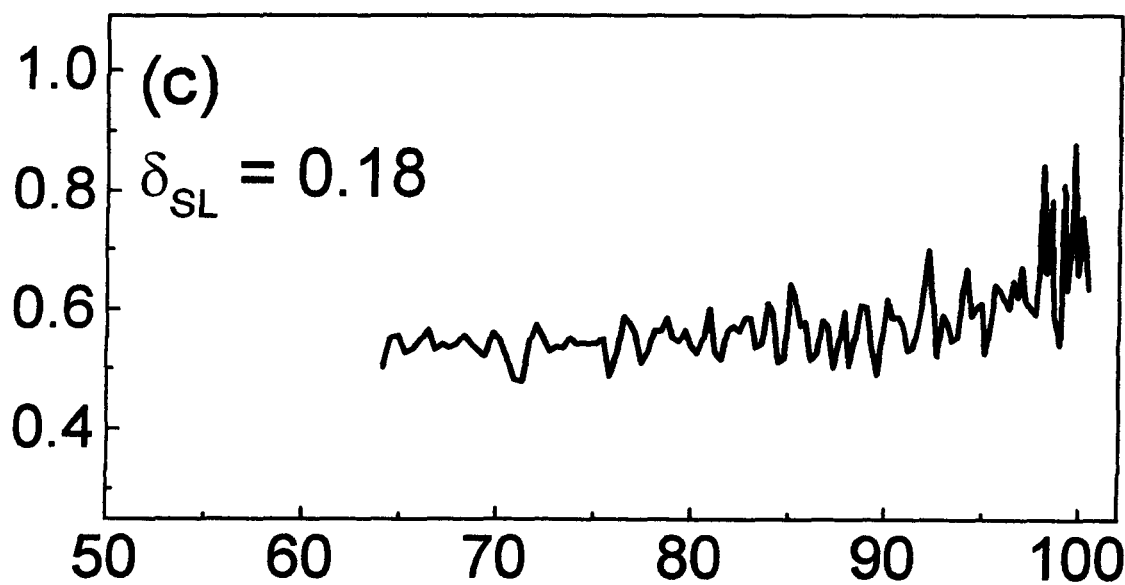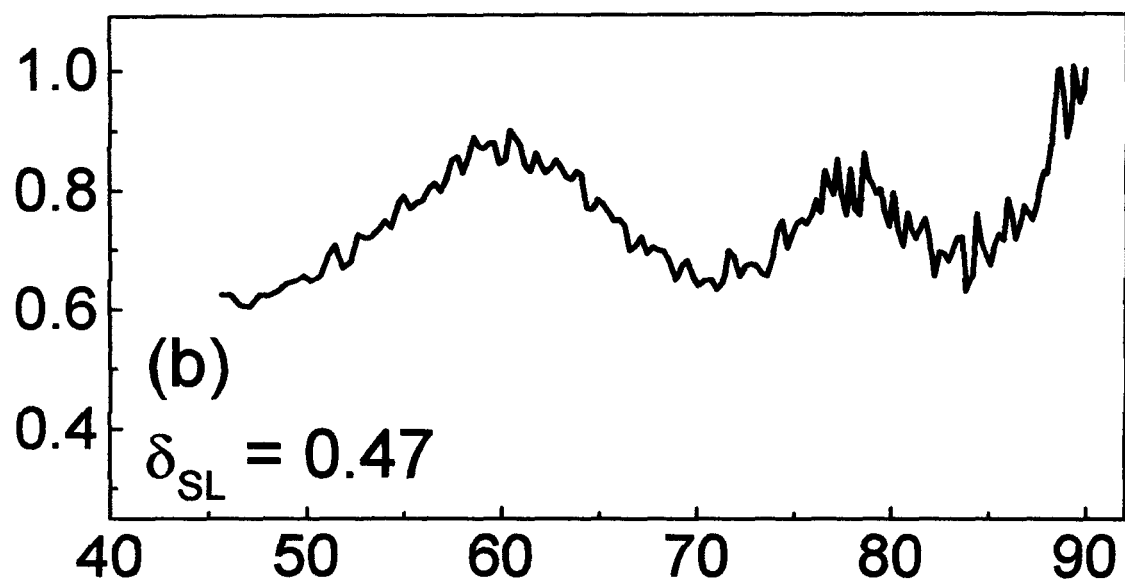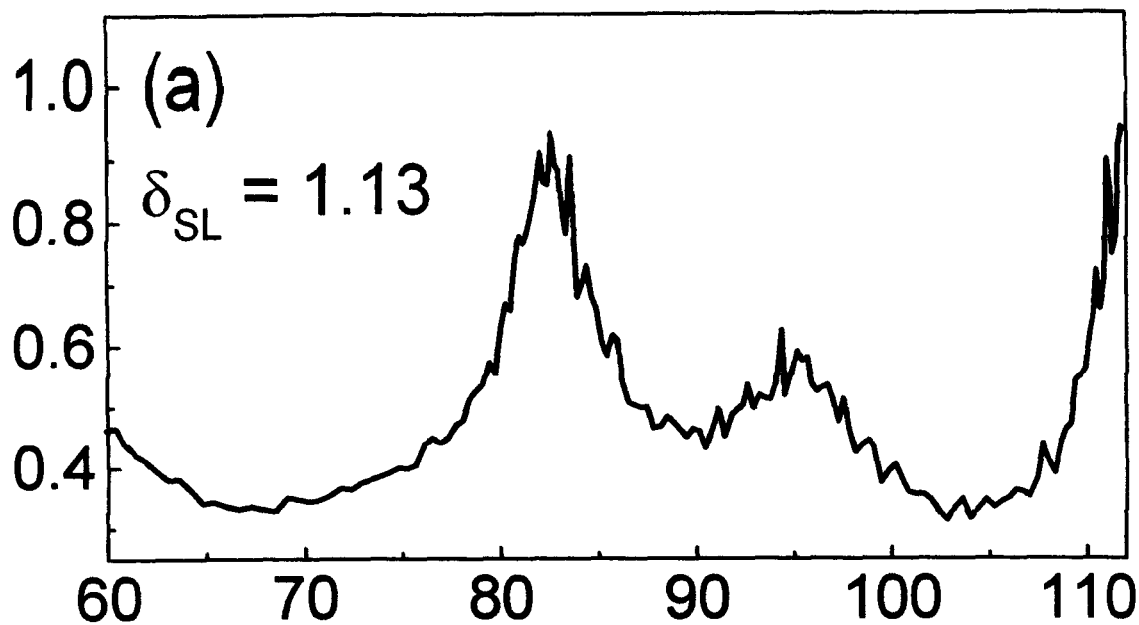
Fig.3. (a) Raman intensity measured at $T = 10 \ K$ in the $(GaAs)_m(Al_{0.3}Ga_{0.6}As)_6$ superlattice with the disorder strength $\delta_{SL} = 0.4$. The dash line is the intensity calculated according to Eq.(1). (b) Weak field vertical magnetoresistance measured in the magnetic field parallel to the layers in the same superlattice at $T = 10 \ K$ (labeled as DSL). Here the dash line was calculated according to Eq.(2). The data marked as $GaAs$ relate to the mesa structure fabricated on the same doped substrate without the superlattice.
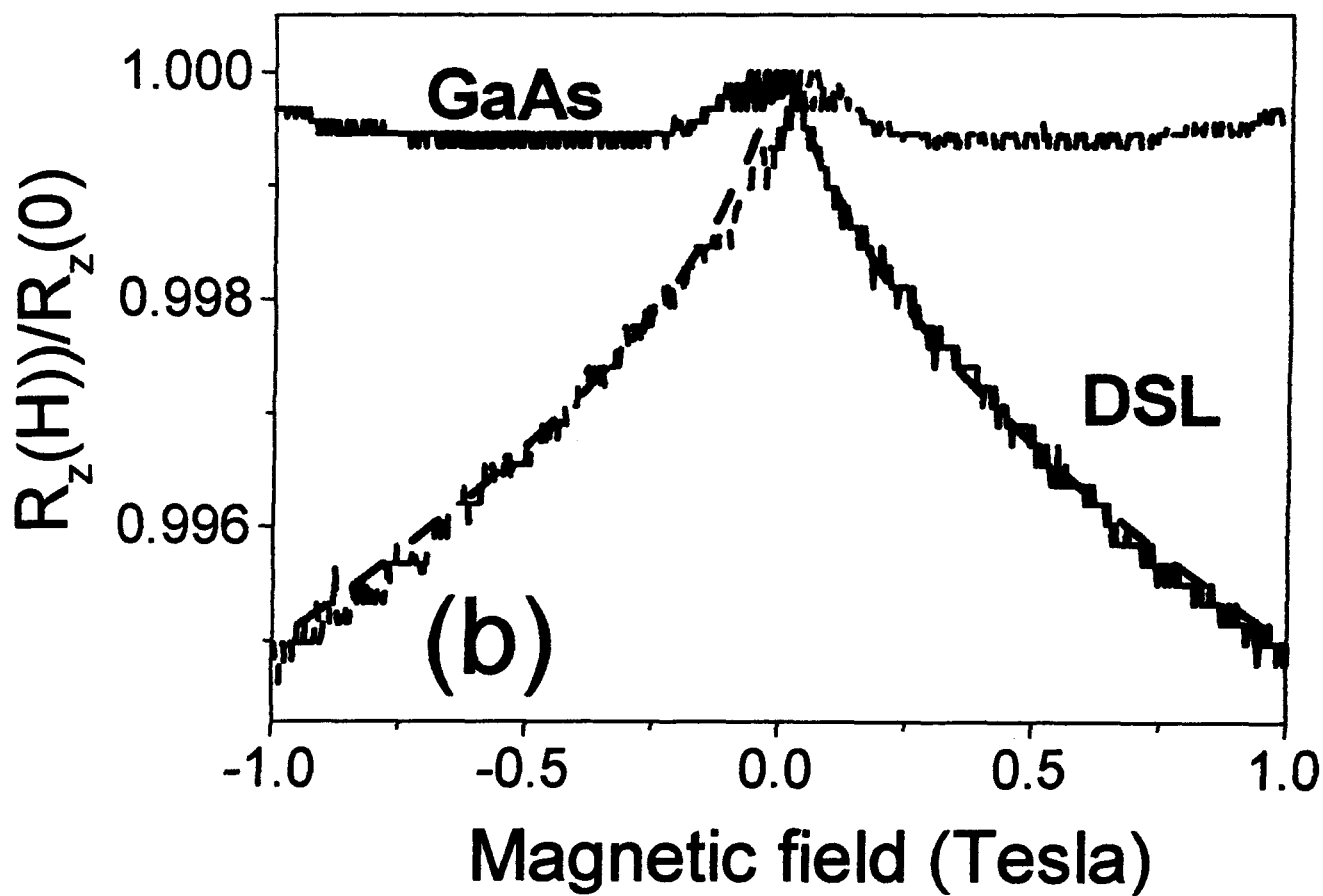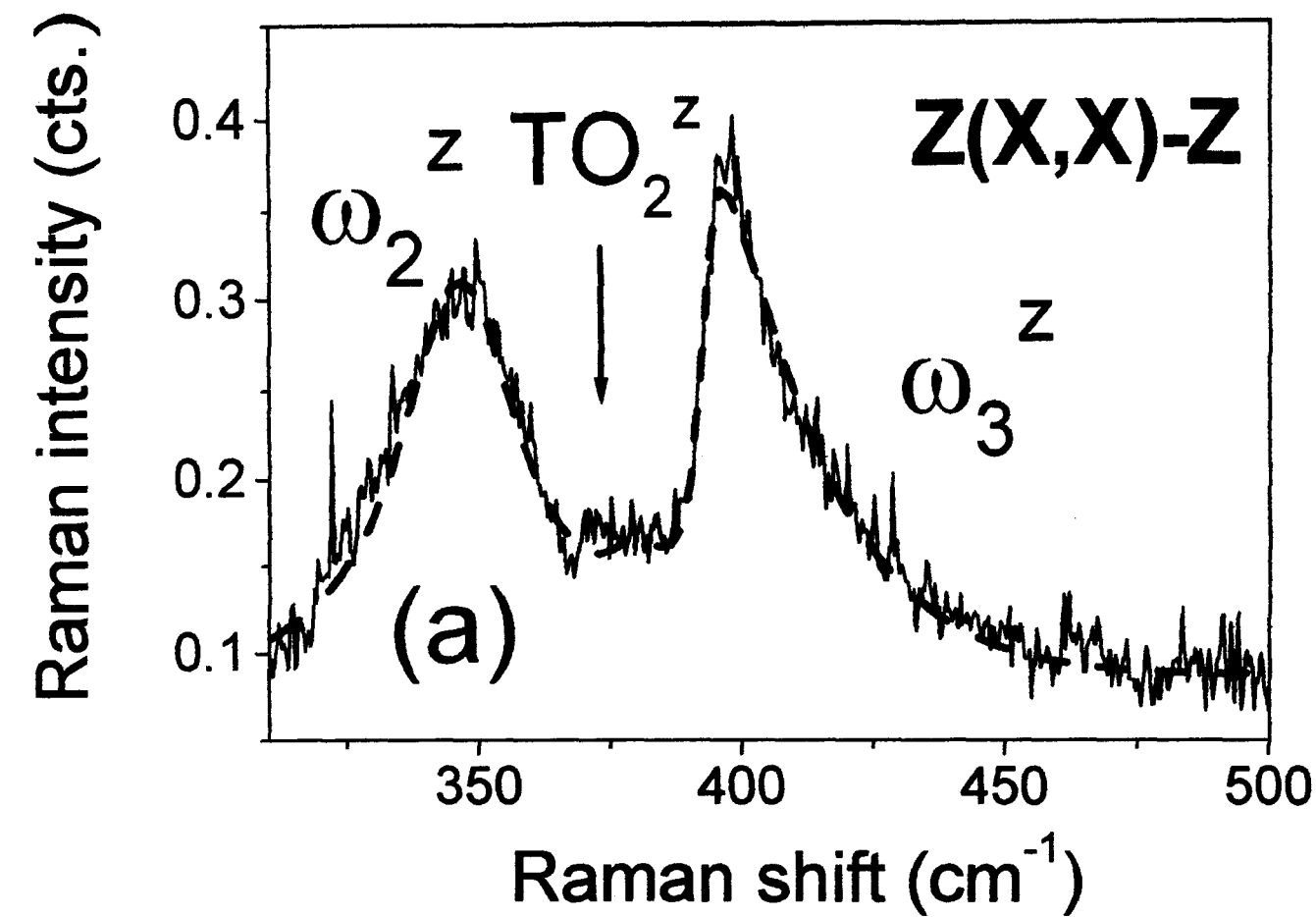
Fig.4. Energy spectra of the vertically propagated single-particle (inset) and collective excitations calculated in the $(GaAs)_{17}(Al_{0.3}Ga_{0.6}As)_6$ superlattice with the electron concentration $n = 6.5x10^{17}cm^{-3}$. The dash and full lines represent the dispersions of the uncoupled plasmons and the plasmons coupled to the $AlAs \ LO$ phonons respectively. The vertical dash-dotted line demonstrates the wave number transferred by the light used for excitation. The right panel shows the calculated Raman intensity obtained by the fit as explained in the text.

Table 1. Parameters determined at $T = 10K$ in two types of the studied disordered $GaAs/AlGaAs$ superlattices

δ_{SL}	n_H, cm^{-3}	$\mu_H, \frac{cm^2}{V_s}$	E_F, eV	$k_F l$	L_{p3}^z, nm	L_φ^z, nm
0.4	6.5x10^{17}	1400	0.036	5.9	5.0	250.0
0.82	2.0x10^{17}	2143	0.015	4.0	7.3	140.0

Fig. 1

(a) $\delta_{SL} = 1.13$

(b) $\delta_{SL} = 0.47$

(c) $\delta_{SL} = 0.18$
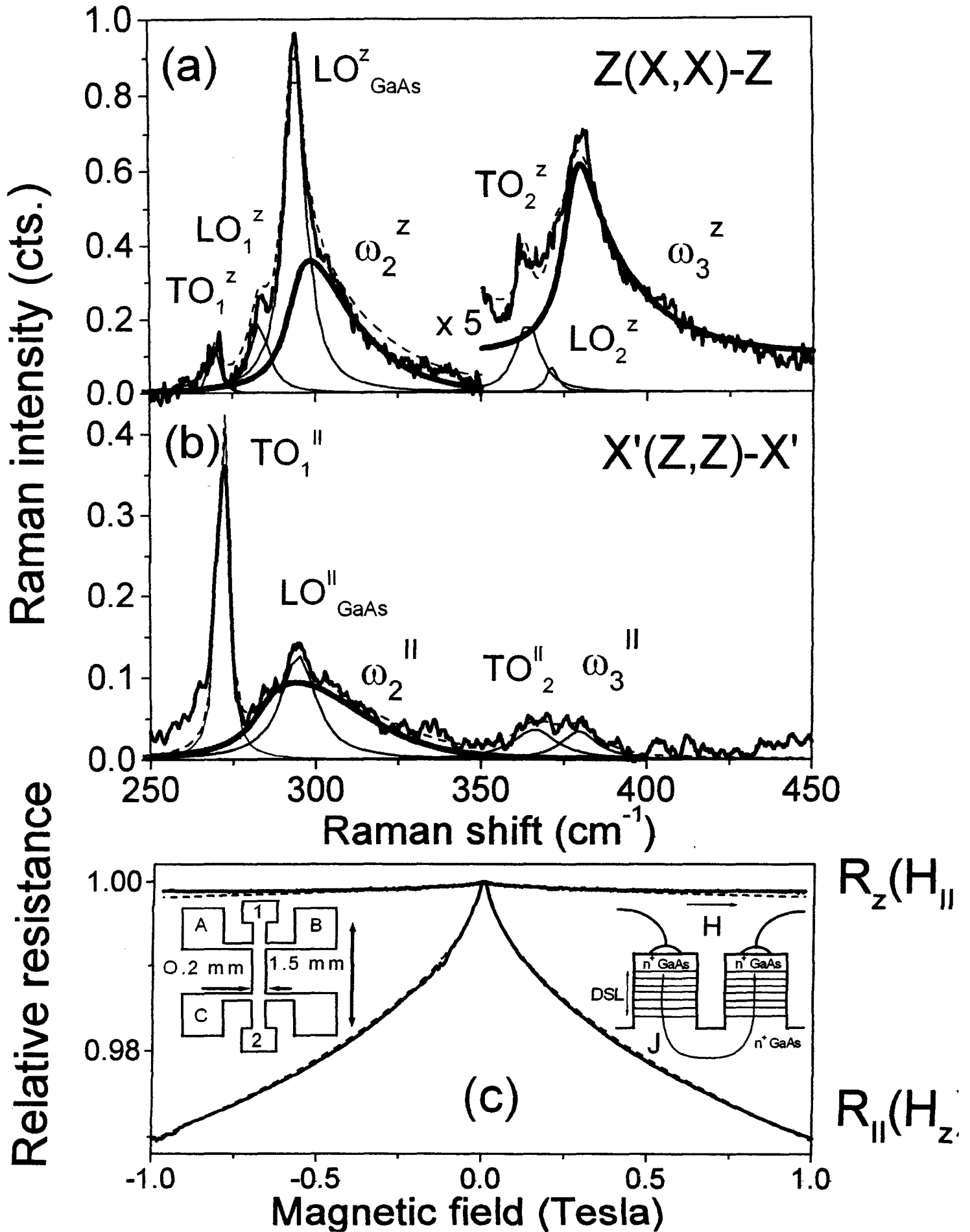
Electron concentration, $\times 10^{18}$ cm^{-3}

Distance Z, nm

Fig.4